AN ABSTRACT OF THE THESIS OF

Gwo-Sheng Peng for the degree of Doctor of Philosophy in Mechanical Engineering presented on January 21, 1992.

Title: Processing of Laser Interferometric Signals for Small Displacement Measurements.

Redacted for Privacy

Abstract approved: _____
Ernest G. Wolff

Algorithms for analyzing laser interferometry signals were developed and adopted to the computer based processing of small displacement measurements. These methods, matrix operation approach and fixed parameters approach, are based on signal phase calculation and are able to replace complex fringe counting electronic circuits. The matrix operation provides an approach for instantaneously displaying the results. The computer fixed parameters analysis allows the laser intensity to vary arbitrarily during a measurement. Displacement caused by a piezoelectric crystal was measured. Second order polynomial curve fitting was performed. The root mean square error is found to be 0.0086 μm in this 8-bit data acquisition system. CTEs of a fused silica plate and a tube were measured by an interferometry system. Signals were analyzed by both manual chart approach and

computer based fixed parameters approach. Results agree well with published data. The accuracy of the CTE measurement system was 4 $\mu\epsilon$, one third of the reference NBS SRM 739 suggested standard deviation. Out-of-plane and in-plane displacements can be measured independently from speckle interferometry. Their resolutions are 0.3164 μm/cycle for the out-of-plane configuration and 0.224 μm/cycle for the in-plane configuration with light incident angle of 45°. Optical systems with Fast Fourier Transform data analysis showed that the minimum detectable vibration amplitudes were 0.0065 μm, 0.0038 μm, and 0.0010 μm for the out-of-plane speckle, the in-plane speckle, and Michelson interferometry systems respectively. Resonance frequency of a steel rod was found by the optical non-contact sensing system. The modulus of elasticity calculated from the resonance frequency was close to the literature data, 182 GPa vs. 200 GPa.

Processing of Laser Interferometric Signals for Small Displacement Measurements

by

Gwo-Sheng Peng

A THESIS

submitted to

Oregon State University

in partial fulfillment of

the requirements for the

degree of

Doctor of Philosophy

Completed January 21, 1992

Commencement June 1992

APPROVED:

Redacted for Privacy

Associate Professor of Mechanical Engineering in charge of major

Redacted for Privacy

Head of Department of Mechanical Engineering

Redacted for Privacy

Dean of Graduate School

Date thesis is presented : January 21, 1992

Presented by : Gwo-Sheng Peng

ACKNOWLEDGMENTS

I would like to express my sincere gratitude to my advisor, Dr. Ernest G. Wolff, associate professor of Mechanical Engineering; without his continuing consultation and valuable guidance, this work would not have been possible. I am also grateful to Dr. David R. Thomas, Dr. Thomas K. Plant, Dr. Timothy C. Kennedy and Dr. William H. Warnes for reviewing the dissertation and participation as Graduate Committee.

This study was supported in part by Lockheed Missiles and Space Co. and the Oregon Metals Initiative. Financial support provided by OSU in the form of teaching and research assistantships is gratefully acknowledged.

I would like to thank all of my teachers at Oregon State University for their advice, help and assistance. I would also like to thank all of the friends in Corvallis for their companionship that made the graduate study at OSU more enjoyable. Special thanks are given to my parents for their love.

However, I praise my wife, Jen-Yu Peng, for her marvelous support, encouragement and understanding throughout my study.

TABLE OF CONTENTS

CHAPTER 1. INTRODUCTION 1
1.1. Thesis Objectives 1
1.2. Thesis Scope 3
1.3. Literature Review 5
1.3.1. Low CTE materials 5
1.3.2. Techniques for measuring CTE . . 6
1.3.3. Reference materials 11
1.3.4. Applications and signal processing of Michelson interferometer 12
1.3.5. Applications and signal processing of speckle interferometers 13

CHAPTER 2. REVIEW OF FUNDAMENTAL PRINCIPLES . . . 16
2.1. General Descriptions of Lightwaves . . 16
2.1.1. Wave equations 16
2.1.2. Polarization 17
2.1.3. Optical Phase Retardation . . . 20
2.1.4. Coherence 21
2.1.5. Interference 22
2.1.6. Lasers 28
2.1.7. Amplitude/Polarizing beam splitters 29
2.1.8. Michelson interferometer . . . 31
2.2. Speckle Interferometry 34
2.2.1. Interference of laser speckle fields 36
2.2.2. Interferometers combining two speckle fields 38
2.2.3. Methods of Correlating Two Speckle Fields 41
2.3. Composite Materials 44
2.3.1. Mechanical/Thermal properties of a lamina 45
2.3.2. Stress-strain relations of a lamina 46
2.3.3. Stress-strain relations of a laminate 48
2.3.4. Thermal expansion of composite materials 49
2.4. Fast Fourier Transform 51
2.5. Temperature Conversion from Thermocouples 53

CHAPTER 3. DERIVATIONS OF SIGNAL PHASE CALCULATION 59
3.1. Interference of Decomposed **E** Fields in Michelson Interferometry 59

3.2. Signal Phase Angles 62
3.3. Signal Trajectory 63
3.4. Signal Phase Calculations 67
3.4.1. Matrix operation approach . . . 67
3.4.2. Fixed parameters approach . . . 69

CHAPTER 4. APPARATUS AND EXPERIMENTAL PROCEDURES . 77
4.1. PZT Calibration Setup 77
4.2. CTE Measurement Apparatus 80
4.2.1. Beam alignment 80
4.2.2. Stability/Drift test 82
4.2.3. CTE measurement procedures . . 84
4.2.4. CTE data Processing 89
4.3. Speckle Interferometry 92
4.3.1. Out-of-plane motion detection system 92
4.3.2. In-plane motion detection system 94
4.3.3. FFT analysis to speckle signals 96

CHAPTER 5. RESULTS AND DISCUSSIONS 98
5.1. PZT Calibration Data 98
5.2. CTE Data 107
5.3. Speckle Interferometry Verification Data 121
5.4. FFT Results of Speckle Signals 127
5.4.1. Characteristic noise in speckle systems 127
5.4.2. FFT outputs with single input frequency 127
5.4.3. Minimum detectable displacements 128
5.4.4. Resonance frequency detection 129

CHAPTER 6. CONCLUSIONS AND RECOMMENDATIONS 144
6.1. Conclusions 144
6.1.1. Signal Analysis Algorithms . . 144
6.1.2. PZT Calibration System 145
6.1.3. CTE Measurement Apparatus . . . 145
6.1.4. Speckle interferometry 146
6.2. Recommendations for the Areas of Future Research 147

BIBLIOGRAPHY 150

APPENDIX A. Thermal expansion of fused silica (SRM 739) 154
APPENDIX B. Temperature Conversion Program 157
APPENDIX C. Matrix Operation Approach Program . . . 163
APPENDIX D. Fixed Parameters Approach Program . . . 165

LIST OF FIGURES

Figure		Page
1.	Two perpendicular waves with initial phase difference ϵ	18
2.	(a) Amplitude and (b) polarizing beam splitters	32
3.	Michelson interferometer	33
4.	Formation of a) objective speckle, b) subjective speckle	37
5.	Double illumination speckle interferometer for measuring in-plane displacement (after Leendertz)	40
6.	Thermocouple junctions a),b) J-type, c) T-type	55
7.	T type thermocouple reference curve (0°C)	58
8.	Decomposition of interference **E** field	61
9.	Simulation signal, voltage vs. phase angle ϕ	65
10.	Signal trajectory with h=0, k=0, a/b=1, δ=45°	66
11.	Flow chart of matrix operation approach	70
12.	Displacements of simulation signal	71
13.	Flow chart of fixed parameters approach	75
14.	Local error within one signal cycle	76
15.	PZT calibration setup	78
16.	CTE measurement apparatus	81
17.	Block diagram of CTE data collection system	83
18.	Automatic PZT On-Off control circuit	85
19.	CTE sample supports and heater/cooler unit	87
20.	Liquid nitrogen flow paths, (a) plate cooler (b) circular cooler	88
21.	Speckle interferometer for out-of-plane motion detection	93
22.	Speckle interferometer for in-plane motion detection	95
23.	PZT induced out-of-plane motion signal, mirror reflection	101
24.	Signals and their reference ellipse : h=0.75, k=0.67, a/b=0.68, δ=35°	102
25.	PZT displacement, input frequency=0.5 Hz	103
26.	PZT displacements with 2nd-order polynomial fitting, input frequency=50 Hz	104
27.	PZT displacement, input frequency=500 Hz	105
28.	PZT displacement, input frequency=1000 Hz	106
29.	Effect of incompletely cured adhesive to CTE	111

30. CTE of fused silica plate, heating/cooling rate=1.5°C/min., chart. 112
31. CTE of fused silica plate, heating/cooling rate=3°C/min., chart 113
32. Typical CTE data trajectory, ellipse parameters : h=-0.19, k=-1.20, a/b=0.61, δ=32° 114
33. Reference ellipses with h=-0.19, k=-1.20, a/b=0.61, δ=32° 115
34. CTE of fused silica plate, heating/cooling rate=3°C/min., fixed parameters 116
35. CTE of fused silica tube, chart 117
36. CTE, composite plate, chart 118
37. CTE, composite tube, fixed parameters. . 119
38. CTE, composite tube, matrix operation. . 120
39. PZT induced out-of-plane motion signal, diffuse tape reflection 124
40. PZT induced in-plane motion signal, diffuse tape reflection 125
41. PZT induced in-plane motion signal cycles against input voltage 126
42. System noise frequency at 120 Hz 132
43. System noise frequencies at 120 Hz, 50 KHz and 100 KHz 133
44. FFT of the out-of-plane speckle interferometry, input signal : A=0.13 μm (λ/5), f=1 KHz 134
45. Doubled FFT output with the same input signal as in figure 44 135
46. Output frequency depends on the input signal position 136
47. Higher orders of FFT output as amplitude greater than half wavelength, input signal : A=0.78 μm (1.2λ), f=1 KHz 137
48. FFT of out-of-plane speckle, input signal : A=0.026 μm, f=5.2 KHz 138
49. FFT of out-of-plane speckle, input signal : A=0.0065 μm, f=5.2 KHz 139
50. FFT of in-plane speckle, input signal : A=0.013 μm, f=5 KHz 140
51. FFT of in-plane speckle, input signal : A=0.0038 μm, f=5 KHz 141
52. Resonance frequency of a steel rod, steel ball excitation, mirror reflection . . . 142
53. Resonance frequency of a steel rod, steel ball excitation, diffuse tape reflection 143

Figure Page

54. CTE of reference material SRM 739 155
55. Instantaneous CTE of reference material SRM 739 156

LIST OF TABLES

Table		Page
1.	Summary of Length Measurement Techniques .	7
2.	Maximum error caused by $\Delta\delta=\pm5°$	74
3.	Maximum error caused by combined effect . .	74
4.	Root Mean Square Errors	100
5.	PZT Characteristic Displacements	100
6.	Properties of Composite Materials	110
7.	In-Plane Speckle system resolutions . . .	123
8.	Vibration amplitudes vs. FFT peak heights	131
9.	Minimum detectable vibration amplitudes .	131

PROCESSING OF LASER INTERFEROMETRIC SIGNALS FOR SMALL DISPLACEMENT MEASUREMENTS

CHAPTER 1. INTRODUCTION

1.1. Thesis Objectives

Dimensional stability is a common requirement for advanced materials and components used in aerospace applications [Blair 1990; Shaffer 1984] or in precision instruments [Haug 1989]. Thermal expansion of materials such as Zerodur, Invar, ULE glass, graphite fiber composites, fused silica, etc., were investigated in this sense. Their coefficients of thermal expansion (CTE) are usually low, thus small displacement measurement techniques are required. Michelson interferometry is one of the contactless interferometry techniques and has been widely and successfully used in measuring coefficients of thermal expansion. Changes of the physical quantities such as sample length or index of refraction "n" are normally related to the change of interference fringes in the interferometry. Fringe counting and signal modulation are common approaches to analyze the interference signals. Digital counter circuits have been developed [Aghdaie 1988; Wolff 1985]. Complex electronic circuits were used in

those systems. This thesis will describe another approach based on signal phase differences calculated by software to simplify the hardware system and increase the resolution. Development of the CTE measurement system for thin plates and thin walled tubes will also be discussed.

Speckle interferometry is another contactless interferometric displacement detection technique. This does not require specular reflecting surfaces. Problems of low signal intensity are commonly encountered. An expensive speckle interferometric camera and image processing system in electronic speckle pattern interferometry is commonly required [Klumpp 1990]. Simple speckle interferometry systems using silicon photodetectors as signal detectors were developed in this work for detecting vibration amplitudes and frequency in both out-of-plane and in-plane direction. Resonance frequencies of a steel rod excited by a steel ball were detected.

The objectives of the study are summarized as follows.

1). To derive a method of analyzing interferometry signals for small displacement measurements. This method should be able to replace the electronic circuit and simplify the apparatus in earlier developed system [Wolff 1985].

2). To demonstrate this method in measuring small displacements caused by a piezoelectric crystal.

3). To develop an interferometric apparatus for measuring inplane CTE of thin composite plates and thin walled tubes.

4). To investigate speckle interferometry for both out-of-plane and in-plane displacement detection.

5). To demonstrate the laser interferometry with FFT data analysis in detection and application of the resonance frequency of a steel rod.

1.2. Thesis Scope

In this work, an approach to analysis of interferometry signals based on the signal phase change is derived. Computer programs were written to calculate the corresponding displacements. Small displacements induced by PZT were obtained with this method. The CTE measurement system requires both displacement and temperature data. Displacement data were provided by the optical system and analyzed by fringe counting methods and/or phase calculation methods. The temperature data were obtained from thermocouple outputs. In speckle interferometry, the signal intensity level was usually lower than that in Michelson interferometry. Factors which can increase the signal to noise ratio were investigated. Both out-of-plane and in-plane motion detection systems were configured. The applications of speckle interferometry to small vibration

and resonance frequency detection with diffuse surfaces were also described. The rest of this chapter reviews the previous studies on the techniques of measuring low CTE materials, reference materials, applications and signal processing approaches of Michelson and speckle interferometry.

In chapter 2, related principles such as interference and coherence of lightwaves, beamsplitters, Michelson interferometry, speckle interferometry, composite materials, temperature conversion of thermocouples were reviewed as a background materials of this thesis. In chapter 3, the signal phase of the Michelson interferometry output was derived. Methods of calculating the phase change and then CTE were presented. Application of signal phase calculation methods to PZT displacement calibration and CTE measurements were given in chapter 4. Developed measurement systems and their experimental procedures were explored in this section. Configurations of speckle interferometry for out-of-plane and in-plane displacements measurement were also included in this chapter. Chapter 5 contained the results and discussions. Chapter 6 gave conclusions and recommendations of the present study.

The CTE measurement system and signal phase calculation approach was presented at the 11th International Thermophysics Symposium at Boulder, Colorado, USA, in June 1991 and submitted to Thermochemical Acta to

publish under the title "Inplane CTE Measurement of Thin Composite Plates". Results of speckle interferometry have been summarized and sent to OMI who sponsored this portion of the research.

1.3. Literature Review

1.3.1. Low CTE materials

Invar type alloys (nominally Fe-36Ni) have the lowest CTE values of metallic systems. Invar sheet decarburized to ≈0.01 wt% C, and treated to 845°C, water quenched, heated to 95°C, and air cooled, showed a CTE of $< 0.05 \times 10^{-6}$/°C (5-30°C) [Marshall 1977]. Super Invar (nominally Fe-30Ni-6Co) has been identified (along with Zerodur) as the material with the best temporal stability at room temperature. It exhibits both low positive and negative CTE values.

Zerodur (manufactured by Schott Glass Works, Mainz, Germany) is a glass ceramic composed of vitreous and crystalline phases of high quartz based solid solutions with Li_2O, Al_2O_3, etc.. The crystallites, ~70-75% of the ceramic by weight, have a negative expansion coefficient. The vitreous phase has a positive expansion, so that by adjusting the relative amounts of the crystalline and amorphous phases it is possible to drive the expansion

coefficient to zero. This ceramic was initially developed as a mirror substrate material. The low CTE ($\pm 5 \times 10^{-8}$/°C or less) near room temperature as compared with 5×10^{-7}/°C for fused silica and its high homogeneity has made Zerodur become one of the most important materials for use when dimensional stability is of prime importance. ULE (manufactured by Corning Glass Works, Corning, N.Y.) is an isotropic single-phase titania-silica glass. Its ultra-low expansion coefficient near room temperature is achieved by precise control of constituent composition, e.g., (SiO_2 + 7%TiO_2).

In composite materials, unidirectional zero CTE is achievable by varying the layup angle θ. Microcracking may start in the fiber reinforced plastic system due to the large thermal stresses between the matrix and the fibers. In metal matrix composite systems, plastic flow of matrix may occur during temperature change. When a negative CTE ceramic, such as β-spodumene (Li_2O-Al_2O_3-$4SiO_2$) [Hawkins 1979], is embedded in a continuous metal matrix, the prospect for isotropic zero CTE with high thermal conductivity is most promising.

1.3.2. Techniques for measuring CTE

Techniques for the measurement of small displacements were reviewed [Wolff 1977; Steel 1983; Jones 1989].

Table 1. Summary of Length Measurement Techniques [Wolff 1977].

Technique	Resolution (m)	Range (m) or $\Delta\epsilon$%	Accuracy m or %Range	Contacting*
A. Metrology				
Air gage	10^{-7}	10^{-3}	1%	SG
Micrometer	$3x10^{-5}$	10^{-1}	10^{-4}	C
Vernier	$3x10^{-5}$	1	$2x10^{-5}$	C
Dial Gage	10^{-5}	10^{-2}	10^{-5}	C
Profile Projector	$8x10^{-6}$	1	10^{-5}	L
Telemicroscopes	10^{-6}	1	10^{-6}	L
Micrometer slides	10^{-6}	10^{-1}	10^{-6}	SG
B. Electrical Transducers				
Resistance Strain Gages	$10^{-7}(\epsilon)$	20%	$5x10^{-7}(\epsilon)$	C
Semiconductor Strain Gages	$10^{-9}(\epsilon)$	1%	$10^{-8}(\epsilon)$	C
Capacitance	10^{-11}	10^{-4}	10^{-10}	SG
LVDT's (dilatometers)	$<10^{-8}$	10^{-2}	10^{-8}	SG
Electronic Gages	10^{-9}	10^{-5}	10^{-9}	C
Resistance Transducers	10^{-5}	3	1%	C
Variable Impedance	10^{-8}	10^{-2}	0.01%	SG
Variable Reluctance	10^{-6}	10^{-3}	3%	C

(continued)

Table 1. (continued) Summary of Length Measurement Techniques

Technique	Resolution (m)	Range (m) or $\Delta\epsilon$%	Accuracy m or %Range	Contacting*
C. Electro-Optical Techniques				
1. Non-Interferometric				
Autocollimators	$3x10^{-6}$ °	3 °	10^{-5} °	L
Optical Levers	10^{-6}	10^{-1}	0.5%	L
Single beam shadowing	$2x10^{-6}$	10^{-2}	0.1%	L
Fiber Optics	10^{-8}	10^{-2}	10^{-7}	SG
Scanning Beams	10^{-6}	10^{-2}	$5x10^{-6}$	L
Detector arrays	10^{-6}	$>10^{-1}$	10^{-5}	L
Photoelectric Microscopes	10^{-9}	10^{-4}	10^{-8}	SG
2. Interferometers				
Michelson	$<10^{-9}$	10^{-3}	10^{-8}	L
Fabry-Perot	$<10^{-9}$	10^{-3}	10^{-8}	C
Fizeau	10^{-8}	10^{-3}	10^{-8}	C
Holographic	10^{-7}	~10%	10^{-7}	L
Speckle	10^{-7}	~1%	10^{-7}	L
Moiré	10^{-7}	~1%	10^{-7}	L

(continued)

Table 1. (continued) Summary of Length Measurement Techniques

Technique	Resolution (m)	Range (m) or $\Delta\epsilon$%	Accuracy m or %Range	Contacting*
D. Miscellaneous Optical				
Ellipsometry	10^{-10}	10^{-5}	10^{-10}	L
Diffraction Pattern Analysis	$<10^{-6}$	$>10^{-5}$	$<10^{-7}$	L
Spatial Filtering	$\sim 10^{-7}$	$>10^{-5}$	10^{-7}	L
E. Subsurface Effects				
X-ray Diffraction	10^{-14}	$<10^{-10}$	10^{-13}	L
Electron Diffraction	10^{-14}	$<10^{-9}$	10^{-13}	L
Neutron Diffraction	10^{-14}	$<10^{-9}$	10^{-13}	L
Ultrasonics	10^{-5}	$5x10^{-1}$	10^{-4}	C
Acoustic Emission	10^{-3}	>1	10^{-3}	C
Beta Radiation Backscatter	10^{-8}	10^{-4}	10^{-7}	SG
Radiance Changes	10^{-5}	$>10^{-3}$	10^{-4}	SG

* C-Contacting, L-Contactless, SG-Small Gap ($<10^{-1}$m).

Table 1 summarizes the linear displacement measurement techniques according to the principle of operation. The accuracy of each method covers wide limits depending on modifications, accessories and/or the ingenuity of the designer of the apparatus. Among these techniques, the Michelson interferometer (two beams), Fabry-Perot and Fizeau interferometers (multiple reflection) are those mainly used for the measurements of low thermal expansion materials with mirror reflections. A speckle interferometry system was designed to measure the thermal expansion of a large class of intermetallic compounds for which surface optical treatments are difficult or even impossible [Costa 1987]. An optical heterodyne interferometric system was used to measure the thermal expansivity and thermoelasticity of high strength organic fibers [Yamaguchi 1989]. CTE of Zerodur has been measured [Bennett 1984]. Here, a computer-aided fringe analysis system (Zygo model GH interferometer) was used to detect the slight movement of fringes (as a change in power) caused by sample bowing. The amount of bowing is directly proportional to the thermal expansion coefficient. An automatic absolute interferometric dilatometer was developed in the National Physical Laboratory in UK [Birch 1988]. The sample length changes were determined by comparing the phase of the heterodyne signal from the interferometer with that from a reference signal. A

bending-beam method (one end free and one end fixed) was used to determine the CTE of printed wiring board [Lamoureux 1987] to avoid the effect of edge damage on length of the sample. CTE was calculated from the deflection measured with a cathetometer (0.05 mm estimable). The CTEs of thin films deposited on a substrate were measured [Iwasaki 1989]. Sample warp measured by an optical lever method was related to the thin film CTE.

1.3.3. Reference materials

Many dilatometers in common use can have significant systematic errors in determining linear thermal expansion. The need for reference materials to check these dilatometers can usually be met by rods of OFHC Cu, semi-conductor grade Si, W, Pt, sapphire etc. which are readily available and for which there are now reliable data. Reference CTE values of Alumina (Al_2O_3), Borosilicate Glass, Copper, vitreous Silica, Silicon, stainless steel (AISI 446) and Tungsten over wide range of temperatures were reviewed by White [White 1991]. Fused silica CTE data and graphs were given in appendix A.

1.3.4. Applications and signal processing of Michelson interferometer

Michelson interferometers have been used in many areas since its invention in the 1880's. Optical configurations and signal processing approaches varies in each case to meet its own requirements. A double Michelson interferometer dilatometer for the study of materials of arbitrary size or shape with time-dependent and near zero coefficients of thermal expansion over the range of 100 to > 450°K was developed [Wolff 1985]. Signal modulation and automatic digital counter-microprocessor combination were employed to analyze the data.

Double Michelson interferometry is also used to measure electrostrictive strain [Sterkenburg 1990]. A lock-in amplifier was used to detect the output signal. Output voltage is linearly proportional to the electrostrictive expansion.

A thin wedge can be combined with two Michelson interferometers to determine the index of refraction "n" of liquids [St-Arnaud 1991]. The system is based on the heterodyne principle and has the advantages of fringe count in both directions.

A Michelson twin interferometer was used for the measurements of the index of refraction n of gases in the visible wavelength range at temperatures between 100 K and

1300 K (Hohm 1990). The evacuated twin interferometer consists of two adjacent identical Michelson interferometers using the same beam splitter and mirrors. Interference fringe counting approach is used to analyze the photodiode signal recorded by a data acquisition system.

Modulation of the spectrum of white light in a Michelson interferometer was derived [Smith 1989]. Displacements were measured by observing the frequency of spectrum of light output from an interferometer and performing a cross-correlation calculation with theoretical spectra.

Michelson interferometry is now becoming a standard device in an advanced undergraduate laboratory [Aghdaie 1988] for a variety of interesting experiments including wavelength, index of refraction, thickness and small vibration measurements [Diamond 1990].

1.3.5. Applications and signal processing of speckle interferometer

The speckle interferometer used for thermal expansion measurements [Costa 1987] is basically a modification of a Michelson interferometer with both mirrors replaced by scattering surfaces. Each speckle grain behaves like an interferometer, its intensity varies cyclically from light

to dark every half-wavelength displacement. The number of cycles is counted over a temperature change ΔT to give the displacements and then the CTE.

A speckle interferometer was used as an optical displacement sensor [Sarrafzadeh-Khoee 1986]. This interferometer can detect both out-of-plane and in-plane disturbances of the object surface, having twice the sensitivity (to in-plane disturbance) of conventional speckle interferometers based on Leendertz's arrangement [Leendertz 1970]. Signal intensity is a function of the optical path length difference introduced by the motion of the diffusive surface.

The grating speckle method was used for in-plane displacement measurement [Tu 1989]. This method combines lensless speckle photography and a high frequency grid applied to the specimen surface. Contact specklegrams were made in white light before and after loading in the double exposure mode. The subsequent specklegram reconstruction yields the various components of in-plane displacement.

In computer speckle interferometry [Chen 1990], two speckle patterns, one before and one after deformation, were captured by a video camera. A resultant "double exposure" speckle pattern was obtained by superposing the two digital images. Fast Fourier transform was performed to analyze the fringe pattern in its spectral domain.

An "Electronic Speckle Pattern Interferometry" (ESPI) system was used to investigate fracture mechanics parameters [Maji 1991]. This technique combines laser interferometry with image processing to create a more versatile method of nondestructive testing. A CCD video camera digitizes and transfers the data corresponding to the speckle image to a computer. The images were acquired and stored by an Image Analysis System. More applications of speckle interferometry techniques were found in various areas [Moore 1990; Ansari 1989].

CHAPTER 2. REVIEW OF FUNDAMENTAL PRINCIPLES

2.1. General Descriptions of Lightwaves

2.1.1. Wave equations

A one-dimensional wave equation can be expressed as

$$\frac{\partial^2 \Psi}{\partial x^2} = \frac{1}{v^2} \frac{\partial^2 \Psi}{\partial t^2} \tag{2.1}$$

where Ψ = wave function

v = wave velocity

A harmonic wave function such as

$$\Psi(x,t) = A \cos(kx-\omega t) \tag{2.2}$$

is one of the solutions of this one-dimensional differential wave equation. This progressive wave travels at a speed $v=\omega/k$ in the positive x direction. Where $k=2\pi/\lambda$ is known as propagation number. The entire argument of this cosine function is known as the phase ϕ of the wave, so that

$$\phi=(kx-\omega t) \tag{2.3}$$

At t=x=0, $\Psi(0,0)=0$, which is certainly a special case. More generally, we can write

$$\Psi(x,t)=A\cos(kx-\omega t+\epsilon) \tag{2.4}$$

where ϵ is the initial phase which is just the constant contribution to the phase arising at the generator and is independent of how far in space, or how long in time, the wave has traveled. The wave function for the three-dimensional case can simply be extended as

$$\Psi(r,t)=A\cos(k.r-\omega t+\epsilon) \tag{2.5}$$

where k is the propagation vector, r is the position vector. Light is an electromagnetic wave. Its electric field, similar to the wave function, thus can be expressed as

$$\mathbf{E}(\mathbf{r},t) = E\cos(\mathbf{k}\cdot\mathbf{r}-\omega t+\epsilon) \tag{2.6}$$

2.1.2. Polarization

We can choose two orthogonal optical disturbances in the form

$$\mathbf{E}_x(z,t) = \vec{i}\, E_{0x}\cos(kz-\omega t) \tag{2.7}$$

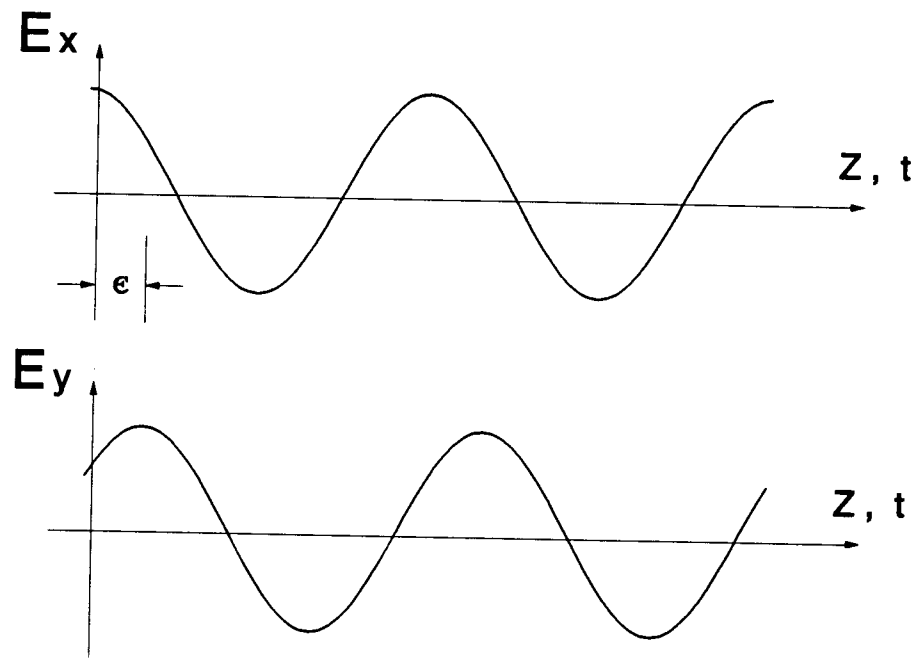

Fig. 1. Two perpendicular waves with initial phase difference ϵ

$$\mathbf{E}_y(z,t) = \vec{j}\, E_{0y} \cos(kz-\omega t+\epsilon) \tag{2.8}$$

both of which are traveling in the z-direction (Figure 1). The resultant optical disturbance is the vector sum of the two perpendicular waves

$$\mathbf{E}(z,t) = \mathbf{E}_x(z,t) + \mathbf{E}_y(z,t) \tag{2.9}$$

If ϵ is 0 or an integral multiple of $\pm\pi$. Then the resultant **E** field becomes

$$\mathbf{E} = (\vec{i}\, E_{0x} \pm \vec{j}\, E_{0y}) \cos(kz-\omega t) \tag{2.10}$$

It has a fixed amplitude equal to $(\vec{i}\, E_{0x} \pm \vec{j}\, E_{0y})$ and is said to be linearly or plane polarized. When both constituent waves have equal amplitudes and their relative phase difference $\epsilon = \mp\pi/2 + 2m\pi$, where m=0, ±1, ±2, ... The consequent wave is given by

$$\mathbf{E} = E_0 \, [\vec{i} \cos(kz-\omega t) \pm \vec{j} \sin(kz-\omega t)] \tag{2.11}$$

Note that the scalar amplitude of **E**, that is E_0, is a constant. But the direction is time-varying, and it is not restricted to a single plane. The tail of this vector moves along a circle. This light is called circularly

polarized. The waves will be called elliptically polarized if ϵ is not those values mentioned above in this section.

2.1.3. Optical Phase Retardation

One of the two constituents of plane polarized waves may somehow be caused to lag in phase behind the other by a certain amount. Upon emerging from the retarder, the relative phase of the two components is different than it was initially, and thus the polarization state is different as well (e.g. polarization changed from linear to elliptical). Indeed, once we have developed the concept of the retarder, we will be able to convert any given polarization state into any other and in so doing create circular and elliptic polarizers as well. Since the optical path length is equal to nL, where n is the index of refraction of the medium and L is the geometric path length. Any change in n or L will cause a change of optical path length difference (OPLD). When light traveling in a direction other than the optical axis of optically anisotropic materials, such as calcite, quartz, mica, etc., the traveling speeds of the two orthogonal components are different because of the difference of index of refractions, n_o and n_e. The relative optical phase difference caused by the material is given by

$$\Delta\phi = k_0 \, |\Delta n| \, L = (2\pi L/\lambda_0) \, |n_o - n_e| \qquad (2.12)$$

The state of polarization of the emergent light evidently depends on the amplitudes of the incoming orthogonal field components and of course on $\Delta\phi$. If $\Delta\phi$ equals to 2π, the relative retardation is one wavelength. This retarder is called a full-wave plate. A retardation plate that introduces a relative phase difference of π radians is known as a half-wave plate. The quarter-wave plate is an optical element that introduces a relative phase shift of $\Delta\phi = \pi/2$ between the constituent orthogonal components of a wave.

2.1.4. Coherence

Suppose that we examine the light emitted by a monochromatic source. The electron transitions responsible for the generation of light have a duration on the order of 10^{-8}s to 10^{-9}s. Because the emitted wavetrains are finite, there will be a spread in the frequencies present. Moreover, since the atoms are in random thermal motion, the frequency spectrum will be altered by the Doppler effect. In addition, the atoms suffer collisions that interrupt the wavetrains and again tend to broaden the frequency distribution. The total effect of all these mechanisms is that each spectral line has a bandwidth $\Delta\nu$ rather than one

single frequency. The time that satisfies the relation of $\Delta\nu \sim 1/\Delta t$ is referred to as the coherence time (Δt_c), and the length given by $\Delta x_c = c\Delta t_c$ is the coherence length. The coherence length is the extent in space over which the wave is nicely sinusoidal so that its phase can be predicted reliably.

2.1.5. Interference

The expression describing the optical disturbance is a second-order, homogeneous, linear partial differential equation (equation 2.1). It therefore obeys the principle of superposition. The resultant electric field intensity **E**, at a point in space where two or more lightwaves overlap, is equal to the vector sum of the individual constituent disturbances. Briefly speaking, optical interference may be termed an interaction of two or more lightwaves yielding a resultant irradiance that deviates from the sum of the component irradiances. Interferometric devices are optical systems which produce interference to be used in detecting optical path length difference that relates to certain physical phenomenon. They are divided into two groups: wavefront splitting and amplitude splitting. In the first instance, portions of the primary wavefront are used either directly as sources to emit secondary waves or in conjunction with optical devices to

produce virtual sources of secondary waves. These secondary waves are then brought together to interfere. In the case of amplitude splitting, the primary wave itself is divided into two segments, which travel different paths before recombining and interfering.

In accordance with the principle of superposition, the electric field intensity $\mathbf{E}$, at a point in space, arising from the separate fields $\mathbf{E}_1$, $\mathbf{E}_2$, ... of various contributing sources is given by

$$\mathbf{E} = \mathbf{E}_1 + \mathbf{E}_2 + \cdots \tag{2.13}$$

Note that the optical disturbance, or light field $\mathbf{E}$, varies in time at an exceedingly rapid rate, roughly in the order of 10^{14}Hz, making the actual field an impractical quantity to detect. On the other hand, the irradiance I can be measured directly with a wide variety of sensors. Consider two point sources, S_1 and S_2, emitting monochromatic waves of the same frequency in a homogeneous medium. Furthermore, let their separation, a, be much greater than λ. Locate the point of observation P far enough away from the sources so that at P the wavefronts will be planes. We will consider, for simplicity, only linearly polarized waves of the form

$$\mathbf{E}_1(\mathbf{r},t) = \mathbf{E}_{01}\cos(\mathbf{k}_1.\mathbf{r}-\omega t+\epsilon_1) \tag{2.14}$$

and

$$\mathbf{E}_2(\mathbf{r},t) = \mathbf{E}_{02}\cos(\mathbf{k}_2.\mathbf{r}-\omega t+\epsilon_2) \tag{2.15}$$

The irradiance at point P is given by

$$I = \epsilon_0 \, C \, \langle \mathbf{E}^2 \rangle \tag{2.16}$$

Inasmuch as we will be concerned only with relative irradiances within the same medium. We will simply neglect the constant and set

$$I = \langle \mathbf{E}^2 \rangle \tag{2.17}$$

What is meant by $\langle \mathbf{E}^2 \rangle$ is the time average of the magnitude of electric field intensity squared, or $\langle \mathbf{E}\cdot\mathbf{E} \rangle$. Accordingly

$$\mathbf{E}^2 = \mathbf{E}\cdot\mathbf{E} \tag{2.18}$$

where now

$$\mathbf{E}^2 = (\mathbf{E}_1+\mathbf{E}_2)\cdot(\mathbf{E}_1+\mathbf{E}_2) \tag{2.19}$$

and thus

$$\mathbf{E}^2 = \mathbf{E}_1^2 + \mathbf{E}_2^2 + 2\mathbf{E}_1\cdot\mathbf{E}_2 \tag{2.20}$$

Taking the time average of both sides, we find that the irradiance becomes

$$I = I_1 + I_2 + I_{12} \tag{2.21}$$

provided that

$$I_1 = \langle \mathbf{E}_1^2 \rangle \ , \quad I_2 = \langle \mathbf{E}_2^2 \rangle \ , \quad \text{and} \quad I_{12} = 2\langle \mathbf{E}_1 \cdot \mathbf{E}_2 \rangle \tag{2.22}$$

The latter expression is known as the interference term. To evaluate it, we form

$$\begin{aligned} \mathbf{E}_1 \cdot \mathbf{E}_2 &= \mathbf{E}_{01} \cdot \mathbf{E}_{02} \cos(\mathbf{k}_1 \cdot \mathbf{r} - \omega t + \epsilon_1) \cos(\mathbf{k}_2 \cdot \mathbf{r} - \omega t + \epsilon_2) \\ &= \mathbf{E}_{01} \cdot \mathbf{E}_{02} \left[\cos(\mathbf{k}_1 \cdot \mathbf{r} + \epsilon_1) \cos(\omega t) + \sin(\mathbf{k}_1 \cdot \mathbf{r} + \epsilon_1) \sin(\omega t)\right] \times \\ &\quad \left[\cos(\mathbf{k}_2 \cdot \mathbf{r} + \epsilon_2) \cos(\omega t) + \sin(\mathbf{k}_2 \cdot \mathbf{r} + \epsilon_2) \sin(\omega t)\right] \end{aligned} \tag{2.23}$$

Recall that the time average of some function f(t), taken over an interval T, is

$$\langle f(t) \rangle = \frac{1}{T} \int_t^{t+T} f(t') \, dt' \tag{2.24}$$

The period τ of the harmonic functions is $2\pi/\omega$, and for our present concern $T >> \tau$. In that case the $1/T$ coefficient in front of the integral has a dominant effect.

After multiplying out and averaging equation (2.23) we have

$$\langle \mathbf{E}_1 \cdot \mathbf{E}_2 \rangle = \tfrac{1}{2}\, \mathbf{E}_{01} \cdot \mathbf{E}_{02} \cos(\mathbf{k}_1 \cdot \mathbf{r} + \epsilon_1 - \mathbf{k}_2 \cdot \mathbf{r} - \epsilon_2) \qquad (2.25)$$

where use was made of the fact that $\langle \cos^2\omega t \rangle = \tfrac{1}{2}$, $\langle \sin^2\omega t \rangle = \tfrac{1}{2}$, and $\langle \cos\omega t \sin\omega t \rangle = 0$. The interference term is then

$$I_{12} = \mathbf{E}_{01} \cdot \mathbf{E}_{02} \cos\delta \qquad (2.26)$$

and δ, equal to $(\mathbf{k}_1 \cdot \mathbf{r} + \epsilon_1 - \mathbf{k}_2 \cdot \mathbf{r} - \epsilon_2)$, is the phase difference arising from a combined path-length and initial phase-angle difference. Notice that if $\mathbf{E}_{01}$ and $\mathbf{E}_{02}$ (and therefore $\mathbf{E}_1$ and $\mathbf{E}_2$) are perpendicular, $I_{12}=0$ and $I=I_1+I_2$, no interference occurred. The most common situation in the work to follow corresponds to $\mathbf{E}_{01}$ parallel to $\mathbf{E}_{02}$. In that case, the irradiance reduces to the scalar quantity.

$$I_{12} = E_{01} \cdot E_{02} \cos\delta \qquad (2.27)$$

Notice that [Verdeyen 1989]

$$I_1 = \langle \mathbf{E}_1^2 \rangle = E_{01}^2/2 \ , \qquad I_2 = \langle \mathbf{E}_2^2 \rangle = E_{02}^2/2 \qquad (2.28)$$

The interference term becomes

$$I_{12}=2\sqrt{I_1 I_2}\cos\delta \qquad (2.29)$$

whereupon the total irradiance is

$$I=I_1+I_2+2\sqrt{I_1 I_2}\cos\delta \qquad (2.30)$$

At various points in space, the resultant irradiance can be greater, less than, or equal to I_1+I_2, depending on the value of I_{12}, that is, depending on δ.

Fresnel and Arago made an extensive study of the conditions under which the interference of polarized light occurs, the so called Fresnel-Arago laws are as follows [Hecht 1987]:

1. Two orthogonal, coherent p-states (plane polarized waves) cannot interfere in the sense that $I_{12}=0$ and no fringes result.
2. Two parallel, coherent p-states will interfere in the same way as will nature light.
3. The two constituent orthogonal p-states of nature light cannot interfere to form a readily observable fringe pattern even if rotated into alignment. This last point is understandable, since these p-states are incoherent.

2.1.6. Lasers

"Laser" is an acronym for Light Amplification by Stimulated Emission of Radiation. These processes involve energy transformations between different states of electrons in an atom. Each atom possesses a certain amount of internal energy, and each tends to maintain its lowest energy configuration - ground state. Atoms can exist in specific, well-defined configurations corresponding to higher energies than the ground state. Any of these are termed excited states. Energy is pumped into the excited atoms. Each atom can then drop back to a lower state either by spontaneous emission or stimulated emission. The latter process is a key to the operation of the laser. In either situation the emerging photon will carry off the energy difference ($h\nu$) between the initial higher state and the final lower state. If an incident electromagnetic wave is to trigger an excited atom into stimulated emission, it must have the frequency ν. A remarkable feature of this process is that the emitted photon is in phase with, has the polarization of, propagates in the same direction as, and has the same frequency, as the stimulating radiation. Thus the photon is said to be in the same radiation mode as the incident wave and tends to add to it, increasing its flux density. Energy would be pumped in to maintain the population inversion, and a beam of light would be

extracted after sweeping across the active medium. The active medium may be solid, liquid, gas or a semiconductor. The He-Ne laser is currently the most popular visible laser, most often providing a few milliwatts of continuous power at 632.8 nm. Its appeal arises primarily because it is easy to construct, relatively inexpensive, and fairly reliable and in most cases can be operated by a flick of a single switch to a high voltage power supply. The appearance on the scientific scene of the laser in the nineteen-sixties set off many new lines of research in the field of physical optics, which it had previously been felt were unprofitable to explore further. Interferometry was an obvious choice, since the greatly enhanced brightness and coherence of laser sources makes the experimentation much easier than when conventional light has to be used. This has enabled length measurement by fringe counting.

2.1.7. Amplitude/Polarizing beam splitters

Amplitude beam splitters (e.g. Melles Griot 03 BTF 007 plate beam splitter) consist of a thin (1mm) plate of optical crown glass on each side of which is deposited a different type of coating. The first-surface is coated with an all-dielectric film having partial reflection properties over either the visible or the near infrared spectrum. The benefit of this type of coating is that it

has low absorption of light at 632.8 nm; 0.5% for a 50/50 splitter at 45°. The second-surface has a broad band antireflection coating optimized for 45°. Polarization states are not considered in total transmittance or reflectance for these splitters.

Unlike the amplitude beam splitters, The emerging irradiance of a polarizing beam splitters (e.g. Melles Griot 03 PBS 043) is strongly dependent on the polarization orientation of the incident beam. These splitters are made of pairs of right angle prisms cemented together with a special multilayer dielectric film in between. Monochromatic unpolarized light which is internally incident at 45° upon the multilayer film is separated into two polarized beams which emerge from the cube through adjacent faces. The beam which passes straight through the cube is the p-polarized component which emerges linearly polarized with the plane of electric field vector parallel to the plane of incidence defined for the multilayer film. On the other hand, the beam which emerges from the cube at right angle to the incident beam (having been reflected by the multilayer film) is the s-polarized component with the electric field vector orthogonal to the plane of incidence defined for the multilayer film. An incident beam of linearly polarized monochromatic light is similarly divided, with the ratio of the emergent beam irradiances

depending on the orientation of the electric field vector of the incident beam. Figure 2 shows these beam splitters.

2.1.8. Michelson interferometer

The Michelson interferometer is one of the best known amplitude-division interference devices. Its configuration is illustrated in figure 3. A light source (discharge lamp or laser) emits a wave, parts of which travels to the left. The beam splitter BS divides the wave into two, one segment travels to the left mirror M_2 and one up to the reference mirror M_1. The two waves are reflected by mirrors and return to the beam-splitter. Interference can be expected after the unification of these two waves. A compensator plate C, an exact duplicate of the beam splitter and parallel to it, is inserted in the arm BSM_2 so that both beams pass through equal thickness of glass. Any optical path difference will arise from the actual path difference. Since the waves travel twice between BS and mirrors, the change of optical path length difference (OPLD) will be $2n\Delta d$ if the movement of M_2 is Δd, where n is the index of refraction of the medium. This means that the phase change will be

$$\Delta\phi = k\cdot\Delta OPLD = (2\pi/\lambda)(2n\Delta d) = 4\pi n\Delta d/\lambda \qquad (2.31)$$

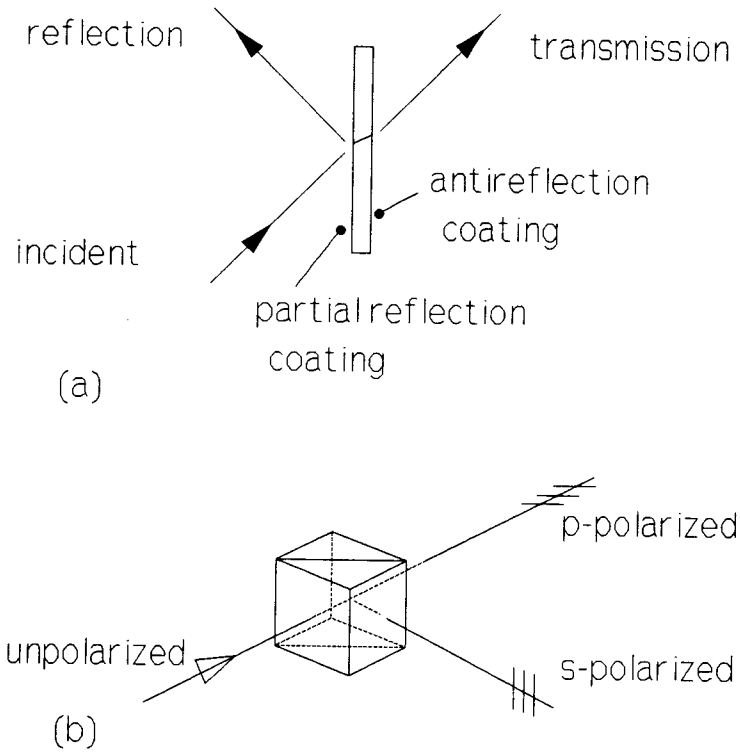

Fig. 2. **(a) Amplitude and (b) polarizing beam splitters**

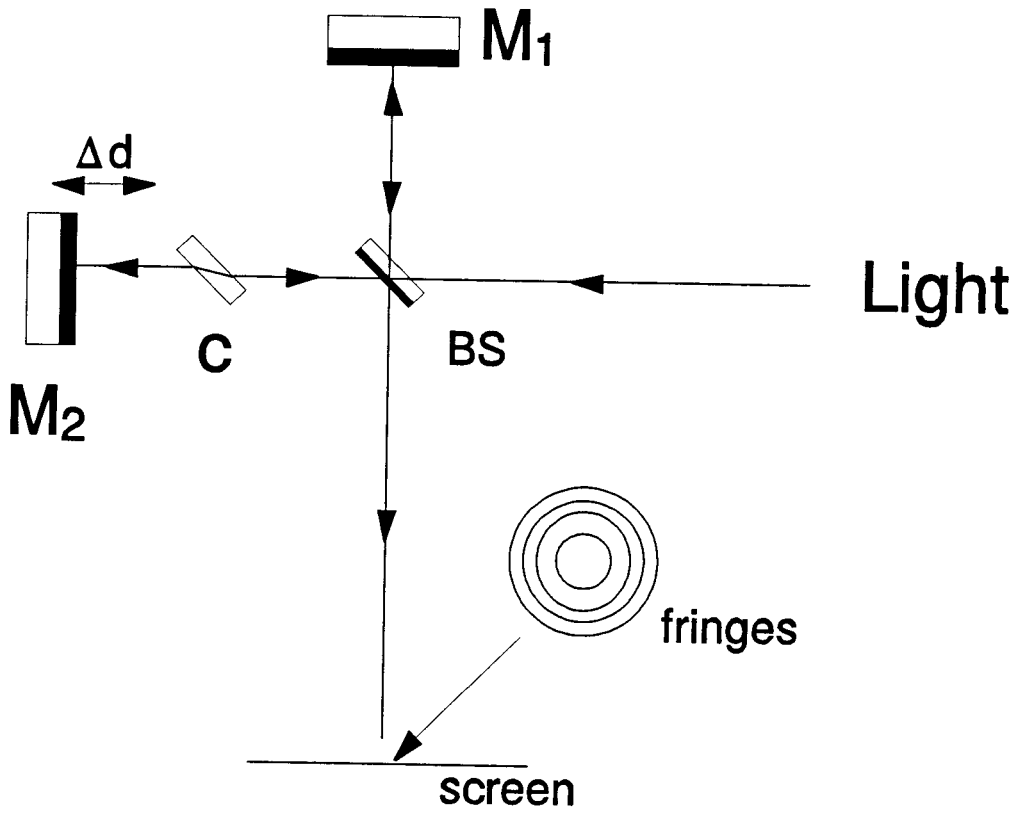

Fig. 3. Michelson interferometer

Recall from section 2.1.5 that the intensity of a two-beam interference, such as the Michelson interferometer output, is a function of ϕ

$$I=I_1+I_2+2\sqrt{I_1I_2}\cos\delta=I_1+I_2+2\sqrt{I_1I_2}\cos(\phi+\epsilon) \qquad (2.32)$$

In vacuum (n=1), when ϕ changes by 2π, the intensity will change by one cycle and Δd will be $\lambda/2$.

2.2. Speckle Interferometry

When coherent light is either reflected from a diffuse surface or propagates through a medium with random refractive index fluctuations, the optical wave at any moderately distant point above the surface consists of many coherent components or wavelets which have traveled a different number of wavelengths and are thus dephased. Their mutual interference results in the granular pattern called speckle.

The speckle effect was an interference phenomenon brought about by constructive and destructive interference between light waves scattered from a rough surface. Interest in speckle patterns lies in six main areas [Dainty 1984];

1. fundamental statistical properties, 2. reducing speckle in optical and holographic systems, 3. measurement of

surface roughness, 4. applications in image processing, 5. applications in metrology, and 6. stellar speckle interferometry.

Our attention will be focused on the applications in metrology of speckle interferometry for measuring out-of-plane and in-plane displacements. Speckle interferometry offers a new way of performing high sensitivity measurements on objects not having a specular reflecting surface. In this sense it strongly parallels hologram interferometry, but there are unique tasks that it can accomplish without the complication of the intermediate holographic process. The speckle effect was initially treated as an additional side effect in the field of holography. However it was quickly realized that light forming each individual speckle was fully coherent, and could take part in optical interference; in addition to the measurable intensity of a laser speckle, the light from it possesses a definite phase that differs from, and can be related to, the phase of neighboring speckles. Experiments thus can be conducted in a new form of interferometry, where the interference effects do not produce a regular pattern of dark and bright fringes, but rather a change in distribution of brightness among individual speckles.

2.2.1. Interference of laser speckle fields

The speckle phenomenon is a three-dimensional interference effect, filling the whole of space where scattered ray paths cross; for most purposes, we are concerned only with the size and brightness distribution of the pattern over a plane, usually that which is normal to the axis of the optical system generating the speckle.

Ennos stated that [Ennos 1984], for a single speckle field, the size of the objective speckles (figure 4a) formed on a screen AB at a distance L by scattering of coherent light from a circular region of diameter D is given approximately by

$$\sigma \approx 1.22\lambda L/D \qquad (2.33)$$

If the speckle field is formed by collecting the scattered radiation field with a lens and focusing it on to a screen, a subjective speckle pattern (figure 4b) is formed. The size of the individual speckles is then related to the effective numerical aperture N.A. of the lens by

$$\sigma \approx 0.6\lambda/N.A. \qquad (2.34)$$

If F is the aperture ratio of the lens and M is the magnification at which the lens is operating in an imaging

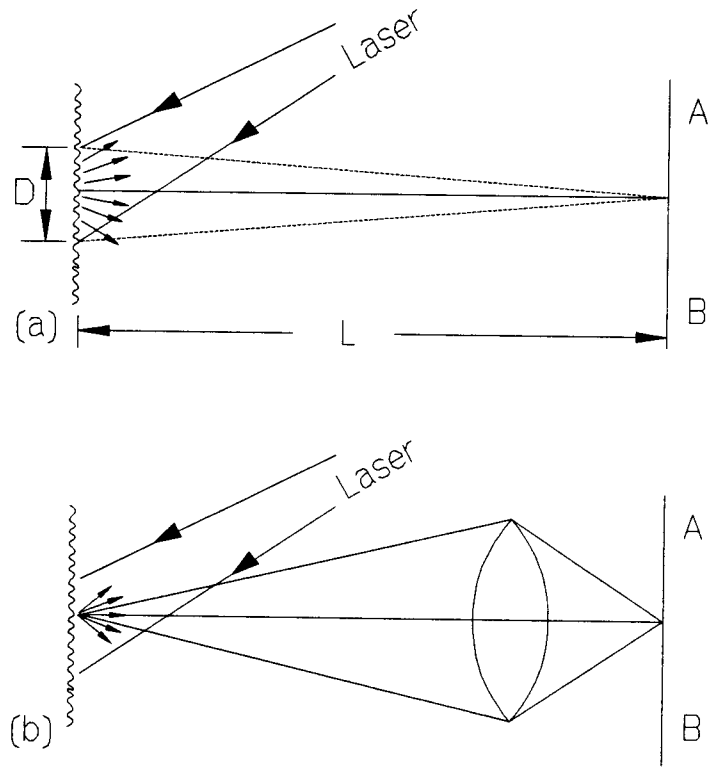

Fig. 4. Formation of a) objective speckle, b) subjective speckle

system, the speckle size is then;

$$\sigma \approx 1.2(1+M)\lambda F \tag{2.35}$$

The distribution of brightness among the speckles of a fully developed pattern is governed by the negative exponential relationship

$$p(I)=(1/I_0)\exp(-I/I_0) \tag{2.36}$$

where p(I) is the probability that a speckle has brightness between the values I and (I+dI), and I_0 is the average brightness.

2.2.2. Interferometers combining two speckle fields

If both mirrors in the Michelson interferometer are replaced by scatters, the coherent addition of the two speckle fields $F_1(x,y)$ and $F_2(x,y)$ derived from the two scatters will result in a third field $F_3(x,y)$, similar in brightness distribution statistics, but differing in detail. The mean intensity of $F_3(x,y)$ will be the sum of the mean intensities of $F_1(x,y)$ and $F_2(x,y)$. If surface 1 is moved in the direction of its normal such that the phase of the light scattered from it everywhere changes by an amount δ, then in general the resulting field $F_3(\delta)$ will

differ from $F_3(0)$ in a random fashion. This means that there will be reduced correlation between the two speckle patterns, before and after the movement has taken place. When $\delta=(2n+1)\pi$, the correlation between them will be zero, but when δ takes the values of $2n\pi$, n is an integer, the patterns will once again correlate, that is $F(0)=F(2n\pi)$. Conceptually, we can think of every individual speckle as having gone through a complete number of bright/dark cycles to end up with the same value as it started with. If it is possible to detect these positions of correlation, the interferometer can be used for measuring the change in phase, or the out-of-plane surface movement in this optical arrangement.

To measure the surface strain, a double illumination speckle interferometer was depicted as figure 5. Each illuminating beam generates its own speckle pattern which combines coherently with the speckle pattern generated by the complementary scattered beam. If the surface moves in the z-direction (normal to the plane), the two interfering beams will suffer equal path length changes, and the combined speckle pattern will remain unchanged. Similarly, there will be no effect due to a y motion in the plane of the surface. However, if an elementary part of the surface becomes displaced by a small distance d_x in the x-direction (defined by the intersection of the surface and the illumination beams), one path length will be increased by

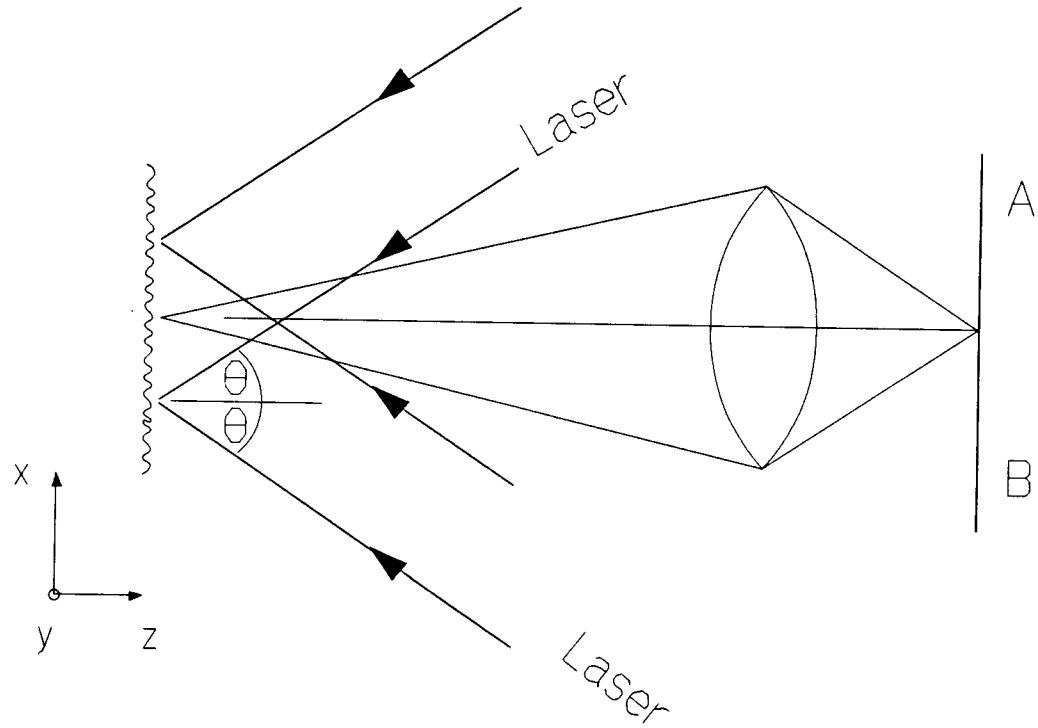

Fig. 5. Double illumination speckle interferometer for measuring in-plane displacement (after Leendertz)

$d_x \sin\theta$, while the other will be decreased by the same amount. Correlation of the combined speckle pattern with the original pattern before surface displacement will take place when

$$2\, d_x \sin\theta = m\, \lambda \qquad (2.34)$$

2.2.3. Methods of Correlating Two Speckle Fields

Since laser speckle interferometry is essentially concerned with differentiating between areas where speckles are correlated and where they are not correlated, it is important to devise means to do this as efficiently as possible. Photographic subtraction is a conventional approach of carrying out a speckle correlation. To do this the two patterns are recorded on separate plates (A and B) and a positive contact print of B is made on a third plate C. Plates A and C are then put together in register, and the fringe pattern is viewed by transmission through the pair. This technique is obviously best suited to cases where the speckles are large, since their registration is then much easier to carry out, and effects due to the non-flatness of the plates are minimized. However, this means using a low-aperture imaging system, which will be inefficient in light utilization.

Double exposure methods can be used to generate speckle correlation fringe patterns if deliberate use if made of the nonlinearity of the photographic processes. Consider an elementary area of the output image of the speckle interferometer corresponding in size to one speckle. The intensity variation is similar to that of the two-beam interference. If the amplitude moduli of the light waves reaching it from the two arms of the interferometer are I_1 and I_2 then the resultant intensity will be the same as equation (2.32). If we record a double exposure in which the phase difference remains the same, or changes by $2n\pi$, the resultant total intensity recorded will be doubled. that is

$$I' = 2(I_1 + I_2 + 2\sqrt{I_1 I_2}\cos\delta) \tag{2.35}$$

On the other hand, if the phase changes by $(2n+1)\pi$ between exposures, the resultant total intensity recorded will be

$$\begin{aligned} I'' &= I_1 + I_2 + 2\sqrt{I_1 I_2}\cos\delta + I_1 + I_2 + 2\sqrt{I_1 I_2}\cos[(2n+1)\pi + \delta] \\ &= 2(I_1 + I_2) \end{aligned} \tag{2.36}$$

In this case the effect is the same as if the light amplitude had been added incoherently. Consider the speckle pattern output from the interferometer as a whole, a double exposure will generate some regions where the

blackening of the plate is caused by two coherently added speckle patterns, and other regions where the patterns have been added incoherently. Speckle correlation fringe patterns are then formed.

Intensity distribution of the speckle patterns can also be recorded by the processes of electro-photography. The so-called Electronics Speckle Pattern Interferometry (ESPI) has an obvious advantage that it converts the visual information into electrical signals which can be manipulated by computers. Displacement, strain, etc., are measured instantaneously.

The intensity of a single grain in the speckle interferometry varies sinusoidally with the surface movement. The relative phase changes of the two constituent components from each arm of the interferometer contain the displacement information similar to that in Michelson interferometer. Such signals can be related to displacements if phase changes were recorded continuously through the entire movement. Multiple speckle grains can be added together of each single grain to increase the total signal intensity;

$$I = \sum_{i=1}^{N} I_i \cos(\phi+\delta_i) = I_0 \cos(\phi+\delta) \qquad (2.37)$$

The resultant intensity still retains its sinusoidal form with respect to its phase but with a different intensity level.

2.3. Composite Materials

A material is called a composite material if it composed of two or more materials, whose properties are superior to either material acting alone. Although man-made composites have existed for thousand of years, the high technology of composites has evolved in the aerospace industry only in the last thirty years. Stephen Tsai summarized the development history of composites in his "Composites Design" [Tsai 1988]. Filament-wound pressure vessels using glass fibers were the first strength critical application for modern composites. Boron filaments came in the 1960's. Graphite and aramid fibers became commercially available in the early 1970's. Soft metals such as aluminum or copper have been used as the matrix. Epoxies are available for various use conditions. Higher temperature matrix materials and thermoplastics have emerged for more demanding applications of the future. The applications of composites have turned to sporting goods, bicycles, and any equipment where weight, stiffness, and strength are important. Nowadays, automotive and electronics industries are all see the impact of composite

materials by not only in their high strength/weight ratio but also in other properties such as low thermal expansion, high thermal conductivity, ..etc.

Composites may be classified [Jones 1975] as 1). Fibrous composite, long fibers of stiff and strong material embedded in a matrix of a flexible, weaker materials. 2). Laminated composites consisting of layers of materials with various properties. 3). Particulate composite, relatively short particles embedded in a matrix. Fibers are normally long and slender with higher stiffness and strength than the matrix which protects the surface of individual fibers, separates the fibers and provides a means by which load is distributed among the fibers. Analysis of shear and normal stress distributions of the fiber conclude that the matrix and the fiber experience the same strain in the (uni-directional) fiber direction of continuous fibrous composites.

2.3.1. Mechanical/Thermal properties of a lamina

Some common in-plane properties of composites are summarized as follows;

Modulus of elasticity:

Longitudinal $E_1 = E_f V_f + E_m V_m$ (2.38)

Transverse $E_2 = E_f E_m \; / \; (E_f V_m + E_m V_f)$ (2.39)

Shear $$G_{12} = G_f G_m / (G_f V_m + G_m V_f) \quad (2.40)$$

Poisson's Ratio:

Longitudinal $$\nu_{12} = \nu_f V_f + \nu_m V_m \quad (2.41)$$

Transverse $$\nu_{21} = \nu_f \nu_m / (\nu_f V_m + \nu_m V_f) \quad (2.42)$$

Coefficient of thermal expansion:

Longitudinal $$\alpha_1 = (\alpha_f E_f V_f + \alpha_m E_m V_m) / (E_f V_f + E_m V_m) \quad (2.43)$$

(Turner equation)

Transverse $$\alpha_2 = V_f \alpha_f^T + V_m \alpha_m^T - \nu_{12}^f V_f (\alpha_1 - \alpha_f^L) - \nu_{12}^m V_m (\alpha_1 - \alpha_m^L) \quad (2.44)$$

where 1,2 represent longitudinal and transverse directions; f,m represent fiber and matrix; V_f and V_m are volume fractions of fiber and matrix of the composites respectively.

2.3.2. Stress-strain relations of a lamina

The stress-strain relations for an orthotropic material with the coordinate aligned along the principle material directions are

$$\begin{bmatrix} \sigma_1 \\ \sigma_2 \\ \sigma_3 \\ \tau_{23} \\ \tau_{13} \\ \tau_{12} \end{bmatrix} = \begin{bmatrix} C_{11} & C_{12} & C_{13} & 0 & 0 & 0 \\ C_{12} & C_{22} & C_{23} & 0 & 0 & 0 \\ C_{13} & C_{23} & C_{33} & 0 & 0 & 0 \\ 0 & 0 & 0 & C_{44} & 0 & 0 \\ 0 & 0 & 0 & 0 & C_{55} & 0 \\ 0 & 0 & 0 & 0 & 0 & C_{66} \end{bmatrix} \begin{bmatrix} \epsilon_1 \\ \epsilon_2 \\ \epsilon_3 \\ \gamma_{23} \\ \gamma_{13} \\ \gamma_{12} \end{bmatrix} \quad (2.45)$$

where the stiffness coefficients C_{ij} may be expressed in terms of the engineering constant as

$$C_{11} = (1-\nu_{23}\nu_{32}) / E_2E_3\Delta$$

$$C_{12} = (\nu_{21}+\nu_{31}\nu_{23}) / E_2E_3\Delta$$

$$C_{13} = (\nu_{31}+\nu_{21}\nu_{32}) / E_2E_3\Delta$$

$$C_{22} = (1-\nu_{13}\nu_{31}) / E_1E_3\Delta$$

$$C_{23} = (\nu_{32}+\nu_{12}\nu_{31}) / E_1E_2\Delta$$

$$C_{33} = (1-\nu_{12}\nu_{21}) / E_1E_2\Delta$$

$$C_{44} = G_{23}$$

$$C_{55} = G_{31}$$

$$C_{66} = G_{12}$$

and $$\Delta = (1-\nu_{12}\nu_{21}-\nu_{23}\nu_{32}-\nu_{31}\nu_{13}-2\nu_{21}\nu_{32}\nu_{13}) / (E_1E_2E_3)$$

For a composite lamina (which is a thin plate), we ignore stresses associated with the axis perpendicular to plane of the plate. If we assume that x_1, x_2, x_3 axes are aligned with the principle material directions, the stress-strain relations are

$$\begin{bmatrix} \sigma_1 \\ \sigma_2 \\ \tau_{12} \end{bmatrix} = \begin{bmatrix} Q_{11} & Q_{12} & 0 \\ Q_{12} & Q_{22} & 0 \\ 0 & 0 & Q_{66} \end{bmatrix} \begin{bmatrix} \epsilon_1 \\ \epsilon_2 \\ \gamma_{12} \end{bmatrix} \qquad (2.46)$$

where

$$Q_{11} = E_1/(1-\nu_{12}\nu_{21})$$

$$Q_{12} = \nu_{12}E_2/(1-\nu_{12}\nu_{21})$$

$$Q_{22} = E_2/(1-\nu_{12}\nu_{21})$$

$$Q_{66} = G_{12}$$

Suppose we want the stress-strain relations for an x-y system at an angle θ relative to the material principle direction. Equation (2.46) becomes

$$\begin{bmatrix}\sigma_x\\ \sigma_y\\ \tau_{xy}\end{bmatrix} = \begin{bmatrix}\bar{Q}_{11} & \bar{Q}_{12} & \bar{Q}_{16}\\ \bar{Q}_{12} & \bar{Q}_{22} & \bar{Q}_{26}\\ \bar{Q}_{16} & \bar{Q}_{26} & \bar{Q}_{66}\end{bmatrix}\begin{bmatrix}\epsilon_x\\ \epsilon_y\\ \gamma_{xy}\end{bmatrix} \qquad (2.47)$$

where

$$\bar{Q}_{11} = Q_{11}\cos^4\theta+2(Q_{12}+2Q_{66})\sin^2\theta\cos^2\theta+Q_{22}\sin^4\theta$$

$$\bar{Q}_{12} = (Q_{11}+Q_{22}-4Q_{66})\sin^2\theta\cos^2\theta+Q_{12}(\sin^4\theta+\cos^4\theta)$$

$$\bar{Q}_{22} = Q_{11}\sin^4\theta+2(Q_{12}+2Q_{66})\sin^2\theta\cos^2\theta+Q_{22}\cos^4\theta$$

$$\bar{Q}_{16} = (Q_{11}-Q_{12}-2Q_{66})\sin\theta\cos^3\theta+(Q_{12}-Q_{22}+2Q_{66})\sin^3\theta\cos\theta$$

$$\bar{Q}_{26} = (Q_{11}-Q_{12}-2Q_{66})\sin^3\theta\cos\theta+(Q_{12}-Q_{22}+2Q_{66})\sin\theta\cos^3\theta$$

$$\bar{Q}_{66} = (Q_{11}+Q_{22}-2Q_{12}-2Q_{66})\sin^2\theta\cos^2\theta+Q_{66}(\sin^4\theta+\cos^4\theta)$$

2.3.3. Stress-strain relations of a laminate

For a laminate (several laminas bonded together forming a plate), the relations between stress resultants N, moments M, strains ϵ and curvatures k are

$$\begin{bmatrix} N_x \\ N_y \\ N_{xy} \end{bmatrix} = \begin{bmatrix} A_{11} & A_{12} & A_{16} \\ A_{12} & A_{22} & A_{26} \\ A_{16} & A_{26} & A_{66} \end{bmatrix} \begin{bmatrix} \epsilon_{x_0} \\ \epsilon_{y_0} \\ \gamma_{xy_0} \end{bmatrix} + \begin{bmatrix} B_{11} & B_{12} & B_{16} \\ B_{12} & B_{22} & B_{26} \\ B_{16} & B_{26} & B_{66} \end{bmatrix} \begin{bmatrix} k_x \\ k_y \\ k_{xy} \end{bmatrix} \tag{2.48}$$

and

$$\begin{bmatrix} M_x \\ M_y \\ M_{xy} \end{bmatrix} = \begin{bmatrix} B_{11} & B_{12} & B_{16} \\ B_{12} & B_{22} & B_{26} \\ B_{16} & B_{26} & B_{66} \end{bmatrix} \begin{bmatrix} \epsilon_{x_0} \\ \epsilon_{y_0} \\ \gamma_{xy_0} \end{bmatrix} + \begin{bmatrix} D_{11} & D_{12} & D_{16} \\ D_{12} & D_{22} & D_{26} \\ D_{16} & D_{26} & D_{66} \end{bmatrix} \begin{bmatrix} k_x \\ k_y \\ k_{xy} \end{bmatrix} \tag{2.49}$$

where

$$A_{ij} = \sum_{k=1}^{N} (\overline{Q}_{ij})_k \, t_k$$

$$B_{ij} = \sum_{k=1}^{N} (\overline{Q}_{ij})_k \, t_k \, \overline{Z}_k$$

$$D_{ij} = \sum_{k=1}^{N} (\overline{Q}_{ij})_k \left(t_k \, \overline{Z}_k^2 + \frac{t_k^3}{12} \right)$$

t_k =thickness of layer k = $Z_k - Z_{k-1}$

Z_k =Z-coordinate of the centroid of layer k

= $(Z_k + Z_{k-1})/2$

Solve the above two equations for $\{\epsilon_0\}$ in terms of N and M

$$\{\epsilon_0\} = ([A^*]-[B^*][D^*]^{-1}[C^*])\{N\} + [B^*][D^*]^{-1}\{M\} \tag{2.50}$$

where

$[A^*]=[A]^{-1}$, $[B^*]=-[A]^{-1}[B]$

$[C^*]=-[B^*]^{-1}$, $[D^*]=[D]-[B][A]^{-1}[B]$

2.3.4. Thermal expansion of composite materials

The coefficient of thermal expansion of a composite lamina in the x or y direction can be transformed from that in the principle directions,

$$\{\alpha_{x,y}\} = ([R][T][R]^{-1})^{-1}\{\alpha_{1,2}\} \tag{2.51}$$

where

$$[T] = \begin{bmatrix} \cos^2\theta & \sin^2\theta & 2\sin\theta\cos\theta \\ \sin^2\theta & \cos^2\theta & -2\sin\theta\cos\theta \\ -\sin\theta\cos\theta & \sin\theta\cos\theta & \cos^2\theta-\sin^2\theta \end{bmatrix}$$

$$[R] = \begin{bmatrix} 1 & 0 & 0 \\ 0 & 1 & 0 \\ 0 & 0 & 2 \end{bmatrix} \quad , \quad [R]^{-1} = \begin{bmatrix} 1 & 0 & 0 \\ 0 & 1 & 0 \\ 0 & 0 & 1/2 \end{bmatrix}$$

If strain is caused by a temperature change ΔT, the laminate thermal strain can be expressed as

$$\{\epsilon_0^T\} = ([A^*]-[B^*][D^*]^{-1}[C^*])\{N^T\} + [B^*][D^*]^{-1}\{M^T\} \tag{2.52}$$

where

$$\{N^T\} = \Delta T \sum_{k=1}^{N} [\bar{Q}_{ij}]_k \{\alpha\}_k (Z_k - Z_{k-1})$$

$$\{M^T\} = \frac{1}{2}\Delta T \sum_{k=1}^{N} [\bar{Q}_{ij}]_k \{\alpha\}_k (Z_k^2 - Z_{k-1}^2)$$

Coefficient of thermal expansion of composite laminate will be

$$\{\alpha_c\} = (1/\Delta T)\{\epsilon_0^T\} \tag{2.53}$$

Software such as GENLAM, SQ5 are available for ply stresses, ply strains, stiffness matrices, coefficient of thermal expansion and other properties calculations.

2.4. Fast Fourier Transform

A physical process can be described either as a function of time h(t), in time domain, or as a function of frequency H(f), in frequency domain. It is useful to think of h(t) and H(f) as being two different representations of the same function. One goes back and forth between these two representations by way of the Fourier transform equations,

$$H(f) = \int_{-\infty}^{\infty} h(t) e^{2\pi i f t} dt$$
$$h(t) = \int_{-\infty}^{\infty} H(f) e^{-2\pi i f t} df \qquad (2.54)$$

The total power in a signal is the same whether we compute it in the time domain or in the frequency domain. This is known as Parseval's theorem

$$\text{Total Power} \equiv \int_{-\infty}^{\infty} |h(t)|^2 dt = \int_{-\infty}^{\infty} |H(f)|^2 df \qquad (2.55)$$

One may just wants to know "how much power" is contained in the frequency interval between f and f+df. In such circumstances, one does not distinguish between positive and negative f, but rather regard f as varying from 0 to ∞. The one-sided power spectral density (PSD) of the function h is defined as

$$P_h(f) \equiv |H(f)|^2 + |H(-f)|^2 \qquad 0 \le f < \infty \tag{2.56}$$

The total power is then just the integral of $P_h(f)$ from f=0 to f=∞. In most experimental work, we are almost never given a continuous function h(t) to work with, but are given a list of measurements of $h(t_i)$ for a discrete set of t_i's. In the most common situations, function h(t) is sampled at evenly spaced intervals in time (Δ). The term 1/Δ is called the sampling rate. There is a special frequency f_c, called the Nyquist critical frequency defined by

$$f_c \equiv 1/(2\Delta) \tag{2.57}$$

If a continuous function h(t) happens to be band-width limited to frequencies smaller in magnitude than f_c, then the function h(t) is completely determined by its samples

$$h_k=h(t_k),\ t_k=k\Delta,\ k=0,1,2,\ \ldots\ N-1. \tag{2.58}$$

With N numbers of input, we will only be able to produce no more than N independent numbers of output. Fourier transform H(f) at the discrete frequency values $f_n=n/(N\Delta)$, n=-N/2,....N/2, can thus be approximated by the discrete sum [Press 1989]:

$$H(f_n) = \int_{-\infty}^{\infty} h(t) e^{2\pi i f_n t} dt \approx \sum_{k=0}^{N-1} h_k \, e^{2\pi i f_n t_k} \Delta = \Delta \sum_{k=0}^{N-1} h_k \, e^{2\pi i k n/N} \qquad (2.59)$$

This equation is called the "Discrete Fourier Transform". If we define;

$$H_n \equiv \sum_{k=0}^{N-1} h_k \, e^{2\pi i k n/N} \qquad (2.60)$$

Equation (2.59) can be rewritten as

$$H(f_n) \approx \Delta H_n \qquad (2.61)$$

To save the computation time, an algorithm called "Fast Fourier Transform (FFT)" was introduced in the mid-1960s. It reduced the number of operations from the order of N^2 to the order of $N \cdot \log_2 N$ and now is widely used in the area of frequency analysis. Algorithm and computer program are available from the "Numerical Recipes" [Press 1989].

2.5. Temperature Conversion from Thermocouples

A continuous current was discovered by Thomas Seebeck in 1821 in the thermoelectric circuit which was made by joining two dissimilar metal wires at both ends and one of the ends is heated. If the circuit is broken at the center, the net open circuit voltage (the Seebeck voltage)

is a function of the junction temperature and the composition of the two metals. All dissimilar metals exhibit this effect. Thus, when using a voltmeter to measure this voltage, one introduces a new thermoelectric circuit between the lead wires of a voltmeter and the thermocouples. Figure 6(a) shows an example of Seebeck voltages generated in a type J (iron-constantan) thermocouple circuit.

The voltages generated at junction 3 and 4 are the same but in opposition to each other if they were kept in an isothermal block and will not affect the result no matter what the absolute temperature it is. Furthermore, if we combine the two isothermal blocks at the same reference temperature, we recall the law of intermediate metals to eliminate the extra junction. This empirical law states that a third metal (in this case, iron) inserted between the two dissimilar metals of a thermocouple junction will have no effect upon the output voltage as long as the two junctions formed by the additional metal are at the same temperature. Figure 6(b) is used in practice to simplify the connections. When using type T thermocouples, both sides of junction J_3 are copper and has no Seebeck effect to the circuit as shown in figure 6(c). The resultant voltmeter reading V will be proportional to the temperature difference between J_1 and J_{REF}.

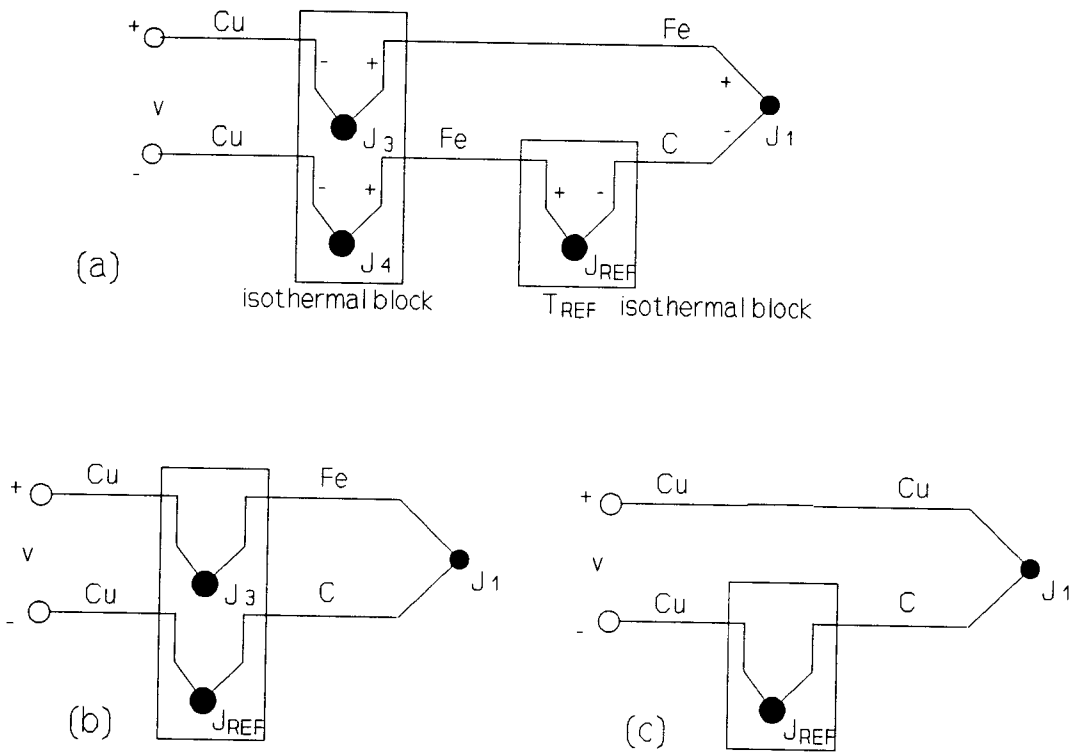

Fig. 6. Thermocouple junctions a),b) J-type, c) T-type

$$V = (V_1 - V_{REF}) = \alpha(t_{J1} - t_{JREF}) \qquad (2.62)$$

This means that we should know the temperature at J_{REF} before we try to measure the temperature at J_1. To determine the temperature of junction J_{REF}, called reference junction, we can physically put the junction into an ice bath and force its temperature to be 0°C. By adding the ice point reference junction voltage we have referenced the reading to 0°C. Since the ice point temperature can be controlled precisely, it is used by the National Bureau of Standards (NBS, now National Institute of Standards and Technology or NIST) as a fundamental reference point for their thermocouple tables, so we can look at the NBS tables and directly convert from voltage V to temperature t_{J1}.

Unfortunately, the voltage versus temperature relationship of a thermocouple is not linear. Figure 7 shows this non-linearity of type T thermocouple as an example. Polynomial curve fitting is commonly used for voltage to temperature conversion. As the order n of the polynomial increases, the accuracy improves. A representative number is n=9 for ± 1°C as stated in OMEGA Temperature Handbook. Better conversion accuracy can be obtained by reading the voltage and consulting the NBS Thermocouple Tables. A data base of T-type thermocouple for every 10°C were extracted from OMEGA Handbook. Piecewise linear interpolation was made to convert voltages

to temperatures at an arbitrary given reference temperature. One finds the reference voltage and adds to the voltage readings. Linear interpolation corresponding to the temperature interval of that voltage reading was made to accomplish the conversion. Maximum midpoint deviation of each temperature interval is 0.1°C from -200°C to 200°C. In most intervals the deviations are less than 0.05°C. High order polynomial curve fitting was eliminated. For other thermocouple conversions, we simply change the database. Appendix B gives a PROLOG program for doing this conversion.

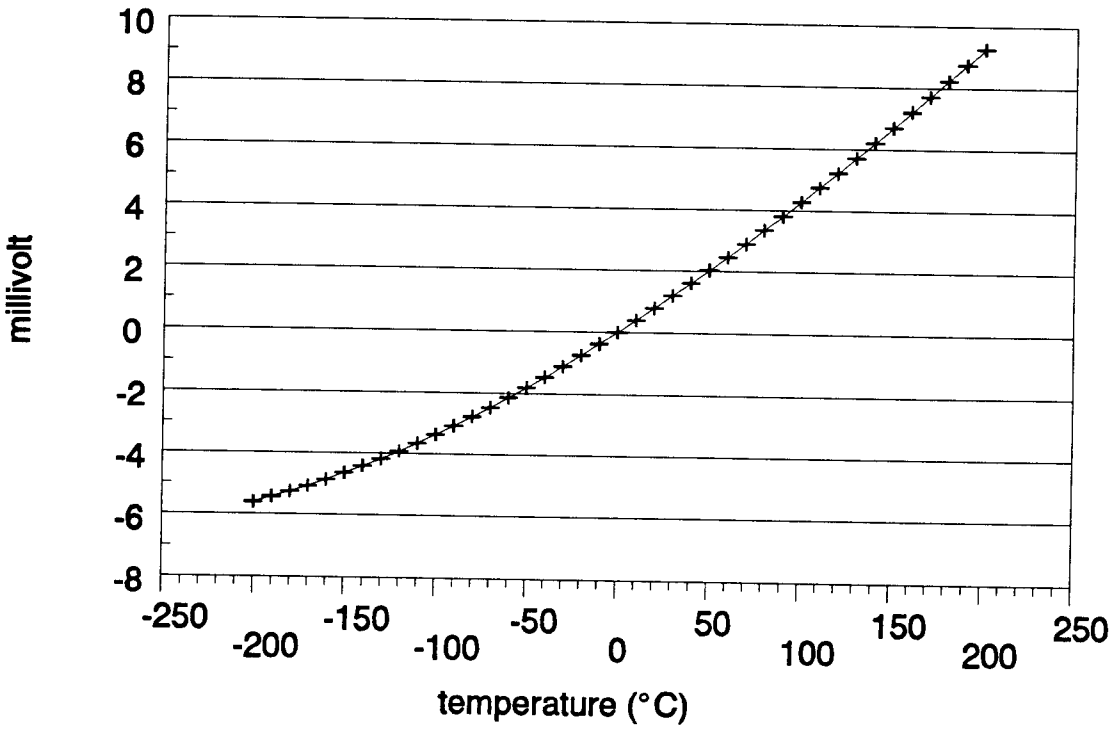

Fig. 7. T type thermocouple reference curve (0°C)

CHAPTER 3. DERIVATIONS OF SIGNAL PHASE CALCULATION

"Signal Phase Calculation" is a new approach to the analysis of the Michelson interferometry signals. This method is similar to the fringe counting method [Aghdaie 1988; Wolff 1985] but calculate the phase changes of every signal points by software instead of counting the number of fringe cycles by electronic circuits. The improvement in displacement-signal linearity and elimination of electronic fringe counting circuits are expected. This method uses the fact that the interfered lightwaves after the beam splitter in the Michelson interferometer (figure 3) is elliptically polarized. One can view the signal moves along an ellipse if we feed the two orthogonal components of the signal into an oscilloscope set in the X-Y mode. Signal phase change can be calculated from two consecutive data points along the ellipse. This chapter describes the optical system, derivation of signal phase angle and computer programs for "Signal Phase Calculation".

3.1. Interference of Decomposed **E** Fields in Michelson Interferometry

The basic relationship between intensity variation and its corresponding displacement in Michelson interferometry has been described in section 2.1.8. "Signal Phase

Calculation" requires two orthogonal electrical field components to interpret the signal. Figure 8 shows the decomposition of the interfered **E** field of an elliptical polarized light in the Michelson interferometer.

A linearly polarized light from a He-Ne laser is split into two beams by the amplitude beam splitter, BS. The reflected beams from the interferometer interfere upon return to this BS. The electrical field of the interfered beam combined from $\mathbf{E}_1$ and $\mathbf{E}_2$ is separated into two orthogonal components, $\mathbf{E}_{1s}$, $\mathbf{E}_{1p}$ and $\mathbf{E}_{2s}$, $\mathbf{E}_{2p}$, by a polarizing beam splitter (SPBS). Because of the anisotropy of these optical components, some phase shift between parallel and perpendicular components was introduced. An optical retarder may be inserted into the optical path to adjust the phase difference. The polarization state of the resultant electric field is no longer linear but elliptical in general. The two orthogonal components of the recombined elliptical polarized light after the polarizing beam splitter are

$$\mathbf{E}_s = (\mathbf{E}_{1s} + \mathbf{E}_{2s}) \qquad (3.1a)$$

$$\mathbf{E}_p = (\mathbf{E}_{1p} + \mathbf{E}_{2p}) \qquad (3.1b)$$

Both $\mathbf{E}_s$ and $\mathbf{E}_p$ are the resultant electrical fields of two beam interference. The corresponding irradiances of these two components are

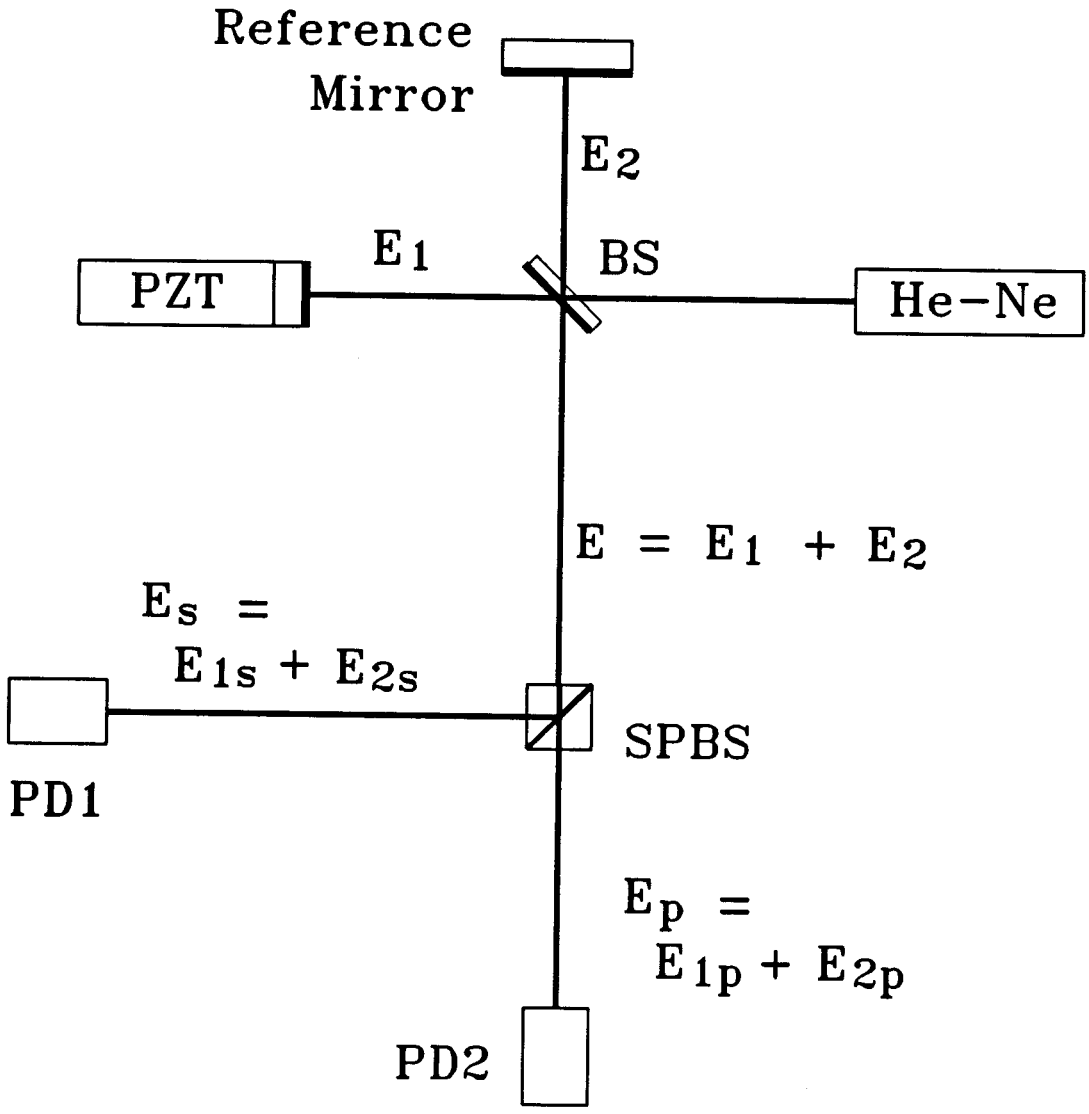

Fig. 8. Decomposition of interference **E** field

$$I_s=I_{1s}+I_{2s}+2(I_{1s}I_{2s})^{1/2}\cos(\phi+\delta_s) \quad (3.2a)$$

$$I_p=I_{1p}+I_{2p}+2(I_{1p}I_{2p})^{1/2}\cos(\phi+\delta_p) \quad (3.2b)$$

where

ϕ = phase difference arising from OPLD

= $(4\pi/\lambda)nL$,

(n, index of refraction;

L, length difference between arms or sample length)

δ_s = initial phase difference between $\mathbf{E}_{1s}$ and $\mathbf{E}_{2s}$

δ_p = initial phase difference between $\mathbf{E}_{1p}$ and $\mathbf{E}_{2p}$

The first two terms of the irradiance represent the DC component while the third term is the AC part or interference term.

3.2. Signal Phase Angles

Since we are considering the change of intensity caused by the change of optical path length difference (OPLD), δ_s can be arbitrarily chosen, say 0, and $\delta=\delta_s-\delta_p$. Irradiance is detected by silicon photodetectors which convert the total power to a current and hence voltage. The above equations can then be written as

$$V_x = (V_x)_{DC} + (V_x)_{AC} = h + a*\cos(\phi) \quad (3.3a)$$

$$V_y = (V_y)_{DC} + (V_y)_{AC} = k + b*\cos(\phi-\delta) \quad (3.3b)$$

Rewrite as

$$\cos(\phi) = (V_x-h)/a \tag{3.4a}$$

$$\sin(\phi) = ((V_y-k)/b-\cos\delta(V_x-h)/a)/\sin\delta \tag{3.4b}$$

Where the triangular equality $\cos(\phi-\delta)=\cos\phi\cos\delta+\sin\phi\sin\delta$ was used. The phase angle ϕ of a given data point (V_x,V_y) can be calculated by

$$\tan\phi=\frac{\sin\phi}{\cos\phi}=\frac{\frac{1}{\sin\delta}\left[\frac{a}{b}(V_y-k)-(V_x-h)\cos\delta\right]}{(V_x-h)} \tag{3.5}$$

The angle ϕ in this equation is defined as the signal phase angle. The displacement ΔL corresponding to two consecutive signal points can be related to the phase angle change $\Delta\phi$ as

$$\Delta L=\frac{\Delta\phi}{2kn}=\frac{\lambda}{4\pi n}\Delta\phi \tag{3.6}$$

3.3. Signal Trajectory

To find the parameters a, b, h, k, and δ in equation (3.5) for any given data point let us take the square of equations (3.3a) and (3.3b) and sum them up;

$$\frac{(V_x-h)^2}{a^2}+\frac{(V_y-k)^2}{b^2}=\cos^2\phi+[\cos\phi\cos\delta+\sin\phi\sin\delta]^2$$

$$=\cos^2\phi+\cos^2\phi\cos^2\delta+\sin^2\phi\sin^2\delta+2\cos\phi\cos\delta\sin\phi\sin\delta$$

$$=\cos^2\phi(1+\cos^2\delta)+\sin^2\phi\sin^2\delta+2\cos\phi\cos\delta\sin\phi\sin\delta$$

$$=\cos^2\phi(\sin^2\delta+2\cos^2\delta)+\sin^2\phi\sin^2\delta+2\cos\phi\cos\delta\sin\phi\sin\delta$$

$$=\sin^2\delta(\cos^2\phi+\sin^2\phi)+2\cos\phi\cos\delta(\cos\phi\cos\delta+\sin\phi\sin\delta)$$

$$=\sin^2\delta+2\cos\phi\cos\delta\cos(\phi-\delta)$$

$$=\sin^2\delta+2\cos\delta\frac{(V_x-h)}{a}\frac{(V_y-k)}{b} \qquad (3.7)$$

We obtain the elliptical equation which represents the trajectory of the data points.

$$\frac{(V_x-h)^2}{a^2}+\frac{(V_y-k)^2}{b^2}-\frac{2(V_x-h)(V_y-k)\cos\delta}{ab}=\sin^2\delta \qquad (3.8)$$

In this equation, (h,k) is the ellipse center. V_x ranges from h-a to h+a and V_y ranges from k-b to k+b. The initial phase difference δ between V_x and V_y determines the opening of the ellipse. Figure 9 shows an example of the two constituent irradiances with V_x leading V_y by $\delta=45°$. Figure 10 shows the elliptical trajectory of these signals.

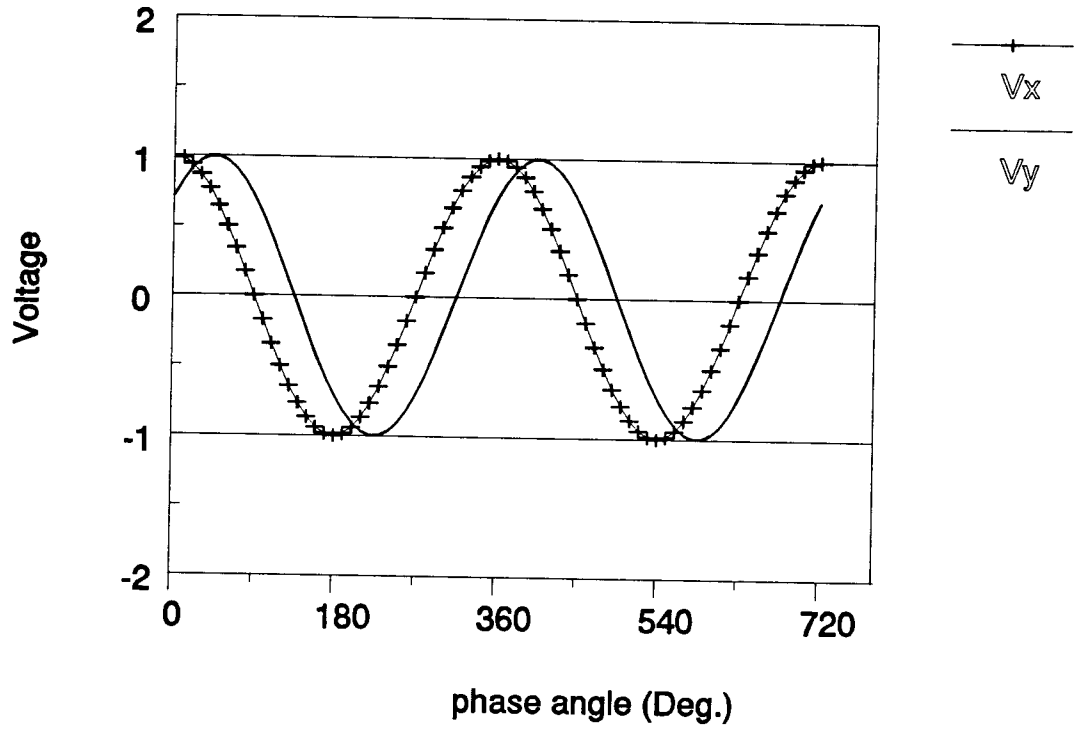

Fig. 9. Simulation signal, voltage vs. phase angle ϕ

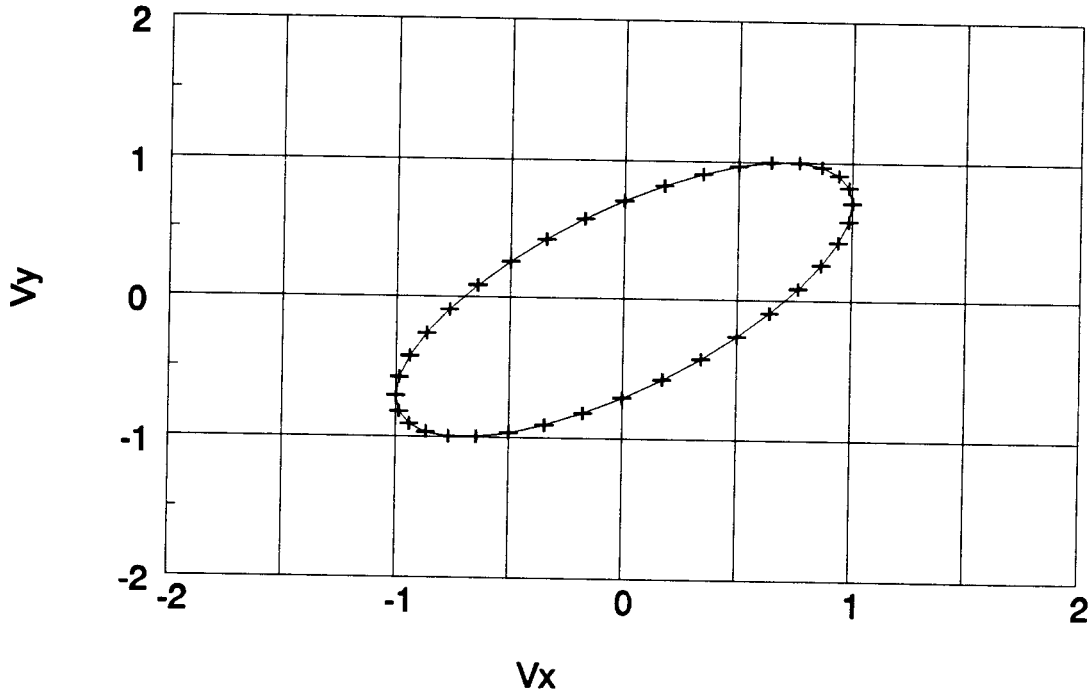

Fig. 10. Signal trajectory with h=0, k=0, a/b=1, δ=45°

3.4. Signal Phase Calculations

3.4.1. Matrix operation approach

Software based approaches to calculate the signal phase ϕ in equation (3.5) and the displacement ΔL in equation (3.6) is desired. Since the signal moves along the ellipse defined by equation (3.8), it is necessary to know the ellipse parameters before we can calculate ϕ and ΔL. To find the parameters in equation (3.8), let us rearrange it as

$$(V_x-h)^2+(a^2/b^2)(V_y-k)^2-2(a/b)(V_x-h)(V_y-k)\cos\delta=a^2\sin^2\delta \qquad (3.9)$$

let $c=a^2/b^2$, $d=2(a/b)\cos\delta$, $e=a^2\sin^2\delta$, $X=V_x$, $Y=V_y$

Alternatively

$$XZ_1-Y^2Z_2+YZ_3+XYZ_4+Z_5=X^2 \qquad (3.10)$$

where $Z_1=2h-dk$,

$Z_2=c$,

$Z_3=2ck-dh$, (3.11)

$Z_4=d$,

$Z_5=dhk-ck^2+e$

Five data points (Vx_i, Vy_i) are read and inserted to form the equation set;

$$X_iZ_1-Y_i^2Z_2+Y_iZ_3+X_iY_iZ_4+Z_5=X_i^2 \quad , \quad i=1,5 \tag{3.12}$$

To eliminate the constant term Z_5, we substitute the first equation of i=1 by every other i's equation and rewrite it in the matrix form

$$[A][Z]=[B] \tag{3.13}$$

where [A] and [B] are

$A(i,1)=x(1)-x(1+i)$

$A(i,2)=-(y^2(1)-y^2(1+i))$

$A(i,3)=y(1)-y(1+i)$

$A(i,4)=x(1)y(1)-x(1+i)y(1+i)$

and

$B(i)=x^2(1)-x^2(1+i)$

Once Z_i has been solved, the parameters h,k,a/b,δ can also be found through the Z matrix (equation 3.11) as

$$h=(2Z_1Z_2+Z_3Z_4)/(4Z_2-Z_4^2) \tag{3.14}$$

$$k=(2Z_3+Z_1Z_4)/(4Z_2-Z_4^2) \tag{3.15}$$

$$a/b=(Z_2)^{1/2} \tag{3.16}$$

$$\cos\delta=Z_4/(2(Z_2)^{1/2}) \quad , \quad 0°\leq \delta \leq 180° \tag{3.17}$$

MATLAB system was used to take the advantages of having build-in matrix operation commands in it. Figure 11 shows the flow chart of the MATLAB program for the matrix

operation approach. It finds h, k, a/b and δ after each reading. These values are used in equation (3.5) and then (3.6) to give one value of ΔL. Procedures continue until the end of the data. In this method, the ellipse parameters are calculated from the acquired data (V_x, V_y). No pre-treatment to the data file is required. Figure 12 shows that a linear displacement of 0.6328 μm (24.91 μin.) was expected for the simulation signal given in figure 9. This method works well except for situations where there is a long period of zero strain or when the signal intensity is not stable. Correct ellipse parameters can not be obtained through the matrix operations in those cases. The computer program written in MATLAB for the matrix operations is given in appendix C.

3.4.2. Fixed parameters approach

In most cases, signals usually deviate from the ellipse such that the calculated parameters h, k, a/b, and δ through the matrix operations do not represent the actual data trajectory. Signal phases are hardly to be found correctly. However, in many cases, the signal intensities on both V_x and V_y components vary with the same percentage. This implies that although the ellipse size changed but the ratio of a/b remain unchanged. The other parameters h, k, and δ can also be thought as constants over certain data

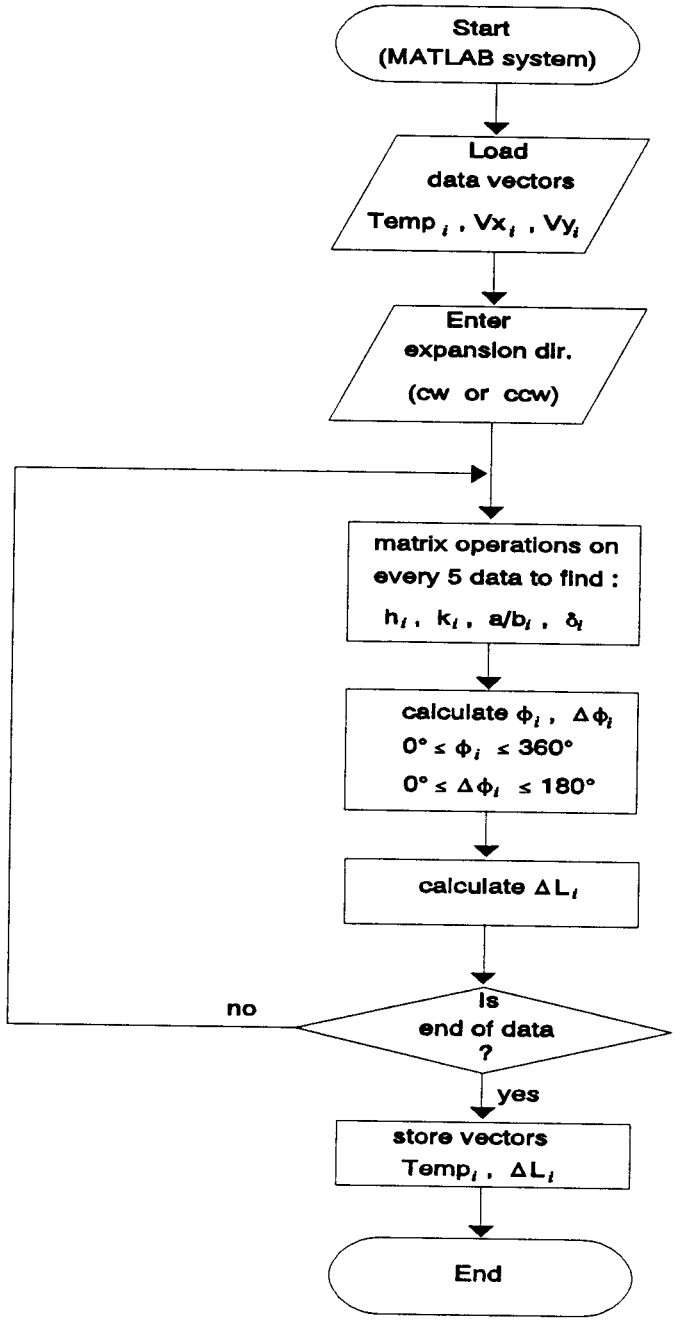

Fig. 11. Flow chart of matrix operation approach

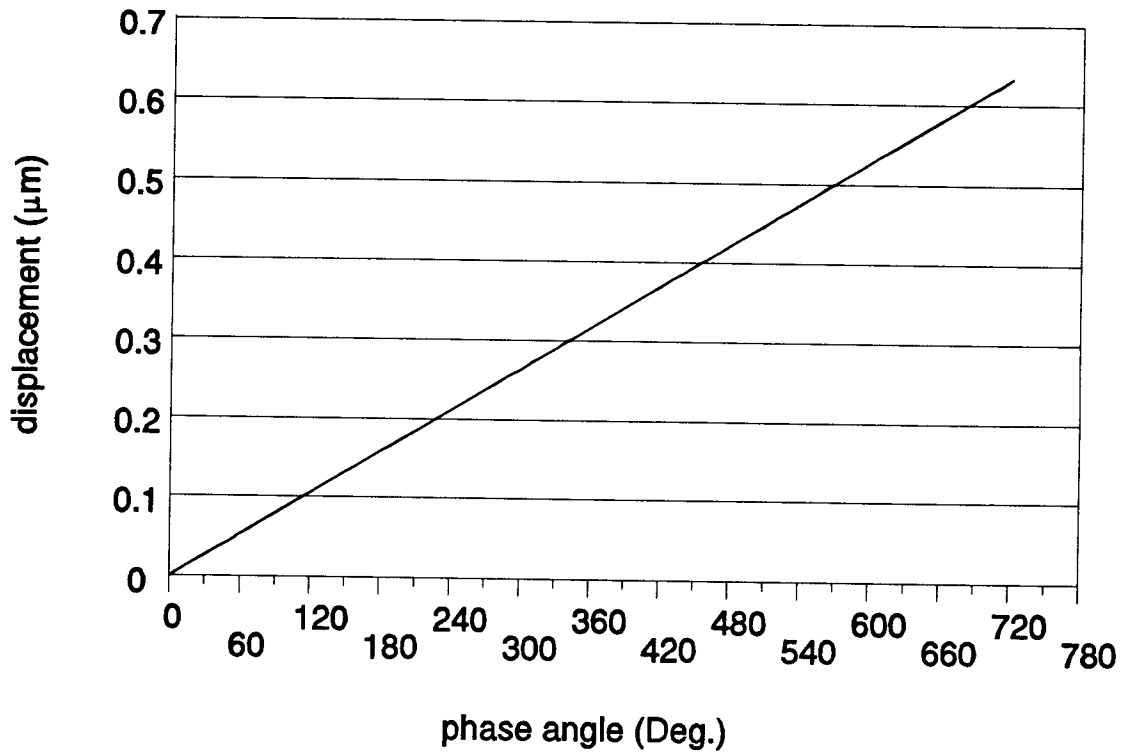

Fig. 12. Displacements of simulation signal

points. New ellipse parameters can be inserted if in the event of signal lost and regain. Updated parameters can be used for the next data group. The procedures of finding these fixed parameters can be listed as follows;

1. Retrieve (V_x, V_y) data into spreadsheet (e.g. Quattro) and plot the data trajectory on screen.
2. Find the maximums and minimums of V_x and V_y.
3. Calculate:

   $h = \frac{1}{2}(V_{x,max}+V_{x,min})$

   $k = \frac{1}{2}(V_{y,max}+V_{y,min})$

   $a = \frac{1}{2}(V_{x,max}-V_{x,min})$

   $b = \frac{1}{2}(V_{y,max}-V_{y,min})$

   δ= an initial guess value
4. Plot a reference ellipse with these parameters together with data points;

   that is :

   $V_{x,ref} = h+a\cdot\cos(\phi)$

   $V_{y,ref} = k+b\cdot\cos(\phi-\delta)$

   where ϕ can be selected as 0°, 10°, 20°, $\cdots$360°
5. Repeat steps 3 and 4 until the shape of the reference ellipse looks on the screen mostly represent the data trajectory.
6. Save h, k, a/b, δ to data file for the use of fixed parameters approach.

Macro commands were written in Quattro to ease these processes.

Figure 13 shows the flow chart of the so-called fixed parameters approach. It reads one line from the data file and update the new parameters if it is recognized. These parameters are used in equation (3.5) to find the signal phases and then the displacements from equation (3.6). Phase change between every two data points should be smaller than 180° to assure the signal moving direction is interpreted correctly. Appendix D list the PROLOG program for this method.

One may concern what will be the error if the parameters are not correctly selected. The analytical error analysis may be done by taking the Taylor series of $\phi=\tan^{-1}(x)$ from equation (3.5). However, for simplicity, we will demonstrate the errors numerically. Table 2 summarizes the errors caused by the effect of $\Delta\delta=\pm5°$. The errors become smaller at higher δ values. This means that we want the signal trajectory close to a circle at which $\delta=90°$. Errors may also be caused by not having a correct ellipse center. Table 3 shows the combined effect of ±5% mismatch of the ellipse center and δ in the range of 45°±5° for the simulation signal. The maximum error is found to be 0.01717 μm. However, this is only a local error within one signal cycle and does not accumulate over the entire test as can be seen from figure 14.

Table 2. Max. error caused by $\Delta\delta=\pm5°$

exact δ	max. error (μm) if $\delta'=\delta\pm5°$
15°	0.01341
25°	0.00839
35°	0.00660
45°	0.00562
55°	0.00511
65°	0.00474
75°	0.00455
85°	0.00441

Table 3. Max. error caused by combined effect

$\Delta h/a$	$\Delta k/b$	range of δ	max. error (μm)
+5%	+5%	40°-50°	0.00885
+5%	-5%	40°-50°	0.01601
-5%	+5%	40°-50°	0.01718
-5%	-5%	40°-50°	0.00802

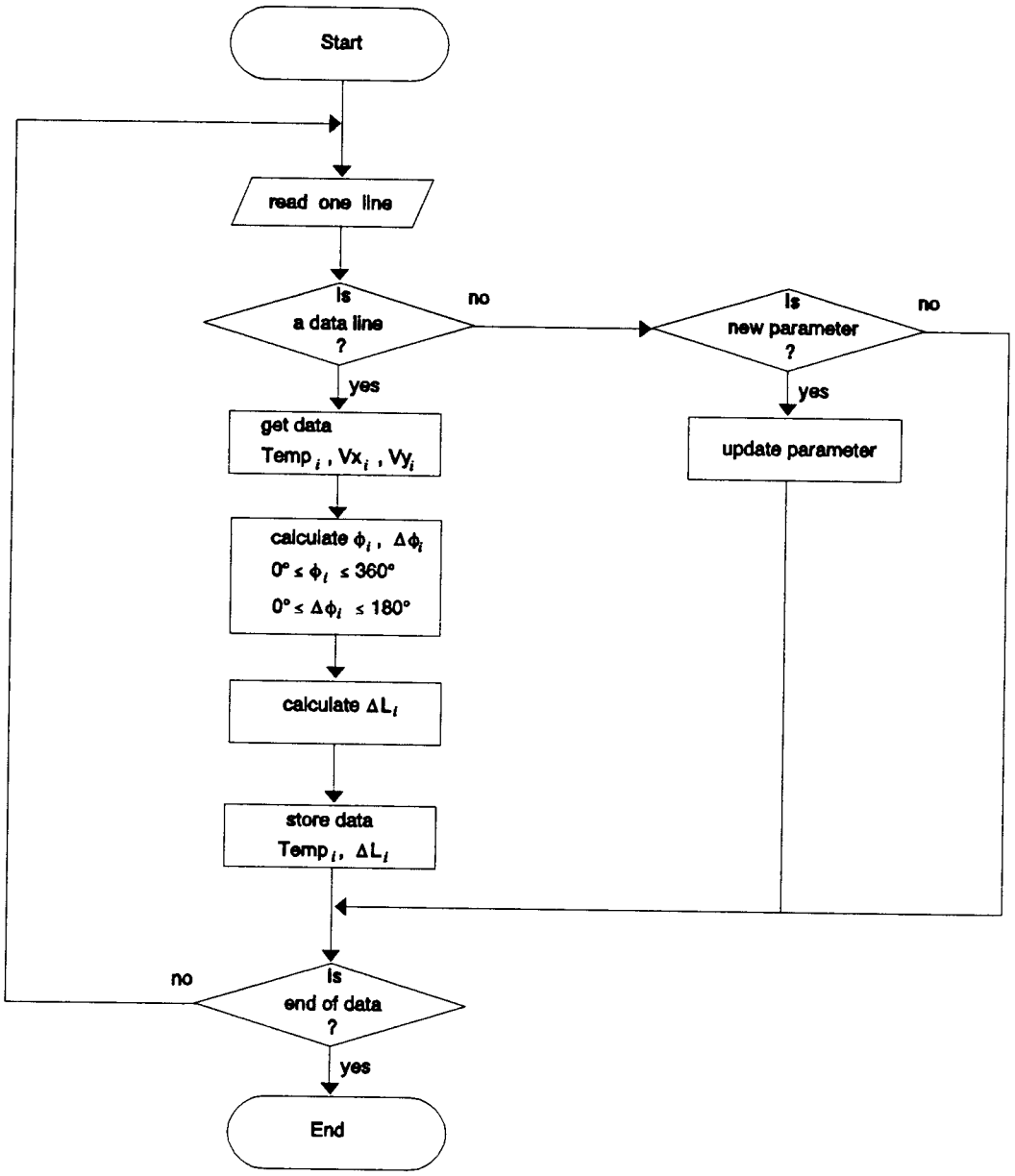

Fig. 13. Flow chart of fixed parameters approach

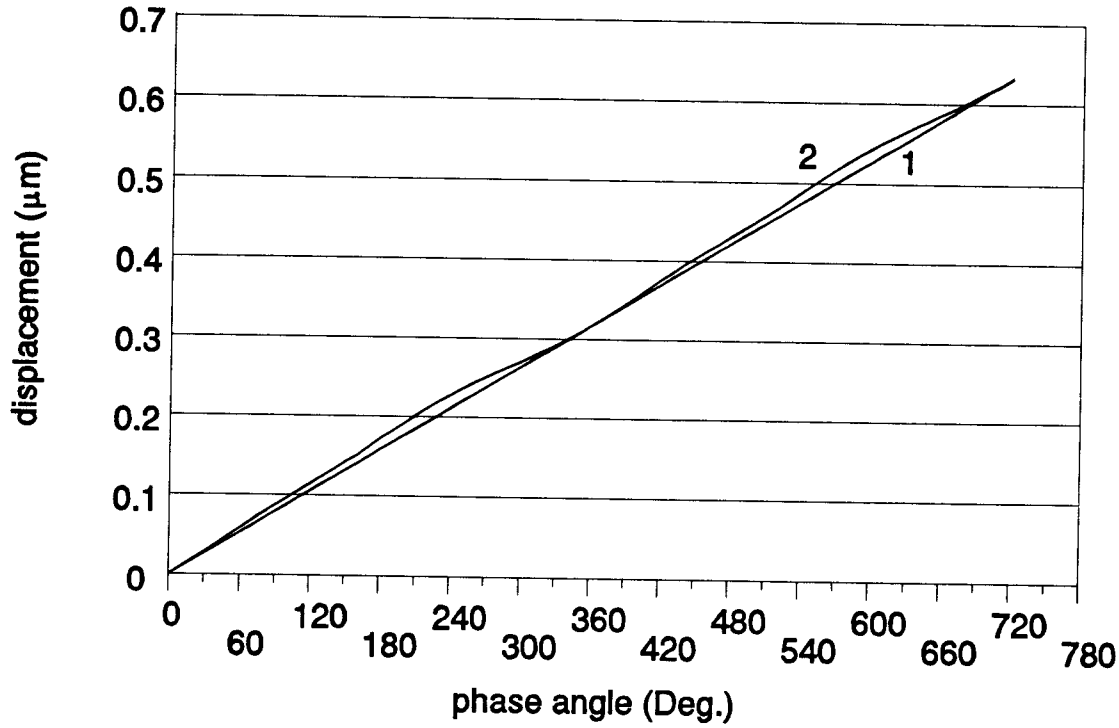

Fig. 14. Local error within one signal cycle, line 1 with exact parameters : h=0, k=0, a=b=1, δ=45°; curve 2 with perturbed parameters : h=-0.05, k=0.05, a=b=1, δ=40°

CHAPTER 4. APPARATUS AND EXPERIMENTAL PROCEDURES

Applications of the "Signal Phase Calculation" method were made in the measurement systems based on Michelson type interferometry. Apparatus and operation procedures for the measurement of small displacements induced by a piezoelectric crystal (PZT) or thermal expansion of materials will be described in this chapter. Speckle interferometry for detecting small displacements were also investigated. The calibrated PZT displacements were used to verify the system performance of speckle interferometry configurations. The frequency contents of the material vibration signals has the potential application to the non-destructive testing (NDT) techniques, thus the FFT analysis to the speckle signals is of prime interest in those systems.

4.1. PZT Calibration Setup

PZT is a common device of providing small displacements. Its characteristic displacement (i.e. μm/volt) describes the main feature of the device. The PZT (Burleigh Model: PZL-15) calibrated here will serve as a known displacement generator and be used in speckle interferometry investigations.

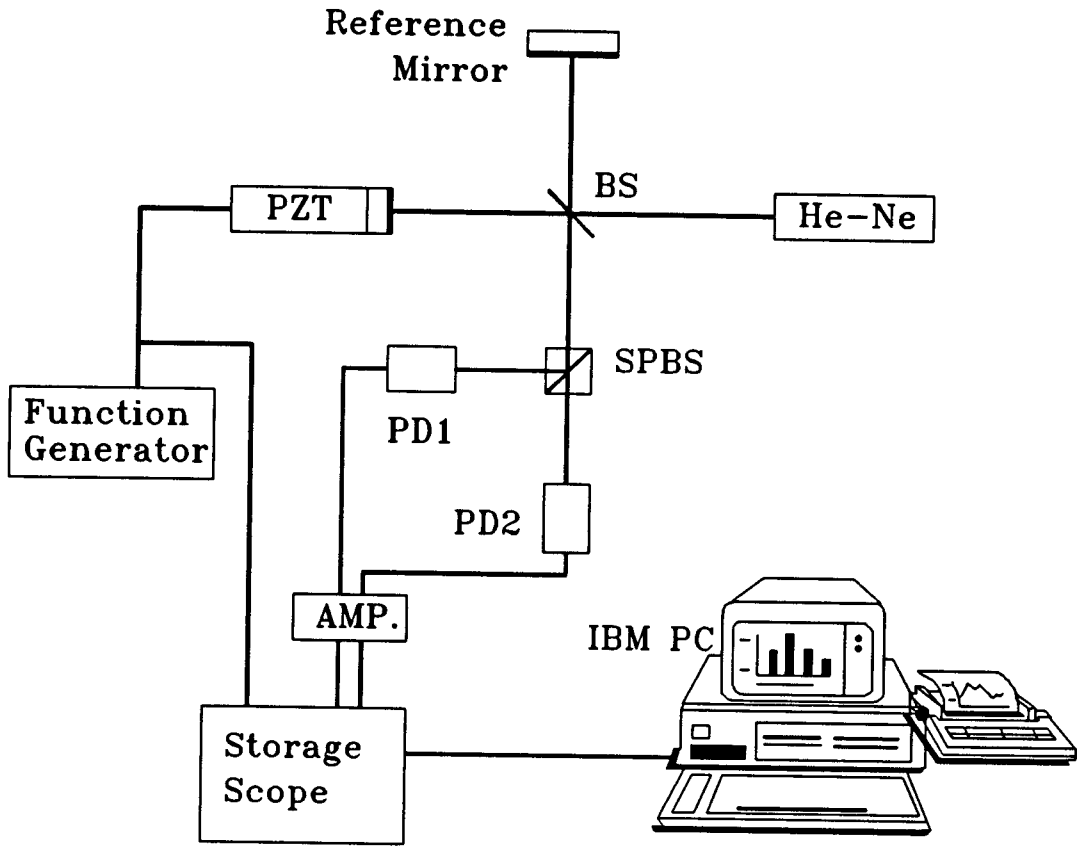

Fig. 15. PZT calibration setup

A Michelson interferometer was set up as in figure 15 to measure the displacements. A 1 mW linearly polarized He-Ne laser (Uniphase Model: 1301P) was used as the light source. Thirty volts peak-peak generated from a function generator was applied to the PZT to introduce displacements in one arm of the interferometer. Total intensities of the interference beams were detected by PIN photodetectors (Model: UDT-555D-177-1). Signals moved along an ellipse in the direction of clockwise (CW) or counterclockwise (CCW) depending on whether the PZT moved toward or away from the beam splitter. Data were recorded by a Tektronix programmable digitizer (Model 7D20) and transferred through IEEE488 interference with the use of the TEKMAP program. Intensities detected from both photodetectors are stored on disk. Displacements were calculated by the fringe counting method and/or fixed parameters approach and plotted against the applied voltages.

The photodetectors' output may saturate and give a flat distorted signal when the total intensity level (AC + DC components) is too high (>15V). A polarizer can be inserted in front of the laser and was able to adjust the light intensity. A signal amplification/processing circuit was placed after the photodetectors to perform both DC offset and AC amplification. If the initial phase difference between I_x and I_y is too small, so that the signal trajectory narrows down to a line, the signal moving

direction (clockwise or counterclockwise) is hard to distinguish. A quarter-wave plate (or any other phase retarders) is able to change the shape of the ellipse by changing the relative initial phase difference between I_x and I_y. This phase retarder can also be used to adjust the signal position at any point along the ellipse. When the displacement to be measured is small and signal moves only part of a cycle, say a quarter cycle ($\lambda/8$ or 0.08 μm), we want the signal moving around the center of the sinusoidal curve where the slope of the curve is large and is in the most sensitive area so that the highest resolution capability of the measurement system is reached.

4.2. CTE Measurement Apparatus

The details of the system operation, such as beam alignment, stability test, sample preparation/support, heating/cooling, finding sample expansion direction, ... etc., were described in this section. Procedure of data recording and analysis including manual chart method and phase change calculation methods were also described.

4.2.1. Beam alignment

Figure 16 shows a reconfigured Michelson type interferometer as a CTE measurement system. A mirror

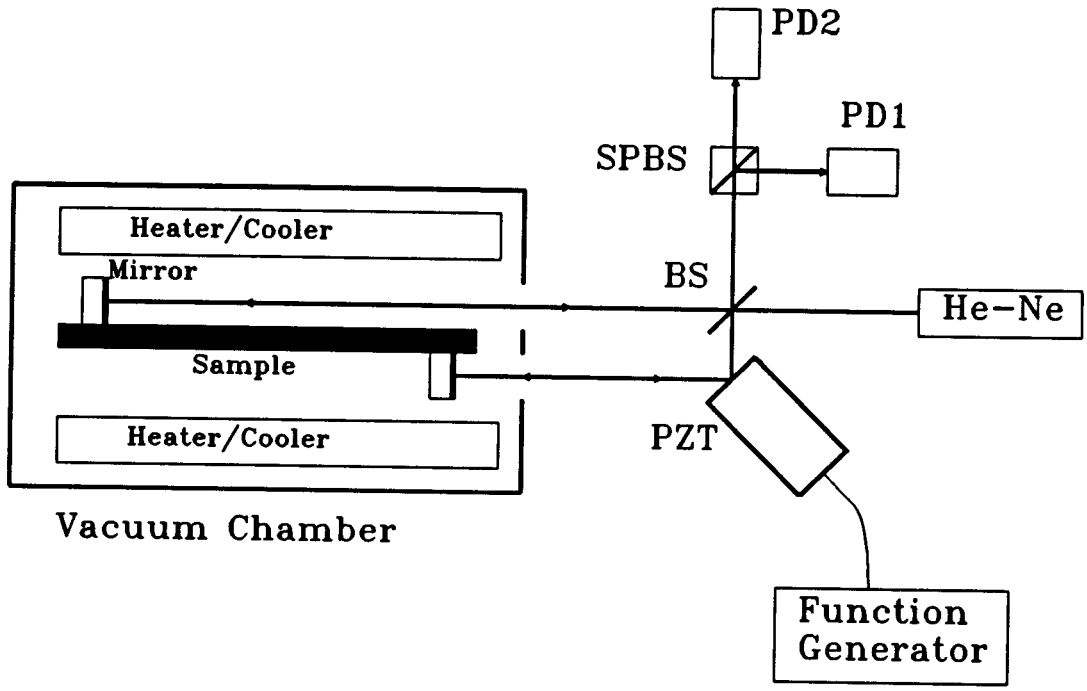

Fig. 16. CTE measurement apparatus

mounted on a PZT which is cemented on an adjustable holder conducts the lower beam to be parallel to the upper one. The interferometric signals were connected to oscilloscope set in X-Y mode, chart recorder and data acquisition system as shown in figure 17. To assure the parallelism of the two beams, one can oscillate the mirror mounted PZT and adjust the orientation of that mirror so that a clear ellipse appears on the scope. The PZT is turned off during the test.

4.2.2. Stability/Drift test

Stability testing of the system was done by recording the signals of both lights reflecting from one mirror over a longer time period, say 24 hours, on chart. Signal amplitude fluctuation was found when it was recorded periodically, once an hour for example, by applying a low frequency voltage to the PZT so that the signal moves a complete cycle and derive a pen to mark the amplitude on the chart. Figure 18 shows the PZT On-Off control circuit. PZT is represented as a parallel connection of a resistor and a capacitor. Since the impedance of the PZT is about on the same order, mega ohms, of a solid state relay, about half of the function generator voltage will still apply to the PZT even the relay is off. A computer controlled mechanical relay which can provide a complete open circuit

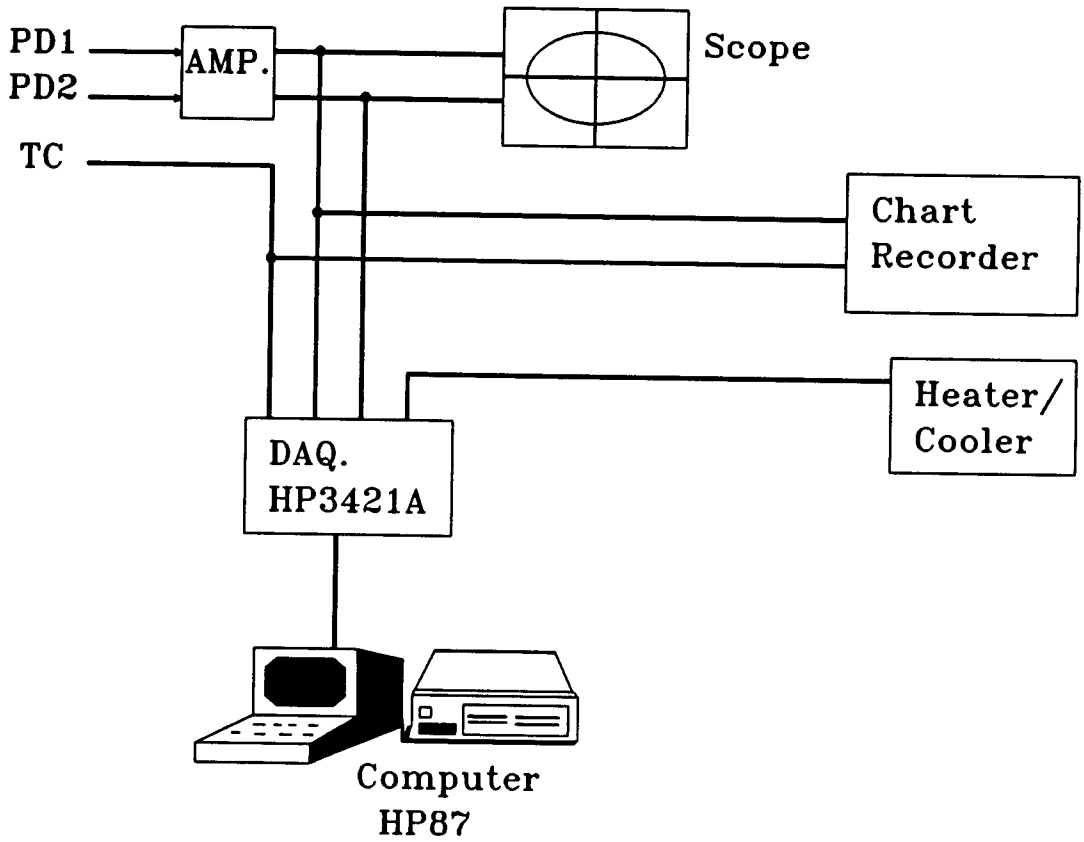

Fig. 17. Block diagram of CTE data collection system

is required to perform this function. The residual electric charges in the PZT can be balanced through the route a-$\bar{x}$-b so that the PZT returns to its neutral position without affecting the testing signals. Signal amplitudes are periodically and automatically recorded on chart.

One hour drift tests are routine for system stability checks prior to heating/cooling. Vacuum chamber and optics are seating on a floating table which isolate the vibrations from the floor.

4.2.3. CTE measurement procedures

Single Michelson mode was used to measure the CTE of thin plate and thin walled tube samples. Low expansion, Al-coated ULE or Zerodur glass mirrors are mounted near the opposite faces of plate samples (typically 150 mm long by 10 to 150 mm wide). Possible edge effects with composites require the mirrors to be >1mm from any sample edge. Mirrors are aligned with another interferometer and held in place until the adhesive (Varian low-outgassing TORR-SEAL) hardens. Postcuring at a temperature lower than highest testing temperature is recommended. For tube samples, similar mirrors were mounted on identical INVAR plates which are spring loaded against the tube ends. The laser beams in all cases were equidistant from and parallel to the plate midplane or tube axis. Cu-Constantan

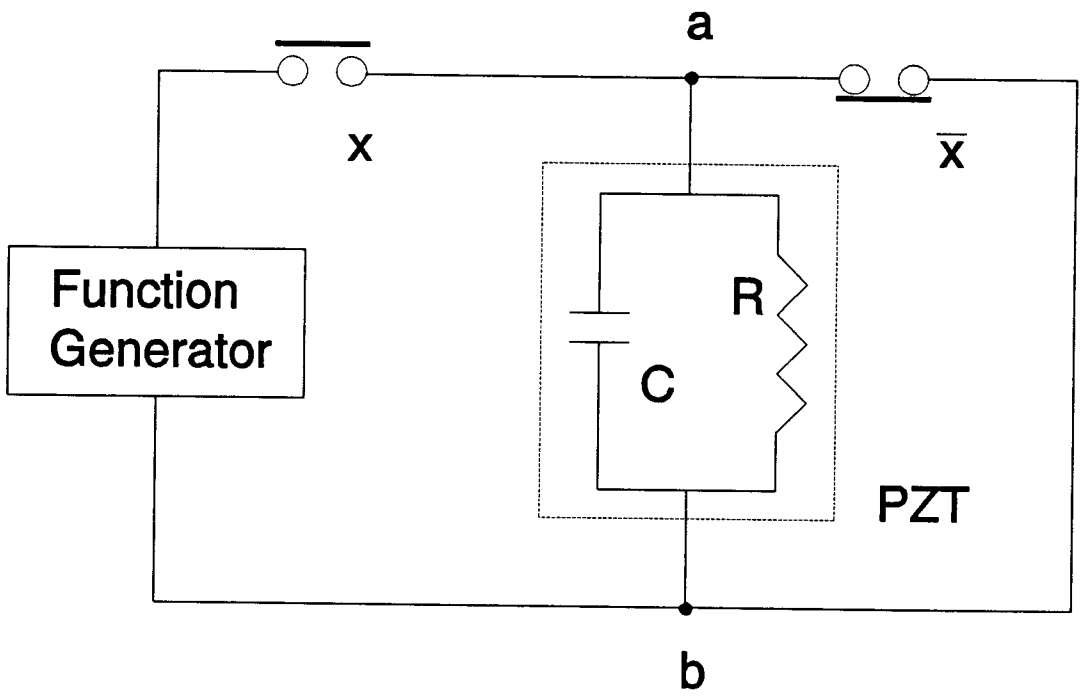

Fig. 18. Automatic PZT On-Off control circuit

thermocouples (0.07 mm dia.) were attached to monitor temperatures.

Figure 19 shows that plates were supported by parallel quartz rods and tubes were supported by vertical ZERODUR posts, all mounted on a quartz plate. The carbon-coated copper heater/coolers are as close as possible to the samples to maximize radiative heat transfer. The flow path of the liquid nitrogen was arranged as in figure 20 to minimize the thermal gradient across the unit. The cooling rate of the liquid nitrogen cooled samples can be augmented by the temporary introduction of helium (lower index of refraction, n=1.000036 compared to n=1.000293 of air at 0°C, 1 atm) into the vacuum system so that the higher heat transfer by convection then by radiation takes place. However, this means certain amount of error was introduced into the interferometer signals. The heating is done with resistive Nichrome wires and the rate is computer controlled.

The signal direction corresponding to sample growth or shrinkage is preset by OPLD adjustment with the PZT mounted mirror. When the PZT moved the mirror forward a distance d, the lower optical path is shortened by an amount of d/cos45°. This shortening effect is equivalent to that of moving the lower mirror to the right and represents a sample growth. Another way of checking the sample growth direction is the temporary introduction of air into the

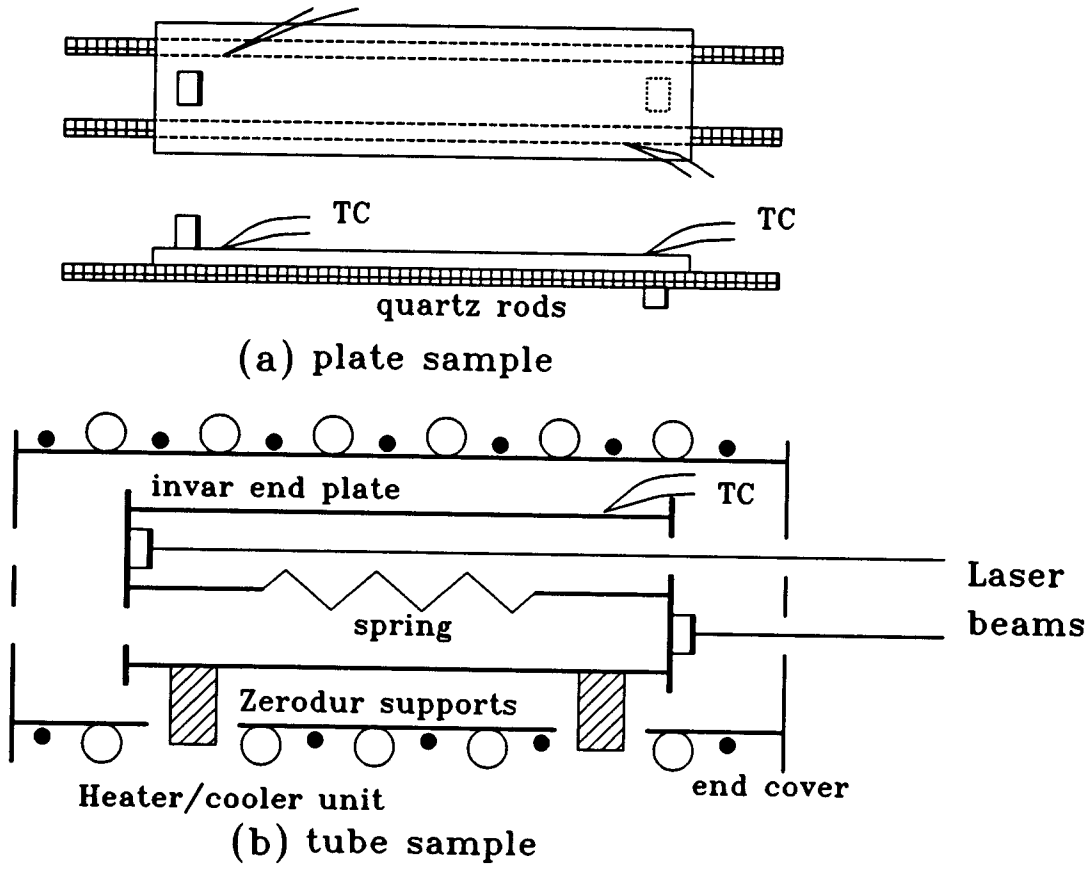

Fig. 19. CTE sample supports and heater/cooler unit

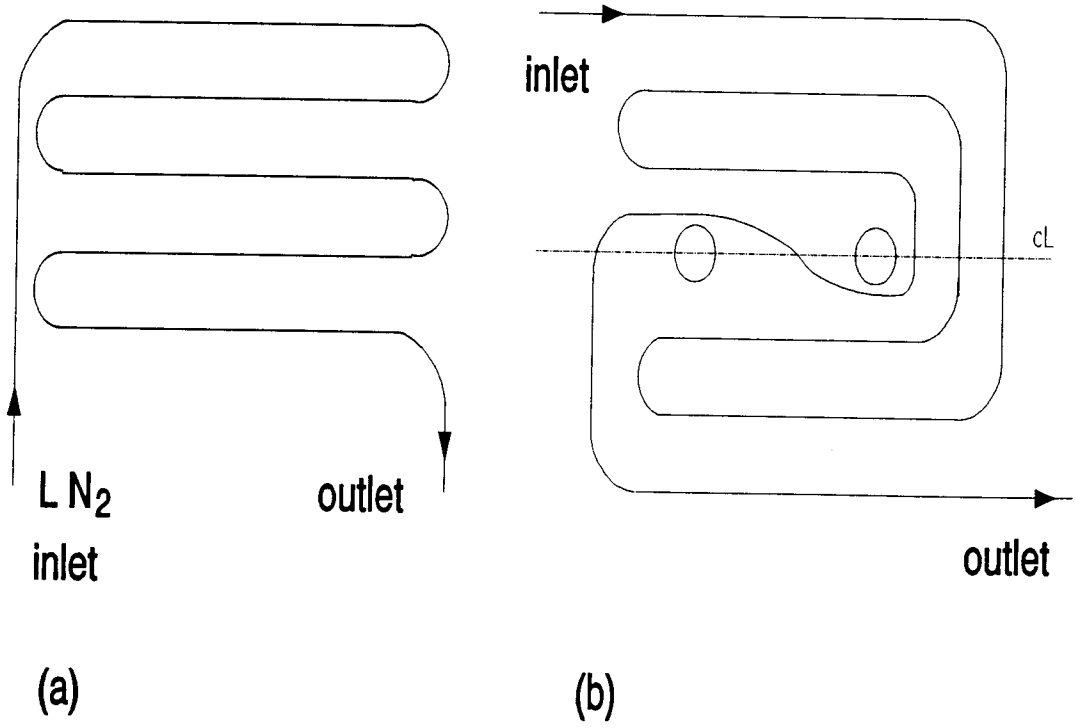

Fig. 20. Liquid nitrogen flow paths, (a) plate cooler (b) circular cooler

vacuum chamber. When air goes into the vacuum, the index of refraction increased by Δn, thus OPLD changed by $\Delta n \cdot L$. This positive value simulates the sample growth.

4.2.4. CTE data Processing

Three methods of analyzing CTE data were used in this work. They are manual analysis, matrix operation approach and fixed parameters approach.

The manual data analysis, based on one of the equations of (3.3), requires only one photodetector trace and a temperature trace to be recorded on chart recorder (SOLTEC-1243 3-pen recorder). The signal moving directions observed from the oscilloscope were marked along with the recorded photodetector trace. One counts the number of cycles, thereafter the sample length change, of the photodetector signal between two thermocouple readings. The temperature conversions of the thermocouple readings were done by the piecewise linear interpolation method described in section 2.4.

During the measurement, interference may disappear due to sample bowing or bending from which the alignment of the two arms of the interferometer is lost. Adjustment has to be made to regain the interference signal. No data except temperature were recorded. This leave a blank interval which needs to be filled in after the data have been

analyzed. By looking at the overall curve, the missed data can be extrapolated with the proper slope. Displacement calculations, extrapolations, and the final curve were done on a spreadsheet such as Quattro in this manual data acquisition procedure.

Since chart recorder was used in the manual analysis method, it is easy to make notes of events, such as vacuum pressure change, expansion direction check or signal jumps due to microcracking, during the test on the chart paper. It is also easy to manipulate the data when the signal is not stable and its DC level (i.e. the ellipse center) is changing. However, this method needs a constant monitoring of the signal moving direction from the oscilloscope. It is also time consuming to convert the row data from chart paper to its final CTE curve.

The photodetector signals and the temperature readings can also be acquired by a data acquisition system and be stored on disk. The data sampling rate should be fast enough so that the signal phase change of every two points is smaller than 180° otherwise the sample expansion/contraction may be misinterpreted. A flag was put into the data sequence during the test to indicate the event of signal loss and regain. The stored data were analyzed by matrix operation method and/or fixed parameters method described in section 3.4. Data reduction, one data point for every one degree celsius for example, can be done

after the calculations. Final curve and missed data extrapolation were made in Quattro.

There is no necessary to monitor the signal moving direction during the test because it was already included in the stored data. Temperature conversion from thermocouple readings was already done by the data acquisition system and stored in disk. Notes can be write into the data file to record the events during the test but it is not that convenient as that on chart paper. Fixed parameters approach allows the AC part of the signal to vary arbitrarily. The local error caused by the changing of the signal DC level to the CTE result can be minimized by given various ellipse centers (h,k) from point to point during the pre-treatment to the data file. This increases the complexity of the data processing procedure and is not used because most of the thermal displacements measured in this work gave more than several signal cycles. The relative large scale of the CTE results were able to smooth out the small local errors. Matrix operation approach requires much more stable signals. Only a few CTE data sets meet the requirements. This method is not recommended in the CTE measurements.

4.3. Speckle Interferometry

Optical configurations of speckle interferometry for measuring out-of-plane and in-plane displacements were investigated. Procedures of system performance verification and FFT analysis to the speckle signals were included.

4.3.1. Out-of-plane motion detection system

Figure 21 shows the out-of-plane speckle interferometry system. Diffuse surfaces such as 3M retro-reflective tape were used to replace the two mirrors in the Michelson interferometer. A 3 mW laser illuminates the diffuse surfaces which form the two speckle patterns. A superimposed speckle pattern was obtained when these two speckle fields came together after the beam splitter. The combined speckle pattern is similar to the individual patterns but sensitive to any out-of-plane disturbances of the two reflecting surfaces. Each speckle grain varies independently but with the same frequency. The beam splitter and the convex lens collect multiple speckle grains to increase the signal intensity level. The calibrated PZT (Burleigh Model: PZL-15) was used to introduce a known displacement to verify the relationship between the speckle signal and the PZT displacement.

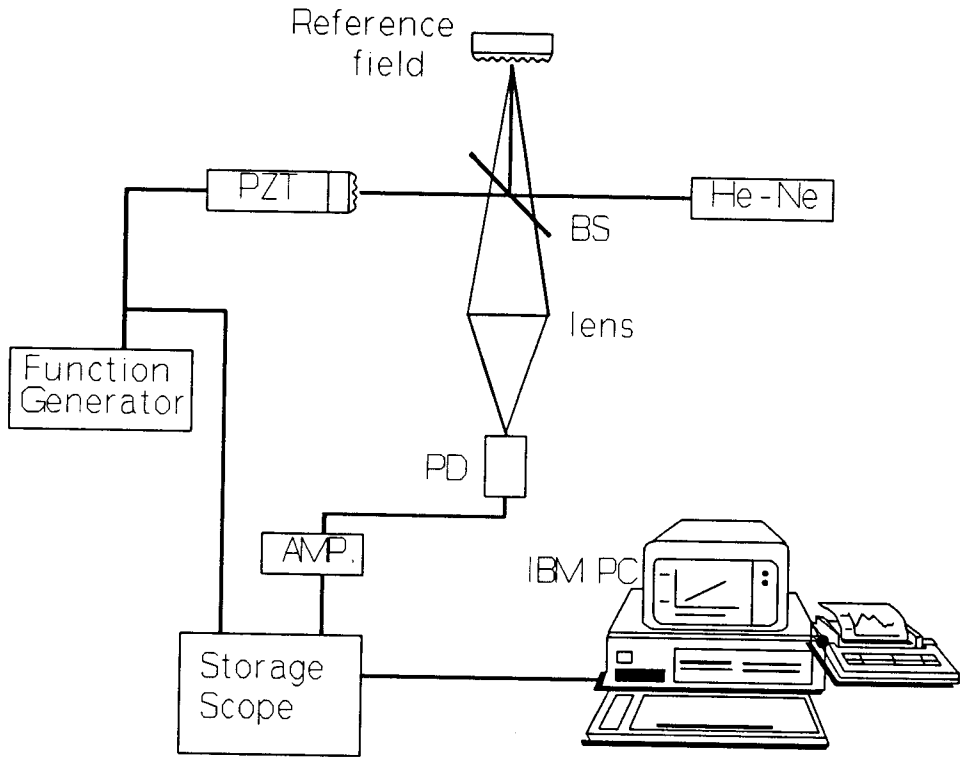

Fig. 21. Speckle interferometer for out-of-plane motion detection

Signals were recorded and stored through the same procedures described in section 4.1. Signal cycles were plotted against applied voltages to verify the out-of-plane motion speckle detection system.

4.3.2. In-plane motion detection system

In-plane displacement can be measured independently of any out-of-plane component with speckle interferometry. The double illumination configuration [Sarrafzadeh-Khoee 1986] was used for the in-plane motion detection system. Two identical but oppositely directed paths were taken by the beams and both form closed loops before they were superimposed. Due to the angular symmetry of the double-illumination beams with respect to the surface normal, only in-plane displacement of the illuminated area gives rise to twice the optical phase change for each beam. The change of the optical path length difference (ΔOPLD) at a point-of-observation (on the interferometric speckle image) were calculated for the obliquely illuminated retro-reflective diffusing surfaces which undergo a displacement, d, as follows;

$$\Delta OPLD = \Delta\phi/k = 4\ d\ \sin\theta \qquad (4.1)$$

or

$$\Delta\phi = (8\pi\ d\ \sin\theta)/\lambda \qquad (4.2)$$

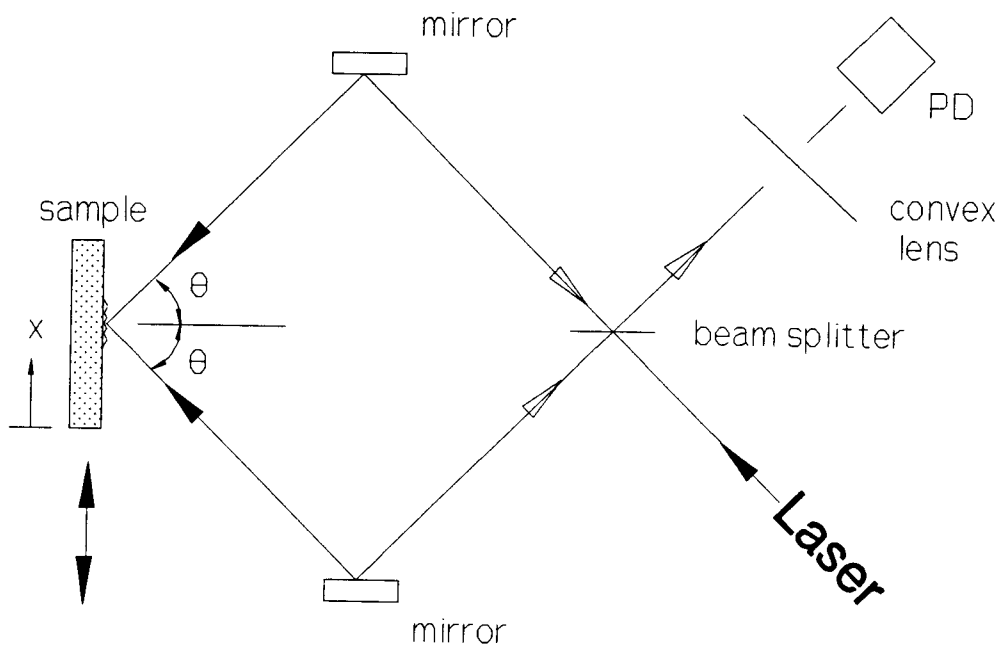

Fig. 22. Speckle interferometer for in-plane motion detection

For $\Delta\phi$ changed by one cycle (2π), d will change by $\lambda/4\sin\theta$. In the common case of θ=45° and assume He-Ne laser is used (λ=632.8 μm), this value will be 0.224 μm. The sensitivity to the in-plane displacement is doubled compared to the conventional speckle interferometer based on Leendertz's arrangement (figure 5). Verification of the in-plane motion speckle detection system was performed similar to that of the out-of-plane system.

4.3.3. FFT analysis to speckle signals

Small vibrations in both out-of-plane and in-plane speckle system were generated by a PZT at various amplitudes and frequencies. Speckle signals correspond to these vibrations were acquired by the same data acquisition system used in PZT calibration setup (section 4.1.). The stored time domain data were transformed by FFT subroutine to their frequency domain. Frequency distribution was then plotted in Quattro.

The speckle signal level was usually low, its amplitude was on the order of 100 mV. The electronic noise became noticeable in this situation. However, the electronic noise level was reduced from 200 mV to 20 mV by separating the high voltage laser power supply from the signal power supply and by using a TEKTRONIX 50 ohm, 2 watt "TERM" connector (Model: 011-0049-01) between the

photodetector and the oscilloscope. The signal to noise ratio was thereby increased from 0.5 to 5.

It was interesting to know how small a vibration displacement can be recognized by the speckle systems with the FFT analysis method. The PZT was oscillating at 5 KHz with various amplitudes determined by the applied voltages to the PZT and its characteristic displacements (μm/volt). The height of the peak at 5 KHz of the FFT results indicated that whether the amplitude can be detected or not. The minimum detectable vibration amplitude was set when the 5 KHz peak got down to about twice of the nearby, 2 to 8 KHz, background frequencies.

Frequency analysis provides many NDT applications. One simple example is to determine the modulus of elasticity of a material from its resonance frequency. A system similar to figure 21, but replace the PZT and function generator by a steel rod and a steel ball, was used to detect the resonance frequency. Both mirrors and diffuse surfaces were used in the optical system for comparison.

CHAPTER 5. RESULTS AND DISCUSSIONS

5.1. PZT Calibration Data

The characteristic displacements (μm/volt) of the PZT at different frequencies were obtained in this work. Figure 23 shows the time series data of the optical signal and the applied voltage at 0.5 Hz. The applied voltage (30 volts peak-peak) and the signal voltage (typically 3 volts peak-peak) were recorded in different scale for convenience in using TEKMAP program. However, it is the signal phase (not the absolute voltage) which relates to the displacement. There are 8 signal cycles counted over 30 volts. The average displacement per volt obtained by the fringe counting method is

(no. of cycles * half wavelength/cycle)/total voltage
= (8.0 cycle * 0.3164 μm/cycle)/30 volts
= 0.084 μm/volt.

Figure 24 shows the data points plotted in the V_x-V_y coordinates on Quattro. A solid line in this figure indicates the reference ellipse for this data set. Reference parameters were calculated in the spreadsheet as h=0.75, k=0.67, a/b=0.68, δ=35. A complete displacement cycle obtained by the fixed parameters approach was given

in figure 25. A PZT is not a perfectly linear device, the forward path is slightly different from backward path. The overall slope of the curve in this figure is 0.084 μm/volt. Second order polynomial fitting was performed on the data for both lower and upper curves. Figure 26 shows an example of original data along with the fitted curve. Root mean square errors (RMSE) were calculated over these data sets. Table 4 summarizes the fitted equations and their RMSE's. An average RMSE of 0.0086 μm is obtained. Higher accuracy can be achieved by increasing the resolution of the data acquisition system from, for example, 8-bit to 12-bit.

Figures 27 to 28 show similar results but with different frequencies of the applied voltages. The overall slope are lower as the frequencies go higher (Table 5).

Table 4. Root mean square errors

Data sets	fitted equation	RMSE(μm)
Fig.25. Lower curve	$y=0.0117x^2+3.246x-0.108$	0.0069
Fig.25. Upper curve	$y=-0.0097x^2+3.242x+4.440$	0.0082
Fig.26. Lower curve	$y=0.0118x^2+2.927x-0.0474$	0.0095
fig.26. Upper curve	$y=-0.0157x^2+2.924x+4.671$	0.0096
Average RMSE=0.0086, STD=0.0011		

Table 5. PZT characteristic displacements

Frequencies (Hz)	Slope (μm/volt)
0.5	0.084
50	0.075
500	0.067
1,000	0.065

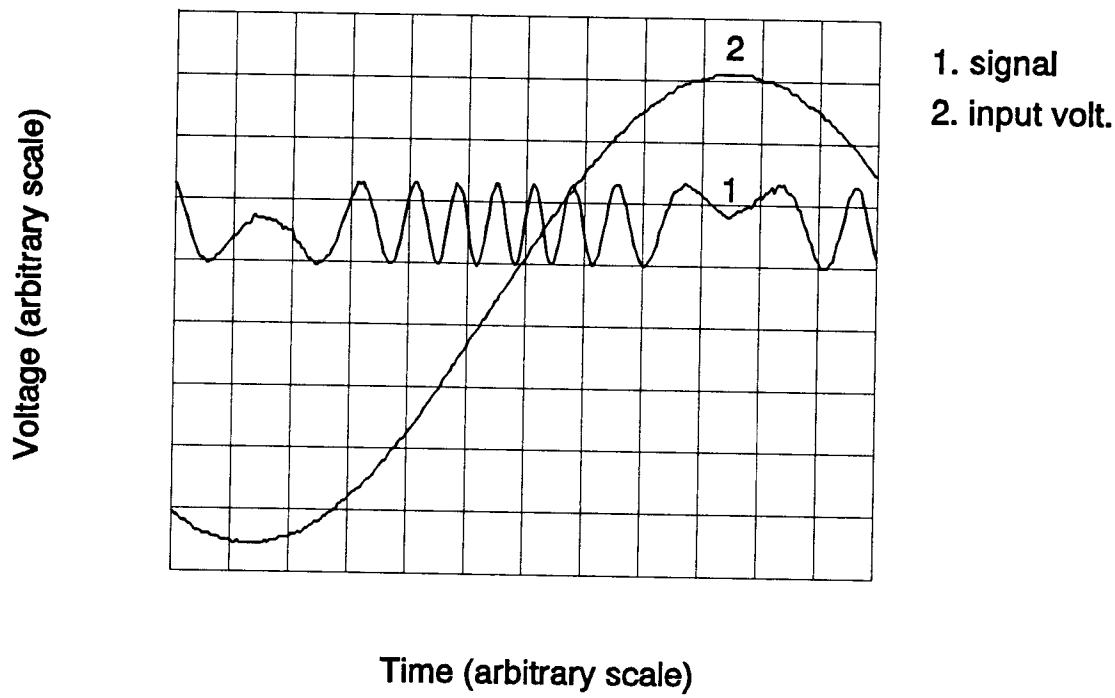

Fig. 23. PZT induced out-of-plane motion signal, mirror reflection

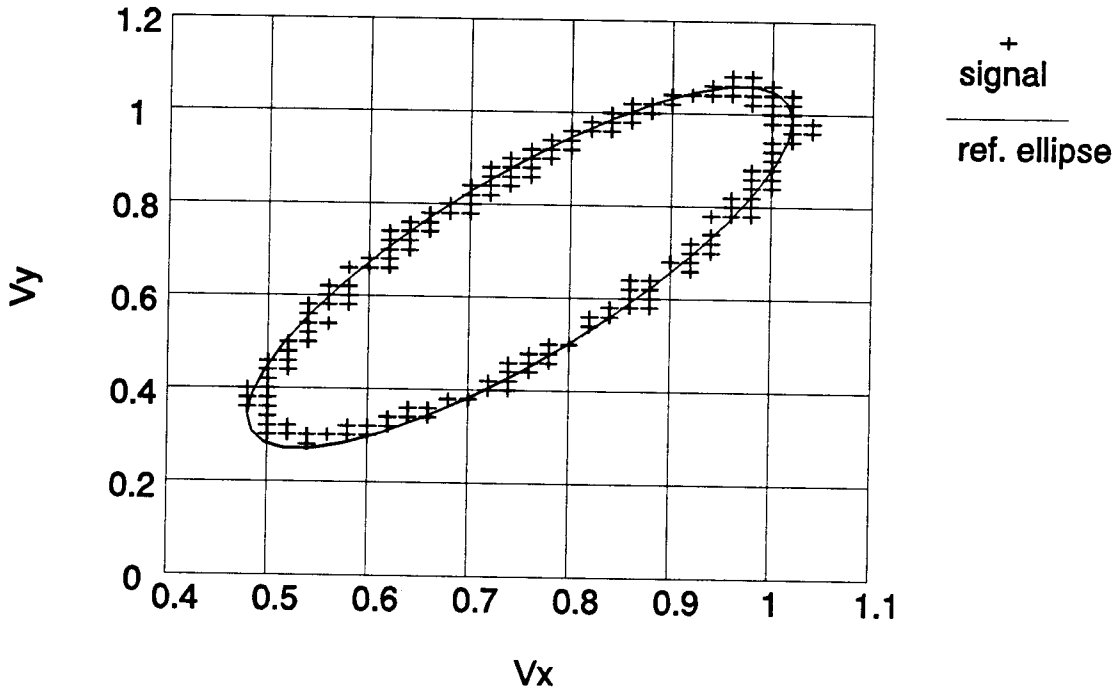

Fig. 24. Signals and their reference ellipse : h=0.75, k=0.67, a/b=0.68, δ=35°

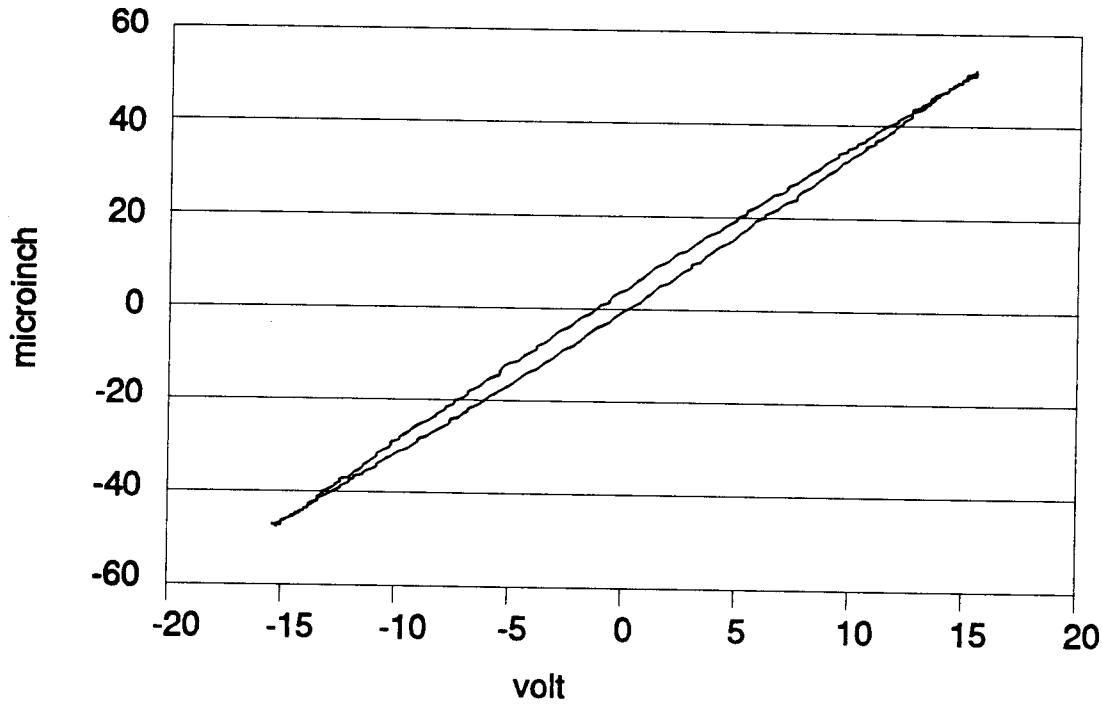

Fig. 25. PZT displacement, input frequency=0.5 Hz

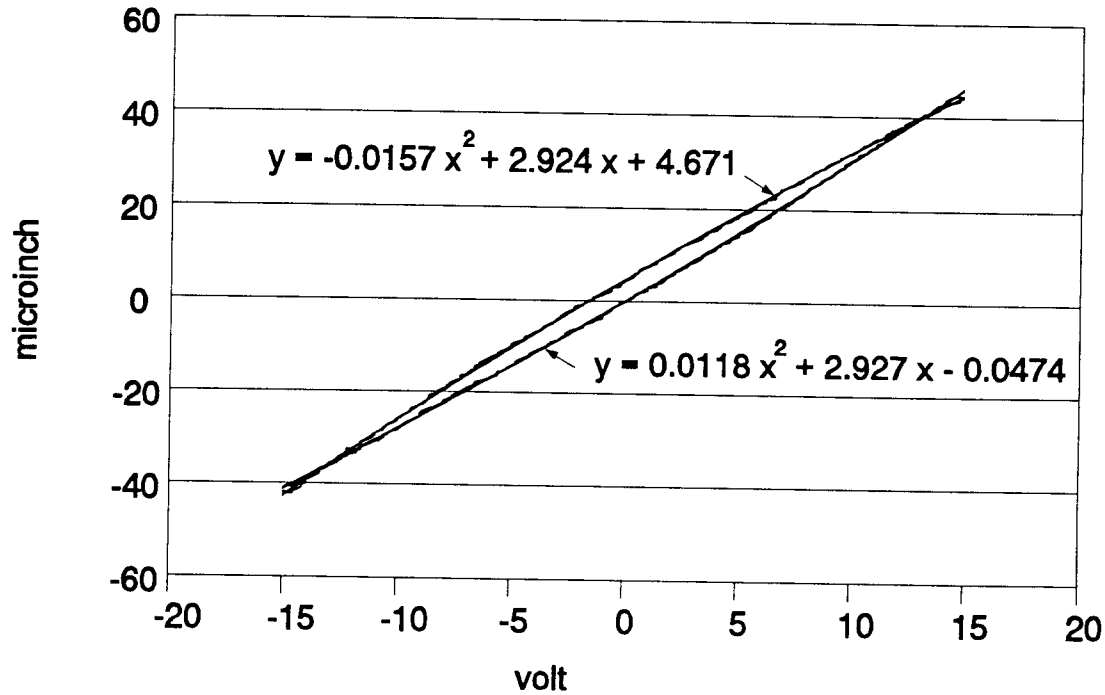

Fig. 26. PZT displacements with 2nd-order polynomial fitting, input frequency=50 Hz

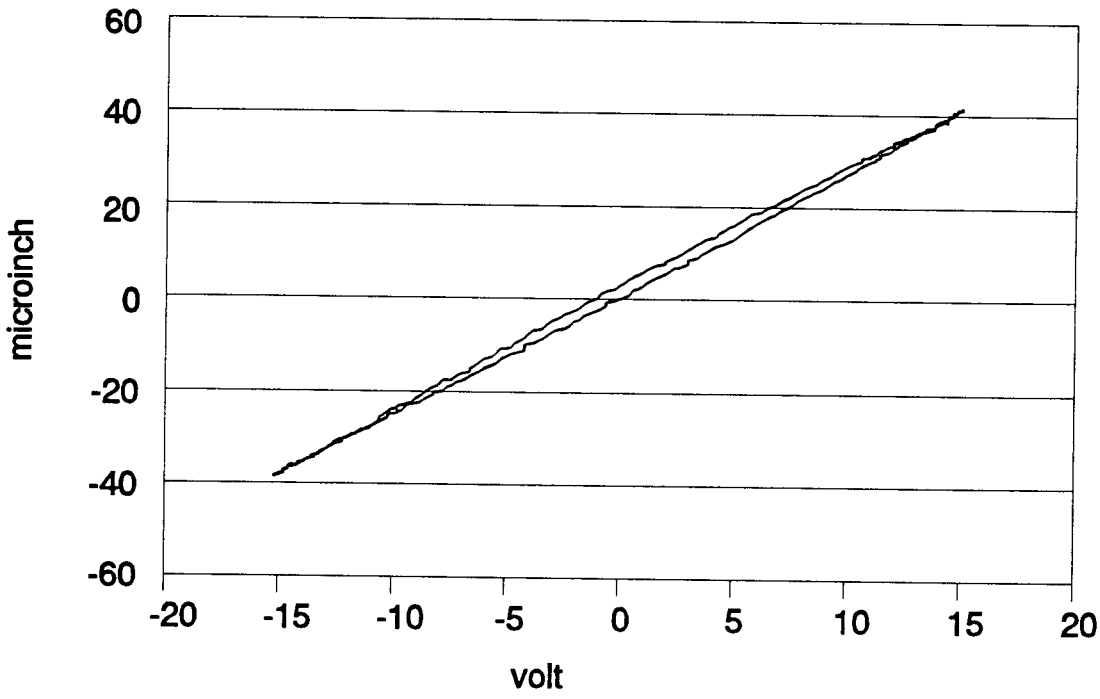

Fig. 27. PZT displacement, input frequency=500 Hz

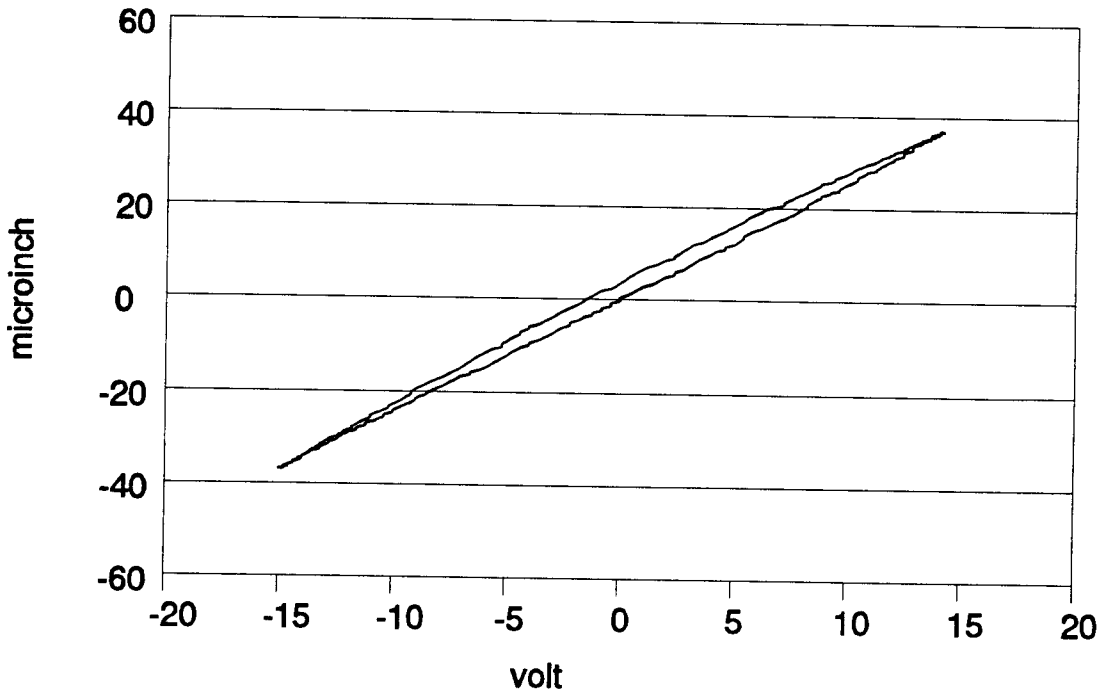

Fig. 28. PZT displacement, input frequency=1000 Hz

5.2. CTE Data

The CTE of a 25mm x 100mm x 1.6mm thick GE type 124 fused silica plate was tested at a heating/cooling rate of 1.5°C/min. Data were analyzed by manual chart method. The first cycle (figure 29) gave a CTE value clearly too low at higher temperature range (0.22 $\mu\epsilon$/°C at 35-60°C) when compared to the reference data listed in appendix A of the similar material (NBS SRM739). Suspicions were given to the incompletely cured adhesive holding the reflective mirrors on the plate sample. Subsequent work emphasized use of the proper resin to hardener ratio and adequate cure time/temperature. Figure 30 shows the next 3 cycles of the CTE curves of this sample after holding it at 60°C for 1 hour. The slope of the curve at room temperature is 0.49 $\mu\epsilon$/°C which is close to the reference data (appendix A). The maximum deviation of the three CTE curves in this figure is 4 $\mu\epsilon$ which is smaller than the NBS SRM 739 standard deviation, ± 6 $\mu\epsilon$.

Due to the relatively low thermal conductivity of silica, hysteresis becomes noticeable (figure 31) at a higher heating/cooling rate (3°C/min.) and the apparent slope is about 0.44 $\mu\epsilon$/°C at room temperature. The same test were also analyzed by the fixed parameters approach. The data trajectory is shown in figure 32. Signal intensity (interpreted as the ellipse size) was changing

during the test. However, one set of the ellipse parameters, h=-0.19, k=-1.20, a/b=0.61, δ=32°, is able to represent the whole data trajectory as can be seen if you superimpose this figure with the reference ellipses depicted in figure 33. The number of CTE data calculated from fixed parameters approach were reduced to one point per °C and plotted in figure 34. It is seen that both manual chart method and fixed parameters method give the same slope of 0.44 $\mu\epsilon$/°C at room temperature. The two curves does not look exactly the same because of the difference of the temperature recording devices, that is chart recorder and data acquisition unit. The latter one has better temperature accuracy because it has the cold junction reference temperature compensation for the thermocouples. However, the overall shapes of these two figures obtained from different analysis methods were very similar.

A 50 mm dia. by 2.5 mm wall thickness GE type 124 quartz tube was tested in the length (203 mm) direction. Figure 35 shows that the results were as expected as when compared to the reference data, with a CTE of 0.50 $\mu\epsilon$/°C near room temperature and 0.56 $\mu\epsilon$/°C at 80°C. The measurement system and analysis methods were verified for the CTE of thin plate and thin walled tube samples.

The CTE of a thin composite plate (M40J/F584, isotropic layup, 12 plies thick) was measured in a similar

manner to the quartz plate. Table 6 gives the properties of the composite materials. Preheating just below the maximum temperature assures both complete sample dryout and mirror adhesive cure. It may also be desirable to subject the sample to a complete heating/cooling cycle prior to taking CTE data because of lower temperature microcracking effects caused by a relief of residual composite curing stresses. The greater thermal conductivity of the carbon fibers means less thermally induced hysteresis than is found with glasses, as shown in figure 36. The measured CTE of the plate, 1.46 $\mu\epsilon$/°C, is about twice of the predicted value, 0.70 $\mu\epsilon$/°C predicted by SQ5. Difference may be arisen from many factors such as incorrect of volume fractions, modulus of elasticity, ··· etc..

The CTE of a graphite epoxy tube (P75/F584, isotropic layup, 12 plies thick) was tested in a similar way to the quartz tube. Results were analyzed by both fixed parameters approach and matrix operation approach. Data reduction, one data point per °C, was performed to reduce the size of the data file. The values of the overall CTE's were very close, 1.18 $\mu\epsilon$/°C (figure 37) and 1.16 $\mu\epsilon$/°C (figure 38) from these two methods respectively. The two flat segments in figure 37 correspond exactly to the signal loss events recorded earlier during the test. Thus, extrapolation for the lost data can be done easily in a spreadsheet. Matrix operations did not pick up these

events exactly. It was also suffered by the signal intensity fluctuations as you compare the curves in these two figures. Fixed parameters approach performed better than the matrix operation approach in the CTE measurement works.

The estimated CTE of this composite was found to be -0.117 $\mu\epsilon$/°C (predicted by SQ5). The relative complex shape, a circular tube rather than a flat plate, of the sample may alter the stress-strain states calculated by the conventional software and made the predictions much difficult. Advanced techniques such as finite element analysis would be a better tool to make the prediction.

Table 6. Properties of composite materials

composite	V_f (%)	E_f (msi)	α_f ($\mu\epsilon$/°F)	E_m (msi)	α_m ($\mu\epsilon$/°F)	ν_{12}
M40J/F584	0.6	55.0	-0.50	0.6	38	0.26
P75/F584	0.6	72.7	-0.73	0.6	38	0.30

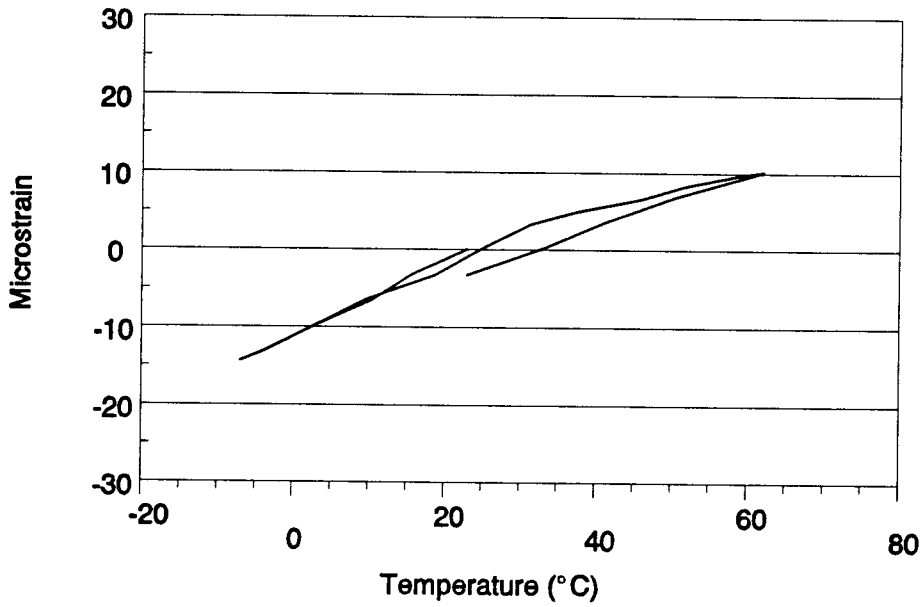

Fig. 29. Effect of incompletely cured adhesive to CTE

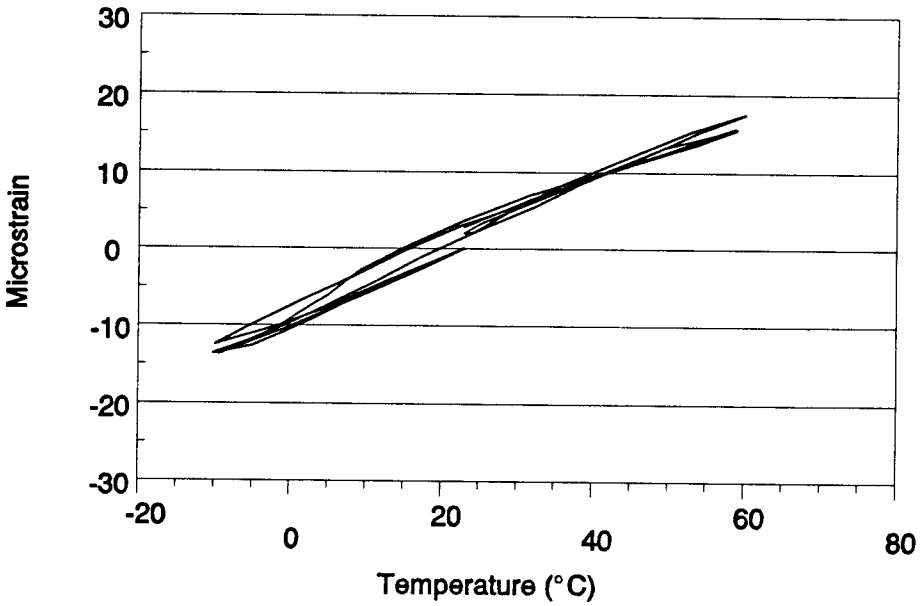

Fig. 30. CTE of fused silica plate, heating/cooling rate=1.5°C/min., chart.

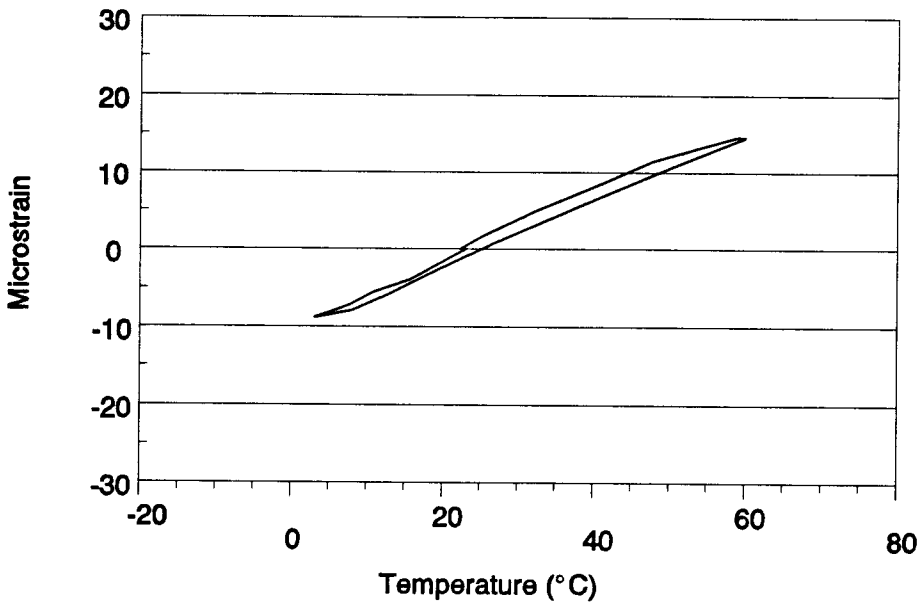

Fig. 31. CTE of fused silica plate, heating/cooling rate=3°C/min., chart

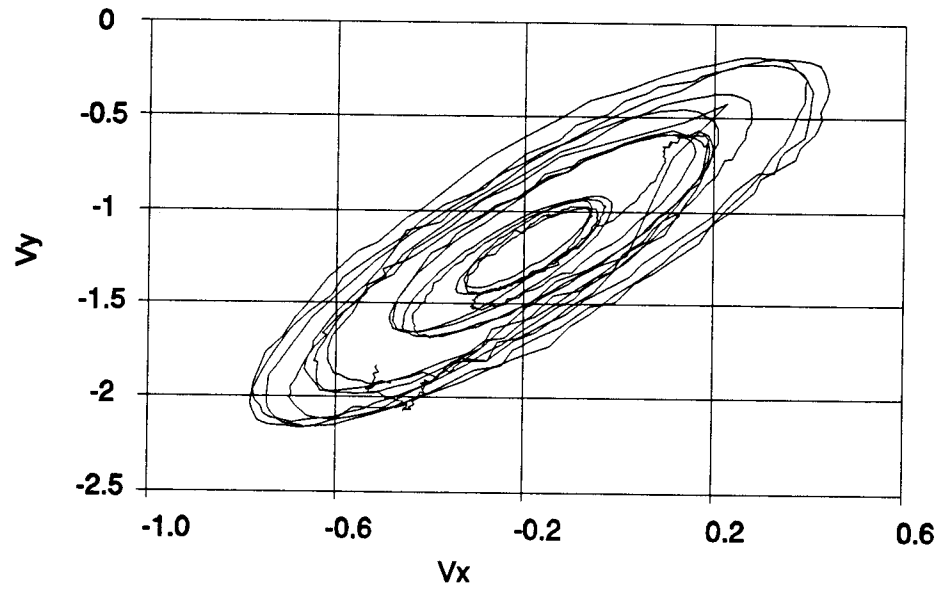

Fig. 32. Typical CTE data trajectory, ellipse parameters : h=-0.19, k=-1.20, a/b=0.61, δ=32°

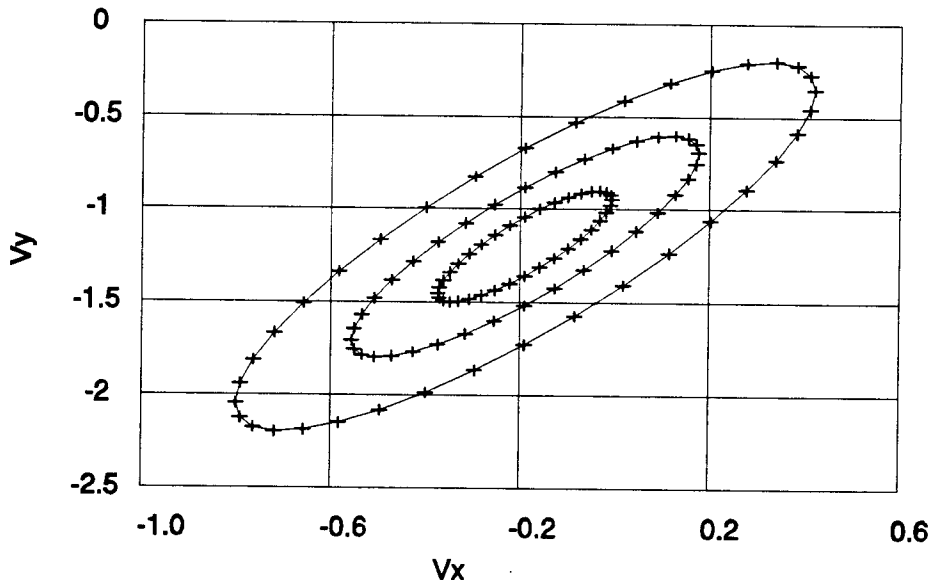

Fig. 33. Reference ellipses with h=-0.19, k=-1.20, a/b=0.61, δ=32°

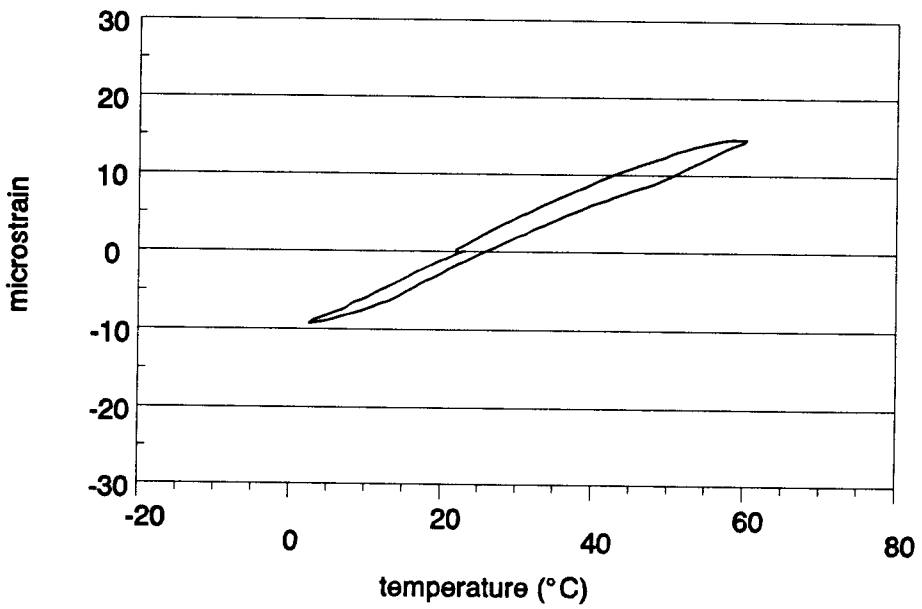

Fig. 34. CTE of fused silica plate, heating/cooling rate=3°C/min., fixed parameters

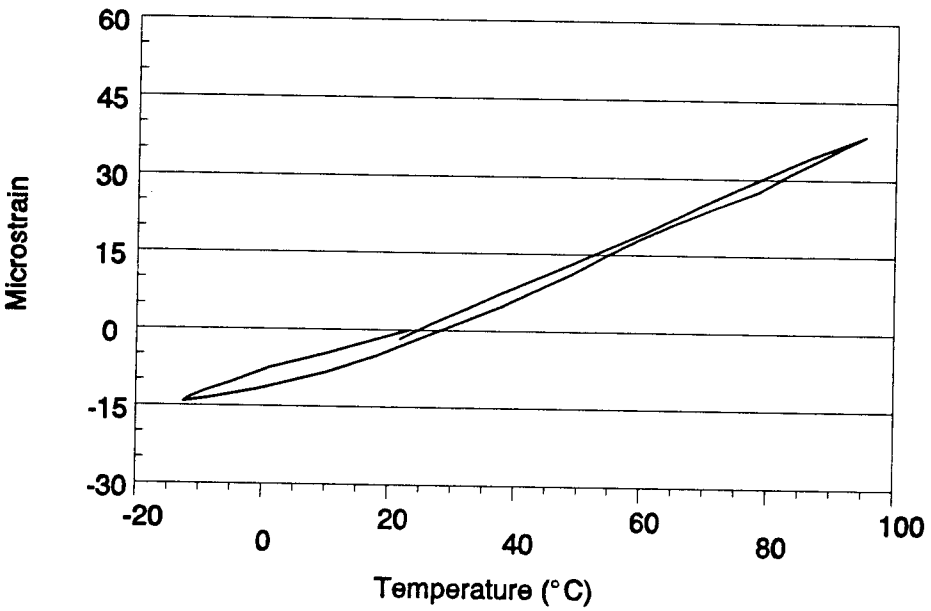

Fig. 35. CTE of fused silica tube, chart

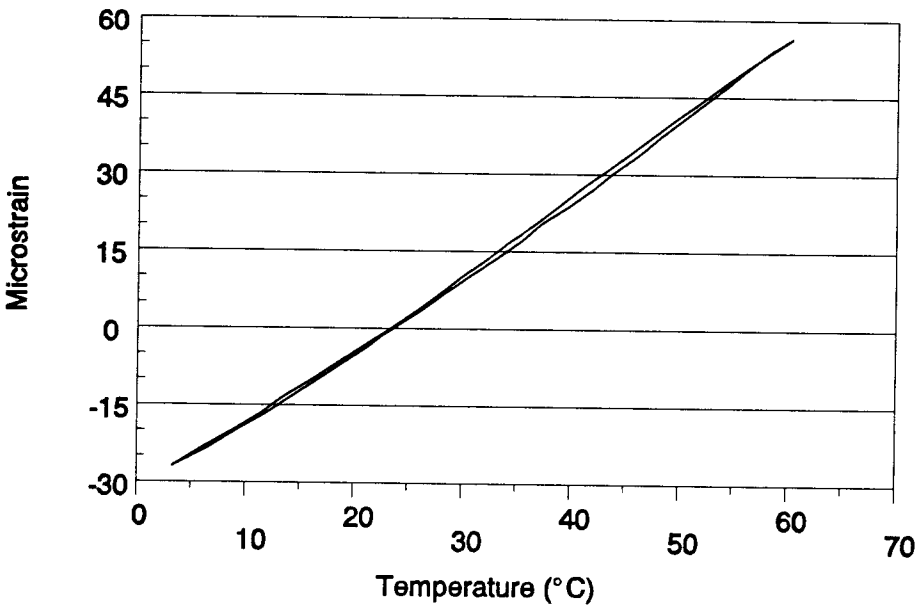

Fig. 36. CTE, composite plate, chart

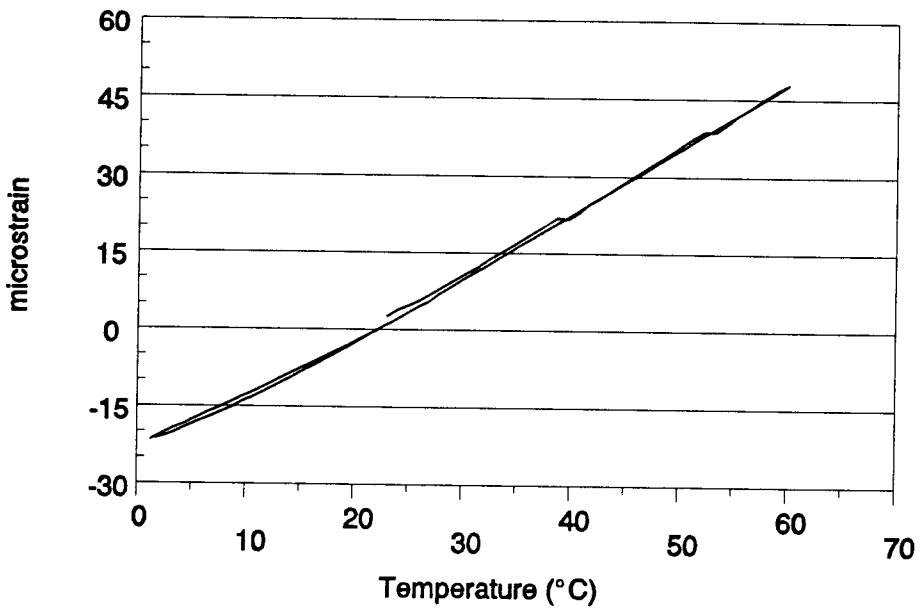

Fig. 37. CTE, composite tube, fixed parameters.

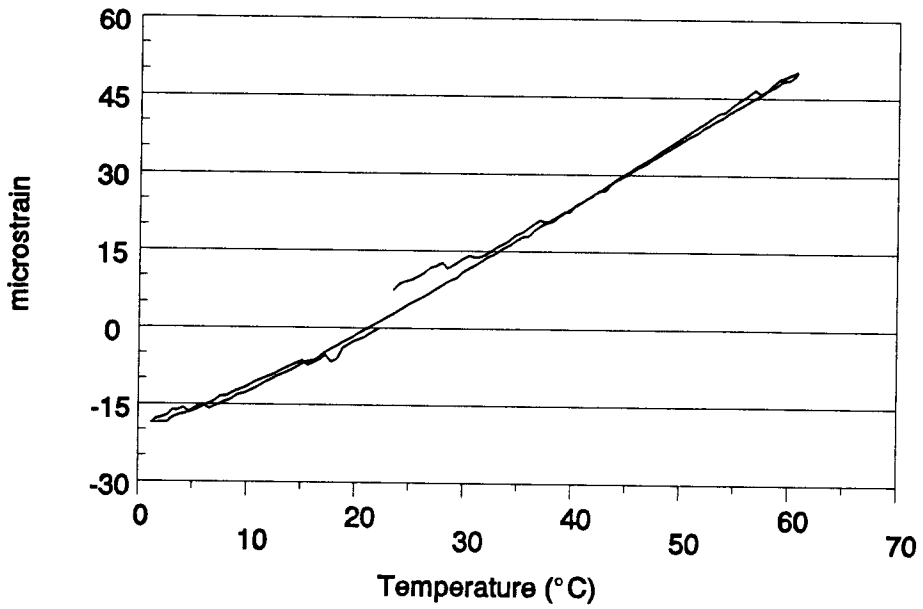

Fig. 38. CTE, composite tube, matrix operation.

5.3. Speckle Interferometry Verification Data

The known displacements introduced by a calibrated PZT were measured by speckle interferometry for both out-of-plane and in-plane configurations. The out-of-plane motion can be detected by the Michelson type speckle interferometer. Although its physical interference phenomena are different from the traditional Michelson interferometer, not only the optical configurations but also the signal variation patterns are similar to each other as one compares figure 39 with figure 23. However, the signals generated from the speckle system were not as clear as that from the Michelson interferometry because of the lower signal intensity level reflected from the diffuse surfaces in the former system than that from the specular surfaces in the latter one. The total PZT displacements over the applied 30 volts were counted as

8 cycles x 0.3164 μm/cycle = 2.53 μm

The same displacement was also introduced in the in-plane motion speckle detection system, double illumination configuration, 11.7 total signal cycles over 30 V was observed in figure 40 , thus the displacement corresponding to one signal cycle in this double illumination system is

2.53 μm / 11.7 cycles = 0.216 μm/cycle

Figure 41 shows a complete displacement cycle obtained from fringe counting method. The overall shape of this curve is similar to those (figures 25 to 28) obtained from Michelson interferometry. Signal variation patterns are the same in each system but resolutions (μm/cycle) are different. The resolution of the double illumination system is adjustable with the light incident angle θ. When the θ in figure 22 changed by moving the sample a distance to the left, the number of signal cycles over the same displacement changed too. Table 7 summarizes the results of 3 different incident angles and their corresponding resolutions. The number of total signal cycles decreased as the angle θ decreased while the total displacements still remained the same. The measured corresponding resolutions of each θ were very close, 3.57 % error maximum, to the calculated values ($\lambda/4\sin\theta$, described in section 4.4.).

Table 7. In-plane speckle system resolutions

Incident angle, θ	# of total cycles	measured (μm/cyc.)	calc. (μm/cyc.)	error (%)
45°	11.7	0.216	0.224	3.57
40°	10.2	0.248	0.246	0.81
17°	4.7	0.538	0.541	0.58

* Total displacements = 2.53 μm

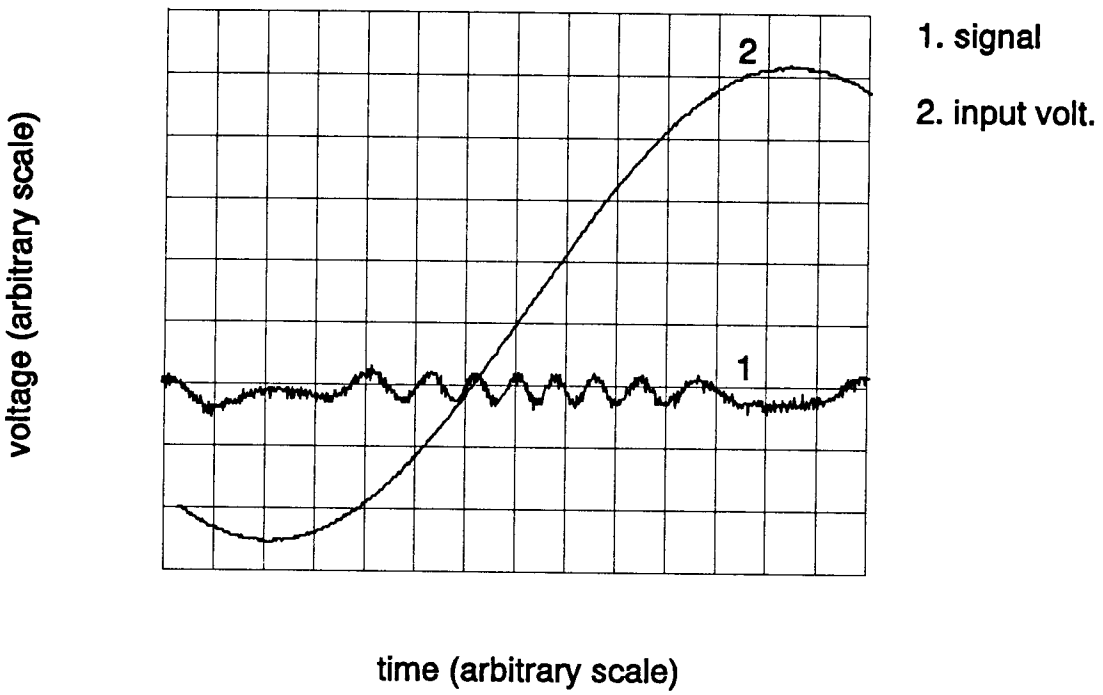

Fig. 39. PZT induced out-of-plane motion signal, diffuse tape reflection

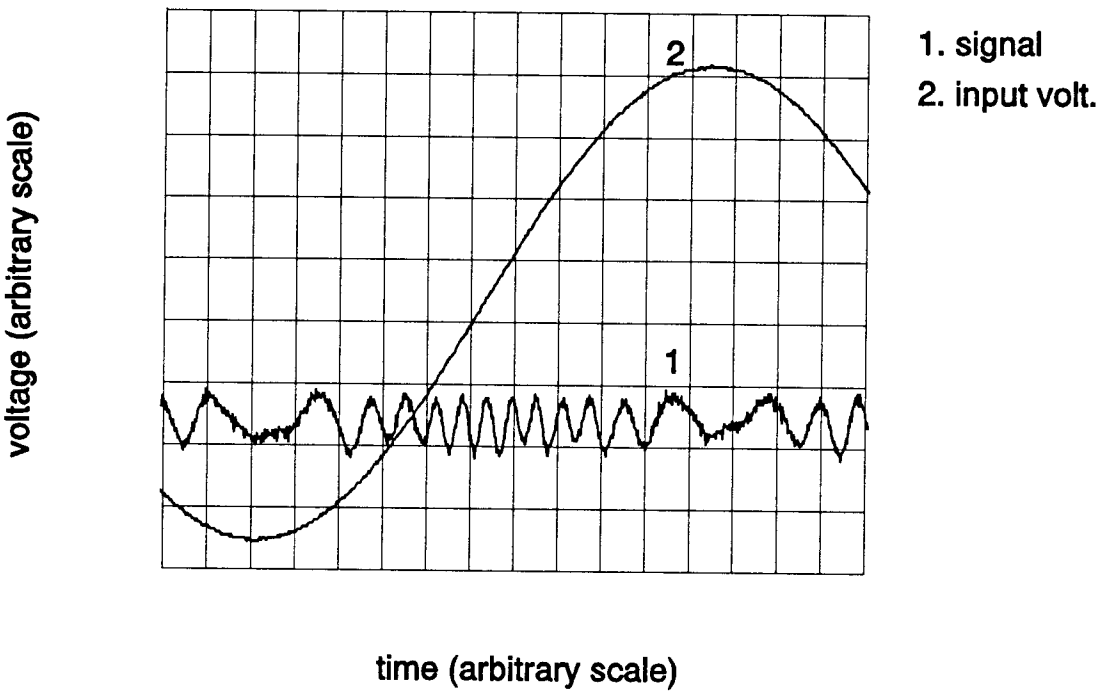

Fig. 40. PZT induced in-plane motion signal, diffuse tape reflection

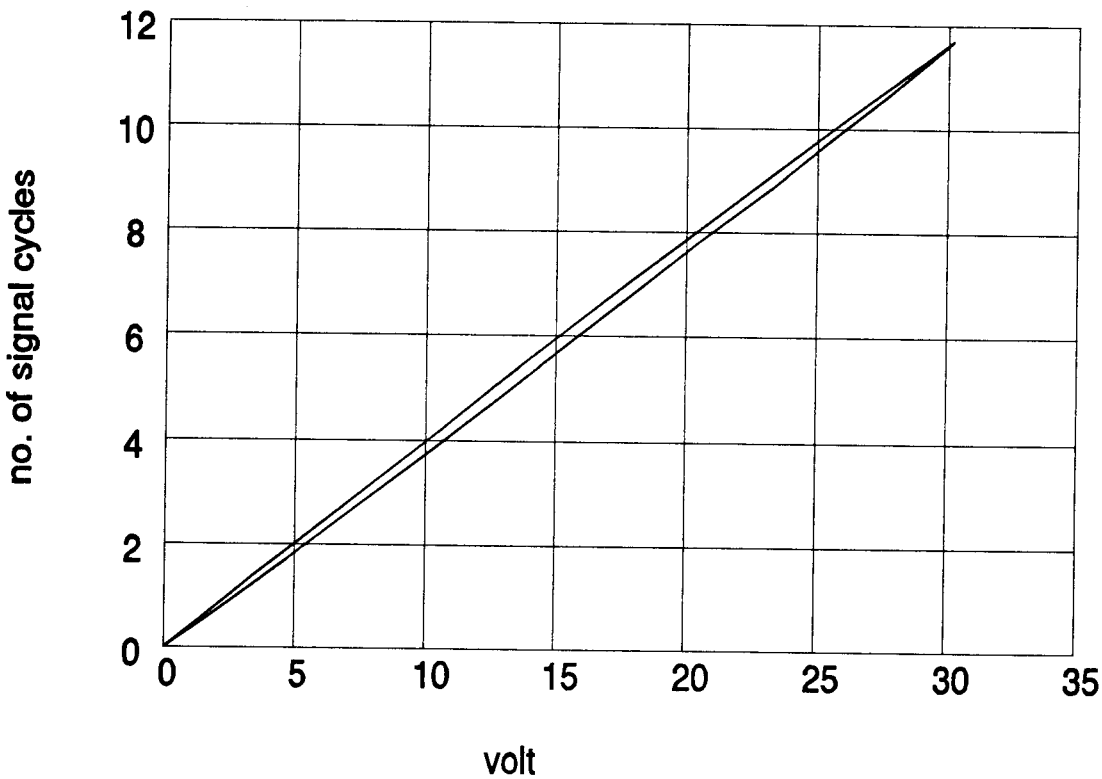

Fig. 41. PZT induced in-plane motion signal cycles against input voltage

5.4. FFT Results of Speckle Signals

5.4.1. Characteristic noise in speckle systems

Two characteristic noise frequencies were found at 120 Hz (figure 42) and 50 KHz (figure 43). 100 KHz noise was also found occasionally. The 120 Hz noise came from the room light and the power line. The 50 KHz noise may come from the amplifier box. These two frequencies will be ignored from the FFT results as we go along.

5.4.2. FFT outputs with single input frequency

The PZT in figure 21 was vibrating at 1 KHz with an amplitude of 0.13 μm ($\lambda/5$). The detected optical signal showed a clear peak at that frequency (figure 44). However, a doubled frequency (2 KHz in figure 45) was also detected with the same vibration conditions. This phenomena is much like the 2nd harmonic effect in the signal amplification/modulation techniques and can be thought of that the optical signal oscillating across a maximum or minimum point. Half cycle of the input signal will generate one cycle in the output as can be seen in figure 46. The phase angles ϕ_{12} and ϕ_{23} are chosen the same, that means the vibration amplitude is the same. If the optical signal oscillates between points 1 and 2, the

output frequency will be the same as the input frequency. On the other hand, if the optical signal oscillates between points 2 and 3, then the output frequency will be doubled of the input frequency because of the symmetry of the output with respect to the midpoint. For a large vibration amplitude, in the cases of more than one signal cycle which is 0.3164 μm in Michelson interferometry system, the output frequency is more complicated. Figure 47 showed the FFT result of vibration at 1 KHz with amplitude of 0.78 μm (1.2λ). Higher order harmonics were also observed at 2 KHz, 3 KHz, ...etc.. The observation that one oscillation frequency generates different FFT output frequencies suggests more caution when interpreting the results in real applications. Analyses of large displacement vibrations are not recommended for the system.

5.4.3. Minimum detectable displacements

To determine the minimum detectable displacements by the speckle system with FFT analysis, one measured the peak heights of the FFT results with various vibration amplitudes at a fixed frequency. Figure 48 showed a typical FFT result with a peak at 5.2 KHz for the out-of-plane speckle system. The peak heights got smaller as the vibration amplitudes was reduced. Table 8 summarized the vibration amplitudes, the peak heights and the signal to

noise ratio at 5.2 KHz. A peak, with signal/noise=2.5, was still found in figure 49 as the vibration amplitude lowered to 0.0065 μm. The last test was repeated 3 times to assure its reproducibility. No peak was observed beyond this point. Thus, the minimum detectable vibration displacement was set to 0.0065 μm for the out-of-plane speckle system.

The same procedures were performed to obtain those values for the in-plane speckle system and the traditional Michelson system. Figures 50 and 51 showed two typical examples of signals at 5 KHz along with two characteristic noise frequencies at 120 Hz and 50 KHz. Table 9 summarized the results. In-plane speckle system has higher resolution than the out-of-plane speckle system, 0.224 μm/cycle vs. 0.3164 μm/cycle, thus a smaller detectable displacement was expected, 0.0038 μm vs. 0.0065 μm. However, the Michelson system has the highest detection capability, 0.001 μm, due to the higher signal intensity level resulted from mirror, instead of diffuse surface, reflections.

5.4.4. Resonance frequency detection

Resonance frequency of a steel rod (22 mm dia.x 230 mm long) excited by a steel ball (8 mm dia.) was detected by both mirror and diffuse surface reflections. Results showed that the resonance frequency was 11.7 KHz in both figures 52 (with mirrors) and 53 (with diffuse tape). The

resonance frequency can be thought of as the reciprocal of the round trip traveling time of the stress wave in the rod. That is;

$$R.F.= 1/(2\cdot L/V) \tag{5.1}$$

where R.F.= resonance frequency (Hz)

L = rod length (m)

V = speed of stress wave (m/sec)

One example of the application of the resonance frequency in NDT techniques is to determine the modulus of elasticity of a material. Since the speed of the stress wave in the rod is $V= 2\cdot L\cdot(R.F.)= 5382$ m/sec, the modulus of elasticity E of the steel rod can be calculated as

$$E = V^2\cdot\rho(1+\nu)(1-2\nu)/(1-\nu) \tag{5.2}$$
$$= 182 \text{ GPa}$$

Where

$\nu= 0.27$, $\rho= 7850$ kg/m^3

There was a 9% error from the book value, E=200 GPa. The difference may arise from the material constants ν and ρ.

Table 8. Vibration amplitudes vs. FFT peak heights

Vibration amplitudes (μm)	FFT peak heights at 5.2 KHz	noise level between 2-8 KHz	signal/noise ratio
0.130	0.610	0	∞
0.026	0.038	0.002	19
0.013	0.018	0.003	6
0.0065	0.010	0.004	2.5
< 0.0065	no peak	NA	NA

Table 9. Minimum detectable vibration amplitudes

Detection systems	Detectable displacements (μm)
Out-of-plane speckle	0.0065
In-plane speckle	0.0038
Michelson	0.0010

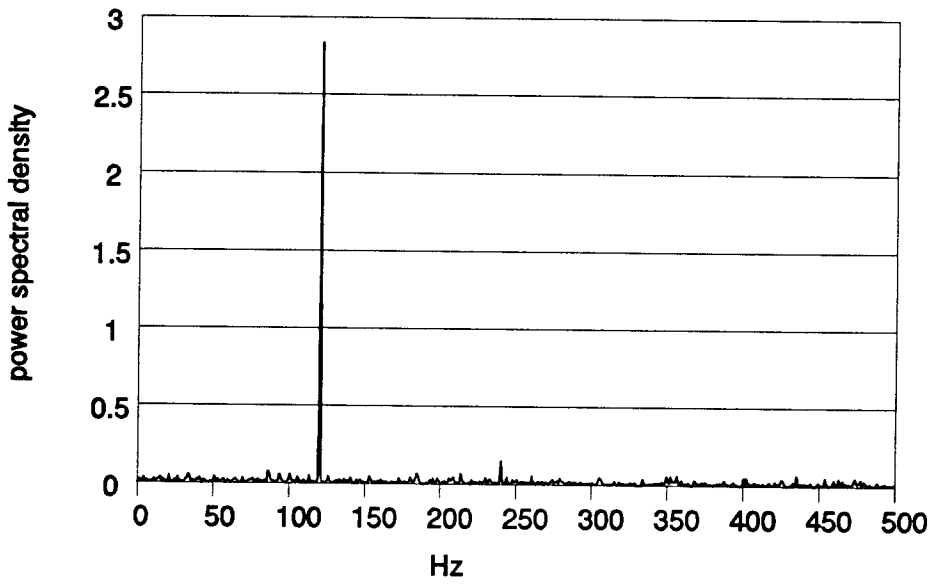

Fig. 42. System noise frequency at 120 Hz

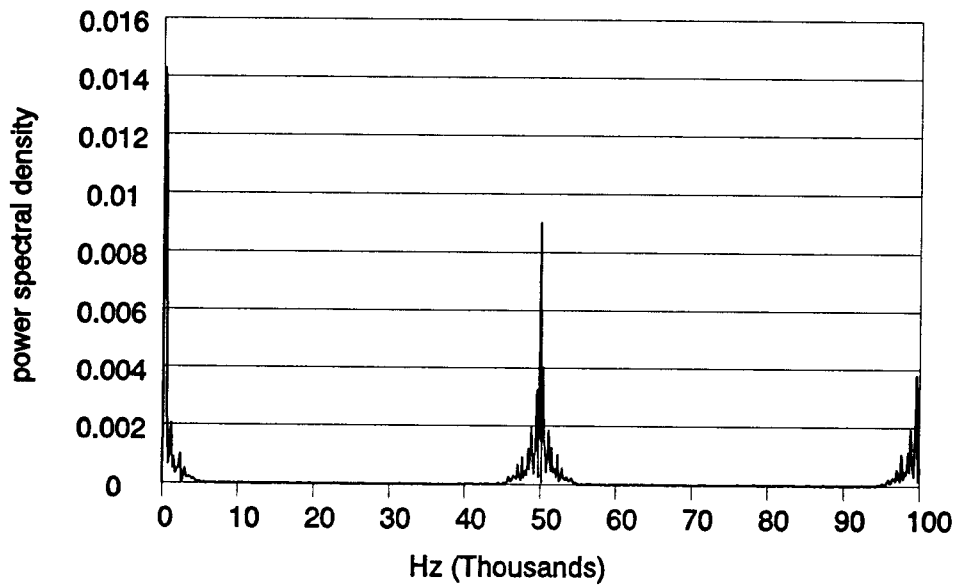

Fig. 43. System noise frequencies at 120 Hz, 50 KHz and 100 KHz

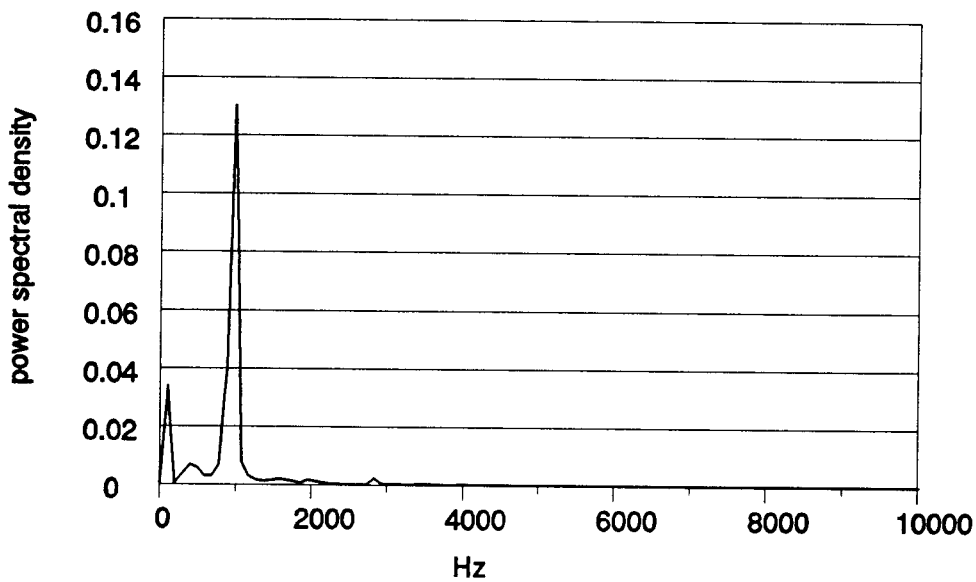

Fig. 44. FFT of the out-of-plane speckle interferometry, input signal : A=0.13 μm (λ/5), f=1 KHz

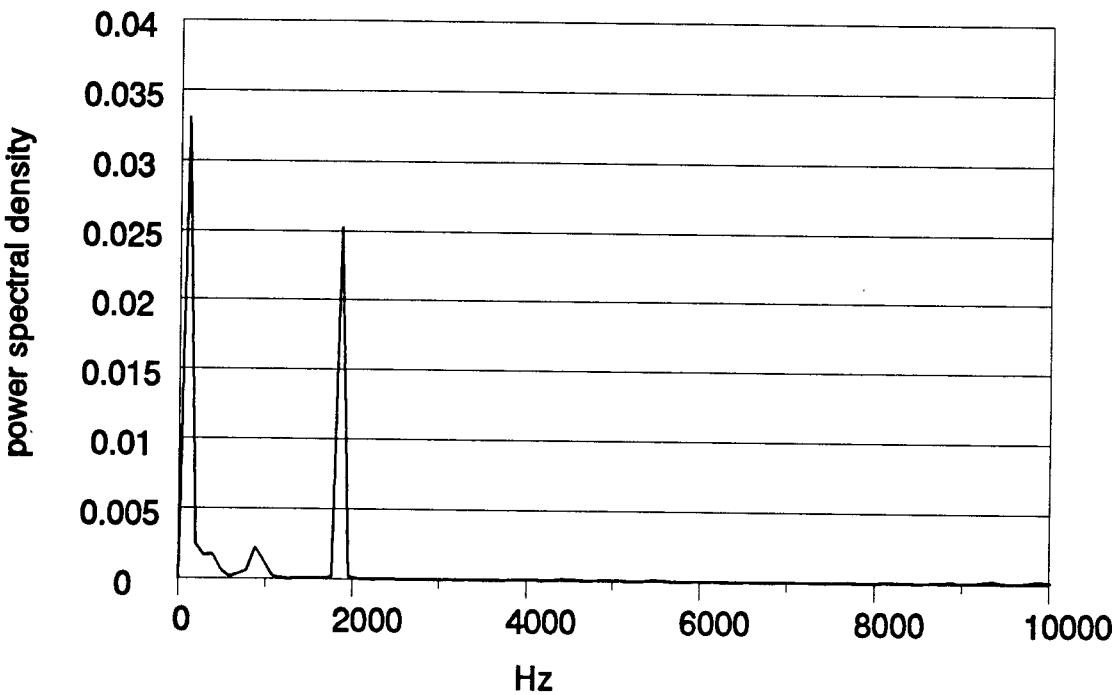

Fig. 45. Doubled FFT output with the same input signal as in figure 44

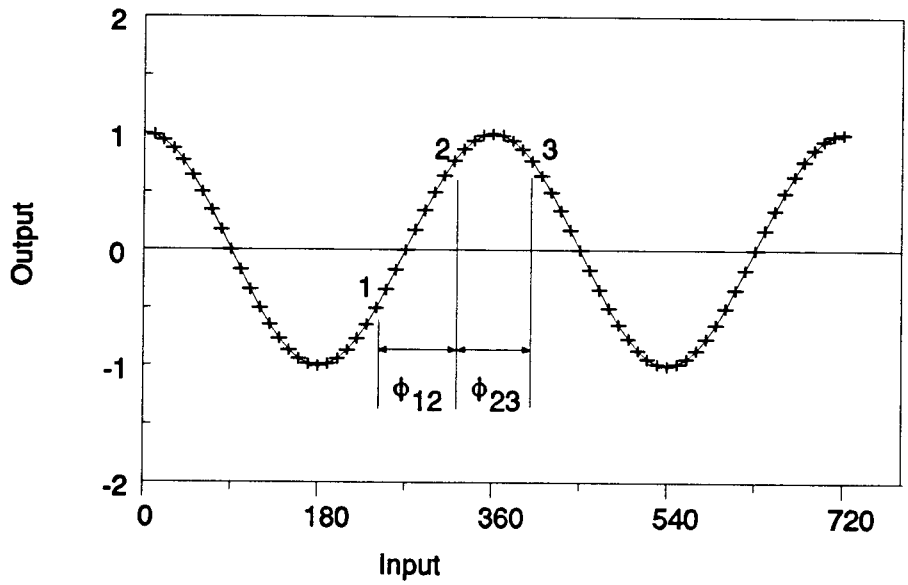

Fig. 46. Output frequency depends on the input signal position

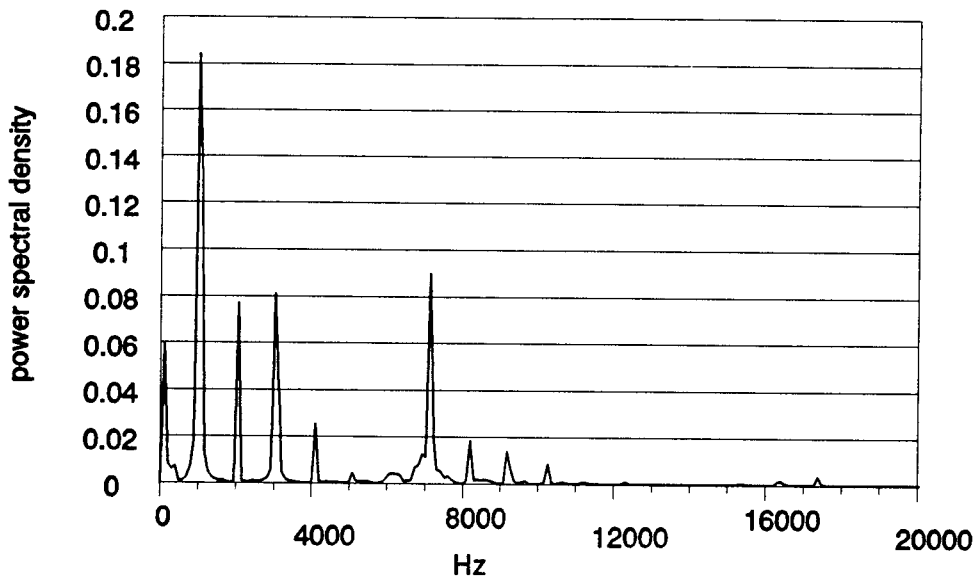

Fig. 47. Higher orders of FFT output as amplitude greater than half wavelength, input signal : A=0.78 μm (1.2λ), f=1 KHz

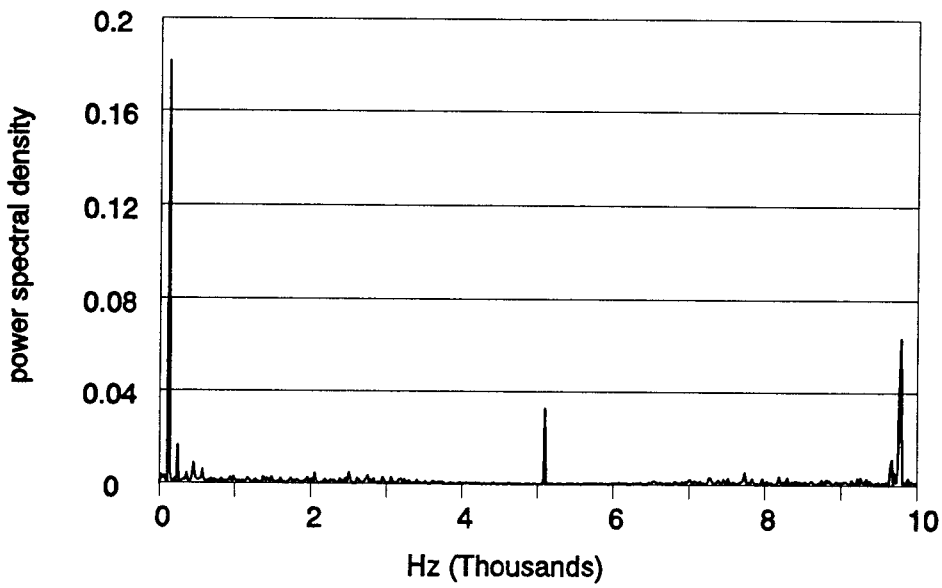

Fig. 48. FFT of out-of-plane speckle, input signal : A=0.026 μm, f=5.2 KHz

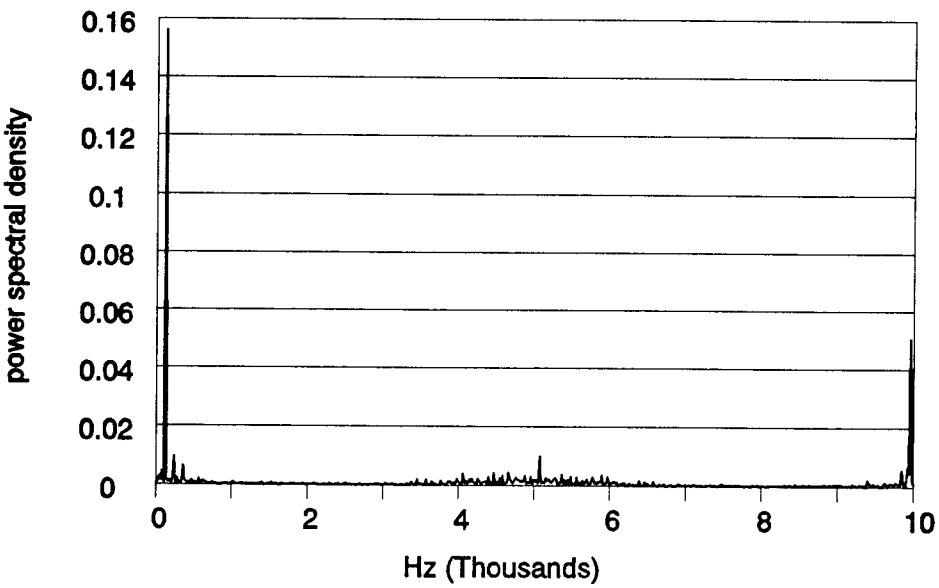

Fig. 49. FFT of out-of-plane speckle, input signal : A=0.0065 μm, f=5.2 KHz

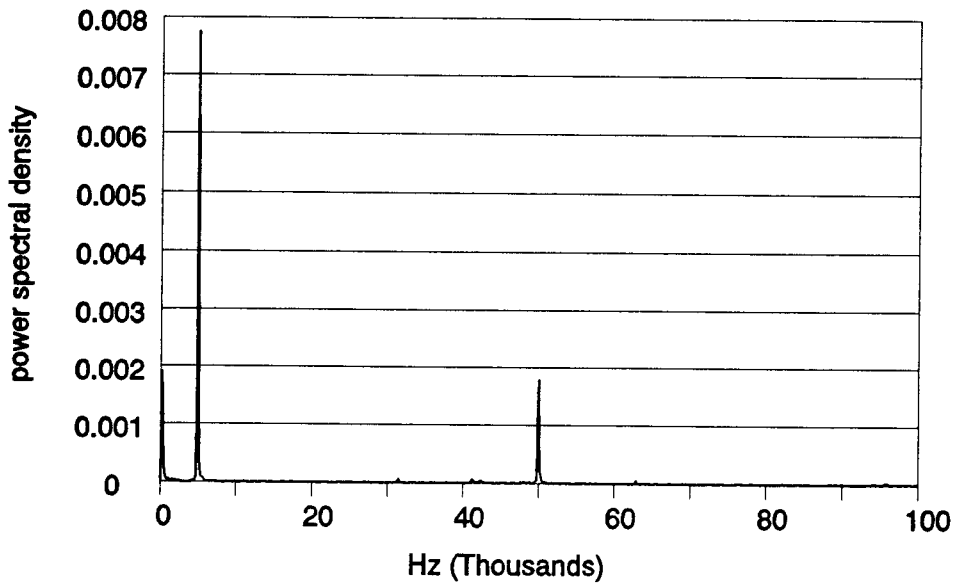

Fig. 50. FFT of in-plane speckle, input signal : A=0.013 μm, f=5 KHz

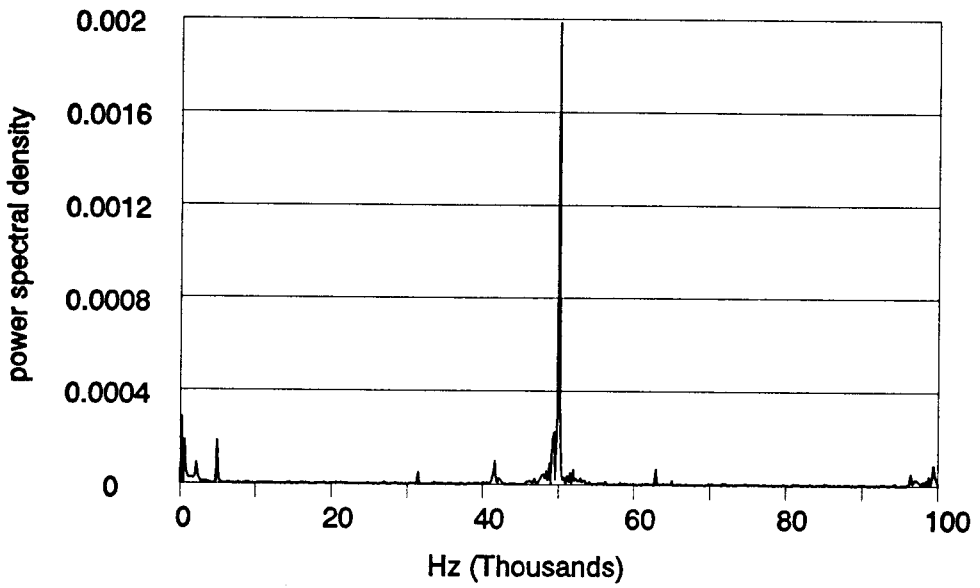

Fig. 51. FFT of in-plane speckle, input signal : A=0.0038 μm, f=5 KHz

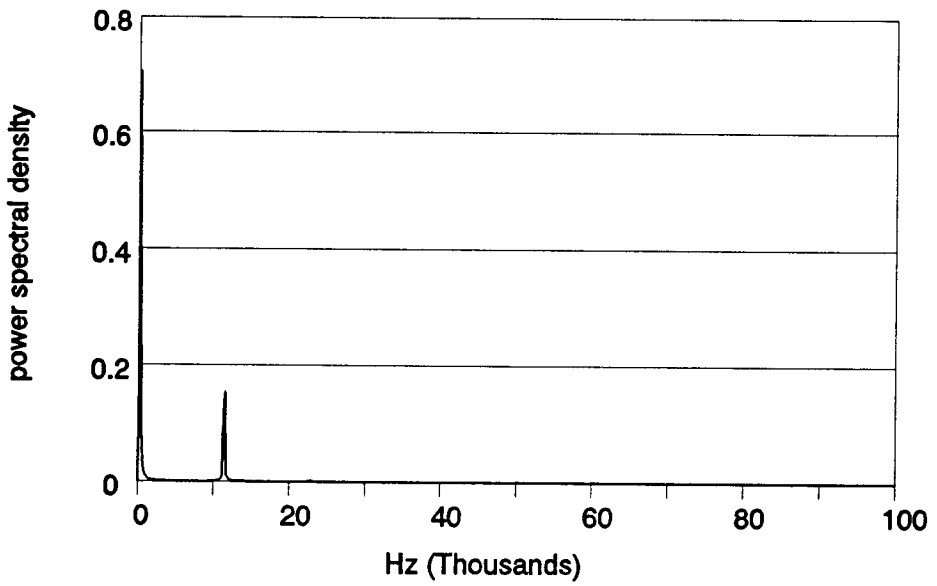

Fig. 52. Resonance frequency of a steel rod, steel ball excitation, mirror reflection

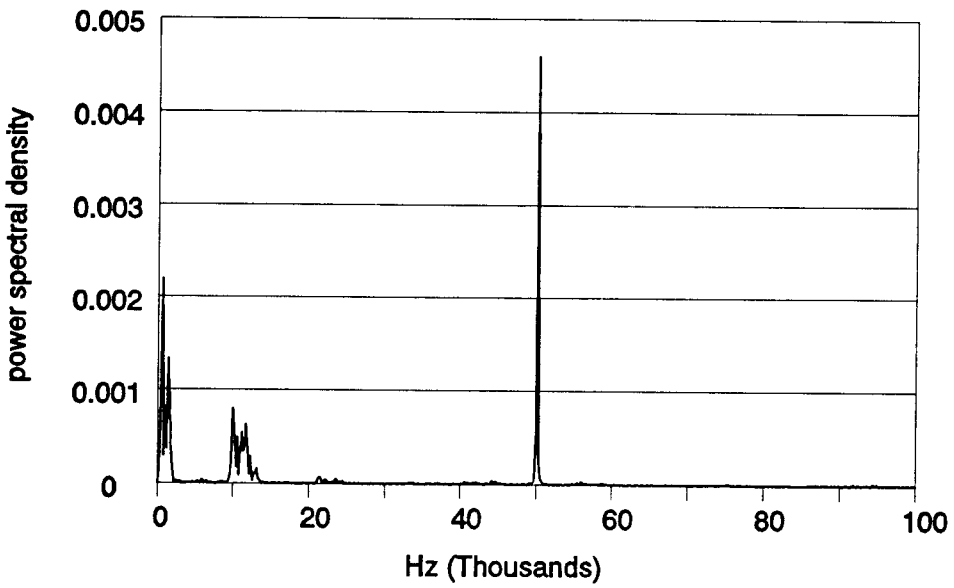

Fig. 53. Resonance frequency of a steel rod, steel ball excitation, diffuse tape reflection

CHAPTER 6. CONCLUSIONS AND RECOMMENDATIONS

A new method called "Phase Change Calculation" of processing laser interferometric signals was derived. Systems using this method to calibrate the characteristic displacements of a piezoelectric crystal (PZT) and to measure the thermal expansion of composite materials were developed. Speckle interferometry for measuring small displacements were verified by the calibrated PZT. These systems, along with the FFT data analysis, were able to pick up vibration signals down to the order of nanometers. Application was extended to NDT techniques. This chapter concludes this work and gives recommendations for the areas of future research.

6.1. Conclusions

6.1.1. Signal Analysis Algorithms

Algorithms for analyzing interference fringes were developed and adopted to the computer based processing of small displacement measurements. The computer fixed parameters analysis allows the laser intensity to vary arbitrarily during a measurement. The calculated phase angles do not depend on the absolute signal amplitudes but on their ratio, a/b. The maximum displacement error was

0.017 μm in the case of $\Delta h/a=\pm 5\%$, $\Delta k/b=\pm 5\%$ and $\delta=45\pm 5°$. It is a local error within one signal cycle and does not accumulate to the next cycles. There is no inherent limitation to the resolution (compare to fringe counting method). The best operational environment is to have a fixed DC signal level through the whole measurement such as in the calibration of the PZT characteristic displacements.

6.1.2. PZT Calibration System

The fixed parameters approach has been successfully applied to measure the small displacements induced by a piezoelectric crystal during oscillation at up to 1 KHz. Displacements per volt were obtained. The non-linear behavior of the crystal wase also observed. The root mean square error calculated from measured displacement data and 2nd order polynomial fitted data was 0.0086 μm. Accuracy can simply be improved by using a higher resolution data acquisition system (12-bit instead of 8-bit).

6.1.3. CTE Measurement Apparatus

Apparatus for measuring thermal expansion of arbitrarily shaped samples was developed. Reference material of fused silica samples were tested. The CTEs agreed well with the published data. The accuracy of the

thermal strain measured by this system is 4 $\mu\epsilon$, one third of the NBS SRM 739 suggested standard deviation, over the temperature range from -10°C to 60°C. The CTEs analyzed by manual chart method and fixed parameters method agreed well with each other. The manual chart method provides a convenient media for recording the events during the test. Manual fringe counting of the signal cycles from chart abolishes the requirements of having a constant DC signal level since its effect can be ousted automatically during the analysis. The fixed parameters approach eliminates the need for polarity tracking during the test and considerable electronics in the system. Since the in-plane CTE measurement of the thin plates was accomplished with mirrors cemented vertically on the plate, sample preheating was suggested to completely dry the adhesive. System accuracy depended on the stability of laser and the sample support system.

6.1.4. Speckle interferometry

Speckle interferometry has the advantage of not requiring specular reflection surfaces but rather diffuse ones. It can also measure out-of-plane and in-plane displacements independently. Speckle interferometry systems for measuring displacements in both directions were calibrated with known displacements introduced by a

calibrated piezoelectric crystal. The relationship between optical signals and displacements in out-of-plane speckle interferometry is the same as traditional Michelson interferometer, that is, one signal cycle represents 0.3164 μm. For double illumination in-plane system, this value becomes 0.224 μm if the incident angle is 45°.

Non-contact optical detection systems along with the FFT data analysis were used to analyze the frequency contents of vibration signals. The minimum detectable vibration amplitudes were 0.0065 μm, 0.0038 μm and 0.0010 μm for out-of-plane speckle, in-plane speckle and Michelson interferometers respectively. The resonance frequency of a steel rod was measured by both the out-of-plane speckle and the Michelson interferometers. This frequency was related to the modulus of elasticity E according to the principle of the stress wave traveling in a medium. The calculated E value was close to the book value, 182 GPa vs. 200 GPa.

6.2. Recommendations for the Areas of Future Research

The main subroutine of the phase change calculation method was developed. The relatively more complexity of the CTE data, than PZT's for example, requires more user friendly subroutines to manipulate these data so that the main subroutine of phase change calculation can be applied correctly and easily. Subroutines which can find the DC

signal levels from point to point in an existing data file are desired to remove the restriction of requiring a constant DC signal level. There is always a need for checking the "air-in direction" (i.e. the sample expansion direction) during a CTE test. A subroutine is desired to automatically determine this direction by reading both the voltages applied to the PZT (figure 16) and the corresponding signal moving directions at the same time.

To increase the accuracy of the CTE measurement system, a better way of sample supporting needs to be designed to minimize the mechanical noise. Electronic and optical noise should also be minimized to enhance the system sensitivity. Both optical and numerical filtering techniques are recommended for this purpose. Double differential interferometers, one for signals and one for system noise, will be another option to improve the system sensitivity.

Speckle interferometry was used to encounter to the problem of low intensity of the optical signals. Efficient use of the laser light should be investigated with lenses and the reflective surfaces. Highly sensitive detection components are desired. Applications can be extended to the areas of optical strain sensor, surface roughness measurement, surface deformation measurement, ··· etc..

Frequency analysis may reveal certain physical phenomena or quantities such as length of a rod, crack

formation and propagation, material properties, flaws in a material ... etc.. Signals detected by the optical systems may be interpreted in their frequency domain or directly be fed into an audio amplifier. It obviously can be applied to the areas of non-destructive testing and acoustic emission techniques. Applications of the current optical system with the FFT data analysis for the future research include specific subjects such as locating of the voids in a cast ingot, material properties, monitoring of the crack formation of a pressure vessel.

BIBLIOGRAPHY

Aghdaie, B., "A fringe-counting circuit for use with the Michelson interferometer",Am. J. Phys. 56(7), p664-5, July 1988.

Ansari, Farhad, "Mechanism of microcrack formation in concrete", ACI Materials Journal, v86, p459-64 September/October 1989.

Bennett, H.E.; Shaffer, J.J.; Burge, D.K., "Simple technique for obtaining approximate thermal expansion cofficients of low expansion materials: application to Zerodur", Appl. opt. Vol. 23 No. 16, 15 August 1984.

Birch, K.P.; and Wilton, P.T., "Thermal Expansion Data for Zerodur from 247 to 373K,"Appl. Opt. 27,2813-2815 (1988).

Blair, Chris and Zakrzewski, Jerry, "Coefficient of thermal and moisture expansion and moisture absorption for dimensionally stable quasi-isotropic high modulus graphite fiber/epoxy composites. SPIE paper, Orlando Fl., pp1303-43, April 1990.

Chen, D.J.; and Chiang, F.P., "Computer speckle interferometry (CSI)", SEM proceedings, November 5, 1990.

Costa, G.P.; and Mangini, S., "Speckle interferometer for thermal expansion measurements", Rev. Sci. Instrum. 58(1), p78-82, January 1987.

Dainty, J.C., "Laser Speckle and Related Phenomena", 2nd. edit., Springer-Verlag, 1984.

Ennos, A.E., "Speckle Interferometry", Laser Speckle and Related Phenomena, Ed. Dainty, J.C., 2nd. edit., Springer-Verlag, 1984.

Haug, R.; Klaas, A.; Pannhorst,W., "Length variation in Zerodur M in the temperature range from -60°C to +100°C", Appl. Opt. v28, p4052-4, October 1, 1989.

Hawkins, G.F.; Wolff, E.G., "7th Thermal Expansion Symposium", Chicago, Ill, November 1979.

Hecht, Eugene, Optics, 2nd edit., Addison-Wesley Publishing, p333-339, 1987.

Hohm, U.; and Kerl, K., "A Michelson twin interferometer for precise measurements of the refractive index of gases between 100 K and 1300 K", Measurement Science & Technology V1 p329-36, April 1990.

Iwasaki, Y.; Kaneko, M.; hayashi, K.; Ochiai, Y.; Hayakawa, M.; and Aso, K, "A new approach for measuring thermal expansion of thin films", J. Phys. E, v22, p498-502, July 1989.

Jones, R.M., "Mechnaics of Composite Materials",Scripta Book Co., 1975

Jones, R., "Holographic and Speckle Interferometry : A Discussion of the Theory, Practice, and Application of the Techniques", 2nd. edit., Camgridge University Press. 1989.

Klumpp, P.A. ; Schnack, E., "Speckle-interferometric camera for displacement measurements", Experimental Mechanics v30 p411-15 December 1990.

Lamoureux, R.T.; Kram, N.P., "Bending-beam method for determining coefficient of thermal expansion", Experimental Techniques, v11 p19-21, November 1987.

Leendertz, J.A., "Interferometric displacement measurement scattering surfaces utilizing speckle effect", J. Phys. E. (Sci. Instrum.), 3, p214, 1970.

Maji, A.K.; Wang, J.L.; Lovato, J., "Electronic speckle pattern interferometry for fracture mechanics testing", Experimental Techniques v15 p19-23 May/June 1991.

Marschall, C.W.; Maringer, R.E., "Dimensional Instability", Pergamon Press, 1977.

Moore, A.J.; Tyrer, J.R., "An electronic speckle pattern interferometer for complete in-plane displacement measurement", Measurement Science & Technology, v1 p1024-30, October 1990.

Press, W.H.; Flannery, B.P.; Teukolsky, S.A.; Vetterling W.T., "Numerical Recipes", Cambridge University Press, 1989.

Sarrafzadeh-Khoee, A.; and Duke, J.C.Jr., "Ultrasonic displacement measurement using laser-speckle interferometry", Exptl. Techniques, 10(10), p18-21, October 1986.

Schwarz, G.; Krahn, F.; Hartwig, G. "Thermal expansion of carbon composites with thermoplastic matrices", Cryogenics v31 p244-7 April 1991.

Shaffer, J.J.; and Bennett, H.E., "Effect of thermal cycling on dimensional stability of Zerodur and ULE", Applied opt. Vol. 23, No. 17, p2852-2853, 1 September 1984.

Smith, L. Montgomery; and Dobson, Chris C., "Absolute displacement measurements using modulation of the spectrum of white light in a Michelson interferometer", Applied Optics, Vol. 28, No. 15, 15 August 1989.

St-Arnaud, J.M.; Ge, J.; Orbriot, J.; and Bose, T.K., "An Accurate Method for refractive index measurements of liquids using two Michelson laser interferometers", Rev. Sci. Instrum. 62(6), p1411-1414, June 1991

Sterkenburg, S.W.P.v.; Kwaaitaal, Th.; and Eijnden, W.M.M.M. van den, "A double Michelson interferometer for accurate measurements of electrostrictive constants", Rev. Sci.Instrum. 61(9), p2318-2322, September 1990.

Steel, W.H., "Interferometry", 2nd. edit., Cambridge University Press. 1983.

Tsai, S.W., "Composite Design", 4th. edit., 1988.

Tu,Meirong; McKelvie,James; Dai, Fu-long; and Post, Daniel "Grating speckle method for in-plane displacement measurement", Appl. Opt., 28(15), p3354-3357, 15 August 1989.

Verdeyen, J.T., "Laser Electronics", 2nd. edit., Prentice-Hall,Inc., 1989.

White, R.G.; and Emmony, D. C., "Active feedback stabilisation of a Michelson interferometer using a flexure element", J. phys. E: Sci.Instrum., Vol. 18, 1985.

Wolff, E.G. and Savedra, R.C.,"Precision interferometric dilatometer", Rev.Sci.Instrum., 56(7),July 1985.

Wolff, E.G., "Development and Testing of Zero CTE Materials", Thermal Expansion -8, Hahn, T.A. (Editor), Plenum Publ. Co., p358-370, 1984.

Wolff, E.G., "Measurement Techniques for Low Expansion Materials", 9th National SAMPE Technical Conference, vol. 9, p57-72, Atlanta Ga, October 1977.

Yamaguchi, Y.; Imai, H., "Interferometric measurements of thermal expansivity and thermoelasticity of high-strength organic fibres", J. phys. E: Sci.Instrum., vol. 22, p9-13, 1989.

APPENDICES

APPENDIX A. Thermal expansion of fused silica (SRM739)

T(°K)	T(°C)	$\Delta L/L_0$ (10^{-6})	α (10^{-6}/°C)
80	-193	-1	-0.7
90	-183	-7.5	-0.61
100	-173	-13	-0.53
110	-163	-18	-0.46
120	-153	-22.5	-0.38
130	-143	-26	-0.31
140	-133	-28.5	-0.24
150	-123	-30.5	-0.17
160	-113	-32	-0.1
170	-103	-32.5	-0.04
180	-93	-32.5	0.02
190	-83	-32	0.08
200	-73	-31	0.13
210	-63	-29.5	0.19
220	-53	-27.5	0.23
230	-43	-25	0.28
240	-33	-22	0.32
250	-23	-18.5	0.36
260	-13	-14.5	0.39
273	0	-9	0.43
280	7	-6	0.45
293	20	0	0.48
298	25	2.5	0.49
320	47	13.5	0.53
340	67	24.5	0.56
360	87	36	0.58
380	107	47.5	0.6
400	127	59.5	0.61
420	147	72	0.62
440	167	85	0.63
460	187	97	0.63
480	207	110	0.63
500	227	122	0.63
520	247	135	0.62
560	287	159	0.61
600	327	183	0.59
640	367	206	0.56
680	407	228	0.54
720	447	249	0.51
760	487	269	0.49
800	527	288	0.47
840	567	307	0.44
880	607	324	0.42
920	647	340	0.4
960	687	356	0.38
1000	727	371	0.37

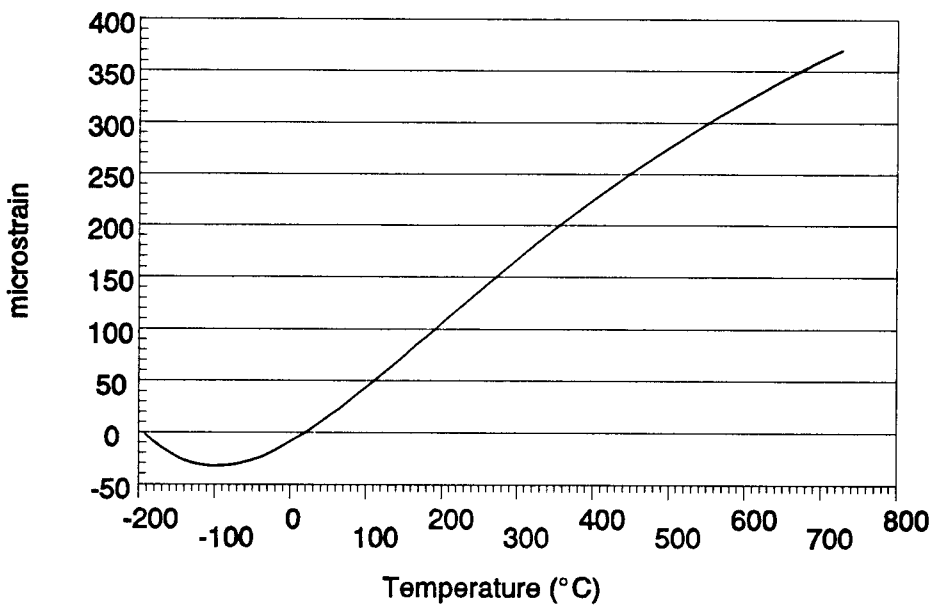

Fig. 54. CTE of reference material SRM 739

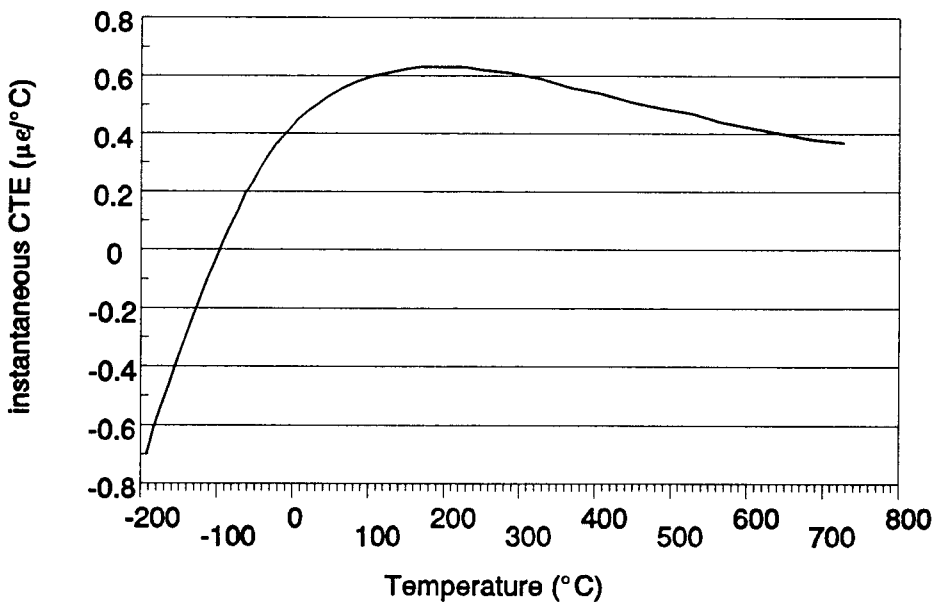

Fig. 55. Instantaneous CTE of reference material SRM 739

APPENDIX B. Temperature Conversion Program

```
/* ****************************************** */
/* ** Thermal Couple Temperature Conversion  ** */
/* **      written in TURBO PROLOG           ** */
/* **  see TemCon.hlp for details, G.S. Peng ** */
/* ****************************************** */
config "PROLOG.SYS"
nowarnings
domains
  file=input;output
  RefT,RefV,Tx,Vx,Mv,D_cyc=real
include "c:\\tprolog\\toolbox\\tdoms.pro"
database
  t_mv(real,real) /*(°C , mv)*/
include "c:\\tprolog\\toolbox\\tpreds.pro"
include "c:\\tprolog\\toolbox\\menu.pro"
include "c:\\tprolog\\toolbox\\status.pro"

predicates
  setup  help  select_mode  operation_mode(integer)
  run_inter  loop_inter(RefV)
  run_batch  loop_batch(RefV)  mv_of(RefT,RefV)
temp_of(Vx,Tx)
  get2Val(string,real,real)  getVal(string,real,string)
  editDataV  checkRest(string)

goal /* ------------------------------ */
  setup, select_mode. /* run and chain to QUATRO */

clauses /* ---------------------------- */
  setup if
    makestatus(7,""),
    makewindow(99,23,0,"",0,0,24,80),/* empty window */
    existfile("TC_T.DBS"), consult("TC_T.DBS").
  setup if
    not(existfile("TC_T.DBS")),clearwindow,
    writedevice(screen),
    write(" database file for T type tc : TC_T.DBS does not
      exist"),
    write("\npress SPACE bar to quit ..."),readchar(_),
      exit.
  help if
    existfile("TemHELP.BAT"),
    clearwindow,makewindow(1,23,2,"H e l p",0,0,22,80),
    writedevice(screen),system("TemHELP.BAT").
  help if
    not(existfile("TemHELP.BAT")),
    clearwindow,makewindow(1,23,2,"H e l p",0,0,22,80),
    writedevice(screen),write("\n TemHELP.BAT doesn't
      exist"),readchar(_).
```

```
   shiftwindow(99),clearwindow,/* empty window */
   Mode1="Batch mode, with input file DATA_V.",
   Mode2="Interactive mode", Mode3="Edit DATA_V.",
   Mode4="DOS", Mode5="Help", Mode6="Quit",
   ModeList=[Mode1,Mode2,Mode3,Mode4,Mode5,Mode6],
   menu_leave(0,0,23,2,ModeList," T.C. Temperature
     Conversion Program ",1,ModeNo),
   !,operation_mode(ModeNo).

   operation_mode(ModeNo):-
     ModeNo=1,run_batch,select_mode.
   operation_mode(ModeNo):-
     ModeNo=2,run_inter,select_mode.
   operation_mode(ModeNo):-
     ModeNo=3,editDataV,select_mode.
   operation_mode(ModeNo):-
     ModeNo=4,system(""),select_mode.
   operation_mode(ModeNo):-
     ModeNo=5,help,select_mode.
   operation_mode(ModeNo):-
     ModeNo=6,writedevice(screen),write("\n Quit"),exit.
   operation_mode(_):-/* keep asking if non of the above
     was selected */
     select_mode.

editDataV:-
  makewindow(2,23,2,"",0,0,24,80), /*local edit window*/
  editmsg("",DataFile,"","DATA_V.","",0,"",Code),Code=0,
    /* when F10 is pressed*/
  openwrite(output,"Data_V"),
  changestatus("save DATA_V."),
  writedevice(output),write(DataFile),closefile(output).

run_inter if /* interactive mode */
  readdevice(keyboard),writedevice(screen),
  makewindow(13,23,6,"reference temp. ",3,20,12,58),
    /* reference temperature */
  write (" Reference Temperature="), readreal(RefT),
    mv_of(RefT,RefV), clearwindow,
  write (" Reference Temperature=", RefT,"----->RefV=",
    RefV),
  makewindow(12,23,6,"interactive mode",5,21,12,58),
  loop_inter(RefV).
loop_inter(RefV) if
  writedevice(screen), write("mv_at_RefT="),readreal(Mv),
  Vx=Mv+RefV, temp_of(Vx,Tx),
  write("-->mv_at_Ref0="),writef("%-7.4f",Vx),
  write(" -->temp="),writef("%-8.2f",Tx),nl,nl,
  !, /* prevent stack overflow */
  loop_inter(RefV).

run_batch if /* reference temperature */
```

```
  existfile("DATA_V"),
  makewindow(11,23,2,"batch mode",2,20,12,58),
  writedevice(screen),write(" processing "),
  openread(input,"DATA_V"),readdevice(input),
  openwrite(output,"DATA_T"),writedevice(output),
  readln(Line),getVal(Line,XRefT,_),RefT=XRefT,
    mv_of(RefT,RefV),
  write("\n     RefT=",RefT," RefV=",RefV),
  write("\n\n     mv(RefT)    mv(Ref0)      temp.
    D_cyc.\n"),
  loop_batch(RefV).
run_batch if
  not(existfile("DATA_V")),readdevice(keyboard),
  writedevice(screen),
  write("\n input file DATA_V. does not
    exist"),readchar(_),
  select_mode.
loop_batch(RefV) if/* ***** main Loop ***** */
  not(eof(input)),
  readln(Line),get2Val(Line,MV,D_cyc),
  Vx=MV+RefV,temp_of(Vx,Tx), writedevice(output),
  writef("%12.4f%12.4f%12.2f%12.4",Mv,Vx,Tx,D_cyc),nl,
  writedevice(screen),write("."),
  !,/* prevent stack overflow */
  loop_batch(RefV).
loop_batch(RefV) if /* skip empty line when get2Val
    failed */
  not(eof(input)),
  beep,changestatus("Skip empty line"),
  !,loop_batch(RefV).
loop_batch(_) if /* end of data file routine */
  eof(input),closefile(input),closefile(output),
  readdevice(keyboard),writedevice(screen),
  makewindow(4,23,0,"",11,22,2,50),/*end of batch job*/
  write(" end of batch job, output file : DATA_T."),
  sound(3,131),sound(4,165),sound(6,196),
  write("\n press SPACE bar to continue    ....."),
  readchar(_),openwrite(output,"flag1"),
  closefile(output) , /* used in CTE.BAT */
  exit.

mv_of(RefT,RefV) if /* Find Reference millivolt */
  t_mv(T1,V1),t_mv(T2,V2),
  T1<=RefT,RefT<T2,T2-T1<10.5,!,/*temp. diff. is 10*/
  RefV=V1+(V2-V1)*(RefT-T1)/(T2-T1).
mv_of(RefT,999) if
  RefT>210 ,write("\n reference temperature(",RefT," °C)
    out of range.\n"),
  run_inter.
mv_of(RefT,-999) if
  RefT<-210 ,write("\n reference temperature(",RefT," °C)
    out of range.\n"),
```

```
    run_inter.
/*Piecewise Linear Interpolation for temperatures*/
  temp_of(Vx,Tx) if
    t_mv(T1,V1),t_mv(T2,V2),
    V1<=Vx,Vx<V2,T2-T1<10.5,!,/* temp. difference is 10 */
    Tx=T1+(T2-T1)*(Vx-V1)/(V2-V1).
  temp_of(Vx,999) if
    Vx>9.82,write("\n mv_at_Ref0(",Vx,"mv) out of
      range.\n").
  temp_of(Vx,-999) if
    Vx<-5.753,write("\n mv_at_Ref0(",Vx,"mv) out of
      range.\n").

/* getVal routines get 1st number in a given text line */
  getVal(Line,Val,Rest):-/* get positive number like 0.5 */
    fronttoken(Line,StrVal,Rest),str_real(StrVal,Val).

  getVal(Line,Val,Rest2):-/*get positive number like .5*/
    fronttoken(Line,StrVal_1,Rest1),StrVal_1=".",
    fronttoken(Rest1,StrVal_2,Rest2),
    fronttoken(X,"0.",StrVal_2),str_real(X,XVal),Val=XVal.
  getVal(Line,Val,Rest2):-/*get negative number like -0.5*/
    fronttoken(Line,StrVal_1,Rest1),StrVal_1="-",
    fronttoken(Rest1,StrVal_2,Rest2),
    str_real(StrVal_2,XVal),Val=-XVal.
  getVal(Line,Val,Rest3):-/*get negative number like -.5*/
    fronttoken(Line,StrVal_1,Rest1),StrVal_1="-",
    fronttoken(Rest1,StrVal_2,Rest2),StrVal_2=".",
    fronttoken(Rest2,StrVal_3,Rest3),
    fronttoken(X,"0.",StrVal_3),str_real(X,XVal),Val=-XVal.
  getVal(Line,Val,Rest2):-/*get positive number like +0.5*/
    fronttoken(Line,StrVal_1,Rest1),StrVal_1="+",
    fronttoken(Rest1,StrVal_2,Rest2),
    str_real(StrVal_2,XVal),Val=XVal.
  getVal(Line,Val,Rest3):-/*get positive number like +.5*/
    fronttoken(Line,StrVal_1,Rest1),StrVal_1="+",
    fronttoken(Rest1,StrVal_2,Rest2),StrVal_2=".",
    fronttoken(Rest2,StrVal_3,Rest3),
    fronttoken(X,"0.",StrVal_3),str_real(X,XVal),Val=XVal.
  getVal(Line,Val,Rest2):-/*skip separator "," */
    fronttoken(Line,StrVal_1,Rest1),StrVal_1=",",
    getVal(Rest1,Val,Rest2).
  getVal(Line,Val,Rest1):- /* repeat when not numbers */
    fronttoken(Line,ExtraChar,Rest),
    concat("Skip extra character(s) : '",ExtraChar,Entry1),
    concat(Entry1,"' for this data -- ",Entry2),
    concat(Entry2,Line,Entry),
    changestatus(Entry),
    !,getVal(Rest,Val,Rest1).

  get2Val(Line,Vx,Vy):-
    XLine=Line,getVal(XLine,XVx,Rest1),Vx=XVx,
```

```
    XRest1=Rest1,getVal(XRest1,XVy,Rest2),Vy=XVy,
    checkRest(Rest2),!./* check for non empty Rest2 */
  get2Val(Line,Vx,Vy):-/* when no 2 numbers in a line */
    /* prompt can be inserted here */
    changestatus(""),fronttoken(Line,_,_),/* return to loop
      if empty line */
    makewindow(95,23,7,"",8,22,5,56),/*correction window */
    writedevice(screen),write("wrong data --> ",Line),nl,
    write("please press a key to correct it ---"),
    readdevice(keyboard),readchar(_),
    edit(Line,Corrected),removewindow,
    shiftwindow(11),/* batch mode window */
    readdevice(input),get2Val(Corrected,Vx,Vy).

  checkRest(Rest):-
    fronttoken(Rest,ExtraChar,_),
    concat("Data line end up with extra character(s) :
      ",Rest,Entry),
    beep,changestatus(Entry),
    !.
  checkRest(_):-/* empty Rest */
    !.

/*data base stored in file TC_T.DBS :*/
t_mv(-210,-5.753). t_mv(-200,-5.603). t_mv(-190,-5.439).
t_mv(-180,-5.261). t_mv(-170,-5.069). t_mv(-160,-4.865).
t_mv(-150,-4.648). t_mv(-140,-4.419). t_mv(-130,-4.177).
t_mv(-120,-3.923). t_mv(-110,-3.656). t_mv(-100,-3.378).
t_mv(-90,-3.089).  t_mv(-80,-2.788).  t_mv(-70,-2.475).
t_mv(-60,-2.152).  t_mv(-50,-1.819).  t_mv(-40,-1.475).
t_mv(-30,-1.121).  t_mv(-20,-0.757).  t_mv(-10,-0.383).
t_mv(0,0).         t_mv(10,0.391).    t_mv(20,0.789).
t_mv(30,1.196).    t_mv(40,1.611).    t_mv(50,2.035).
t_mv(60,2.467).    t_mv(70,2.908).    t_mv(80,3.357).
t_mv(90,3.813).    t_mv(100,4.277).   t_mv(110,4.749).
t_mv(120,5.227).   t_mv(130,5.712).   t_mv(140,6.204).
t_mv(150,6.702).   t_mv(160,7.207).   t_mv(170,7.718).
t_mv(180,8.235).   t_mv(190,8.757).   t_mv(200,9.286).
t_mv(210,9.820).

************  TemCon.HLP  ******************************
DATA BASE of T_type thermal couple with arbitrary Ref.
Temp.
*********************************************************
*Enter a number for RefT, program will find the RefV then
  all input millivolt will be shifted by RefV.
*Enter millivolt ---> give you a corresponding temperature.
*volts range for RefT=0 : -5.603 to 9.286 mv -->temp: -200
to 200 Deg.C
*in batch mode : input file=DATA_V, output file=DATA_T"
                 first number in DATA_V should be reference
                 temp. data format in file DATA_V:
```

```
  Millivolt,D_cycles
Typical example of DATA_V :

Ref temp = 24.5
0     0
0.12  2
0.25,2

.....
```

(any extra characters contained in a data line will be skipped)

*Flies included:

- CTE.BAT (main batch file)
- CTE2.EXE (main prolog program, Enter from DATA_V. and output to DATA_T.)
- TemCon.HLP (this file)
- CTE2.PRO (prolog source file)
- CTE_FORM.WKQ (QUATTRO MARCO file for CTE calculation)
- TemHelp.BAT (contain DOS command to print TemCon.HLP)
- PROLOG.SYS (configuration file)
- PROLOG.ERR (prolog error message)
- TC_T.DBS (T type thermal couple datafile)
- DATA_V.(millivolt, D_cyc data file)
- DATA_T.(intermediate temperature and D_cyc data file)
- QUATTRO system files

APPENDIX C. Matrix Operation Approach Program

```
% ****************************************
% ** Calculate strain from CTE test data **
% **   written in MATLAB                **
% **   Read STRAINM.HLP for details, GSP **
% ****************************************

% * read CTEdata from file CTEDATA.DAT
disp('loading CTEDATA.DAT ...')
load CTEdata.dat;

% * resolve data into 4 column vectors
[Row,Col]=size(CTEdata);
disp('reading time'), time=CTEdata(1:Row,1);
disp('reading x'),    x=CTEdata(1:Row,2);
disp('reading y'),    y=CTEdata(1:Row,3);
disp('reading Temp'), Temp=CTEdata(1:Row,4);
clear CTEdata;
disp(''),disp('count down data points to be processed')

for I=1:Row,  disp(Row-I)
while I<=5
A11=x(I)-x(I+1);                A21=x(I)-x(I+2);
A31=x(I)-x(I+3);                A41=x(I)-x(I+4);
A12=-(y(I)^2-y(I+1)^2);         A22=-(y(I)^2-y(I+2)^2);
A32=-(y(I)^2-y(I+3)^2);         A42=-(y(I)^2-y(I+4)^2);
A13=y(I)-y(I+1);                A23=y(I)-y(I+2);
A33=y(I)-y(I+3);                A43=y(I)-y(I+4);
A14=x(I)*y(I)-x(I+1)*y(I+1);    A24=x(I)*y(I)-x(I+2)*y(I+2);
A34=x(I)*y(I)-x(I+3)*y(I+3);    A44=x(I)*y(I)-x(I+4)*y(I+4);
B1=x(I)^2-x(I+1)^2;  B2=x(I)^2-x(I+2)^2;
B3=x(I)^2-x(I+3)^2;  B4=x(I)^2-x(I+4)^2;
break,  end

while I>5
A11=x(I)-x(I-4);                A21=x(I)-x(I-3);
A31=x(I)-x(I-2);                A41=x(I)-x(I-1);
A12=-(y(I)^2-y(I-4)^2);         A22=-(y(I)^2-y(I-3)^2);
A32=-(y(I)^2-y(I-2)^2);         A42=-(y(I)^2-y(I-1)^2);
A13=y(I)-y(I-4);                A23=y(I)-y(I-3);
A33=y(I)-y(I-2);                A43=y(I)-y(I-1);
A14=x(I)*y(I)-x(I-4)*y(I-4);    A24=x(I)*y(I)-x(I-3)*y(I-3);
A34=x(I)*y(I)-x(I-2)*y(I-2);    A44=x(I)*y(I)-x(I-1)*y(I-1);
B1=x(I)^2-x(I-4)^2;  B2=x(I)^2-x(I-3)^2;
B3=x(I)^2-x(I-2)^2;  B4=x(I)^2-x(I-1)^2;
break,  end

% solve[A][Z]=[B]
A=[A11 A12 A13 A14;
   A21 A22 A23 A24;
```

```
   A41 A42 A43 A44];
B=[B1; B2; B3; B4];
Z=inv(A)*B;
HK=inv([2 -Z(4); -Z(4) 2*Z(2)])*[Z(1); Z(3)];
h=HK(1);  k=HK(2);
% or h=(2*Z(1)*Z(2)+Z(3)*Z(4))/(4*Z(2)-Z(4)^2);
% or k=(2*Z(3)+Z(1)*Z(4))/(4*Z(2)-Z(4)^2);
aob=sqrt(Z(2));
delta=acos(Z(4)/(2*sqrt(Z(2)))); % 0< delta <180
atan2Y=(1/sin(delta))*(aob*(y(I)-k)-(x(I)-h)*cos(delta));
atan2X=x(I)-h;
Phi(I)=atan2(atan2Y,atan2X)*180/pi;
if Phi(I)<0, Phi(I)=Phi(I)+360;end
end % of I=1:Row loop

CCW=input('Expansion dir. (CCW=1, CW=-1) >> ');
disp('calculating displacements ...')
DPhi(1)=0;  DSPL(1)=0; % initial value
for I=2:Row,
  DPhi(I)=(Phi(I)-Phi(I-1))*CCW;
  if DPhi(I)>180, DPhi(I)=DPhi(I)-360;end
  if DPhi(I)<-180, DPhi(I)=DPhi(I)+360;end
  DSPL(I)=DSPL(I-1)+12.456*DPhi(I)/360;
end
disp('save (temp,dsplmt) onto file CTE.MAT')
save cte Temp DSPL
disp('Hit RETURN to continue'),pause
plot(Temp(1:Row),DSPL(1:Row))


************  STRAINM.HLP ******************************
Use of Matrix Operation Approach to calculate strain from
CTE data
**********************************************************

*Data file is CTEDATA.DAT
*Data format:
     column 1 is time,  column 2 is Vx,  column 3 is Vy and
     column 4 is temperature.  Only numbers are allowed in
     the data file.
*Output file is CTE.MAT which can be TRANSLATEd to ASCII
 file .
```

APPENDIX D. Fixed Parameters Approach Program

```
/* ****************************************** */
/* ** Calculate STRAIN from CTE test data ** */
/* **   written in TURBO PROLOG           ** */
/* **   see STRAIN.HLP for details, GSP   ** */
/* ****************************************** */
code=4000
nowarnings
domains
  file=input;input1;input2;output
  L0,H,K,Eps,AoB,CCW,Time,Vx,Vy,Temp,Val=real
  Phi0,Phi1,DPhi=real
  line,restline,keyword,airInDir,Unit=string
  keywords=keyword*
database
  inpfile(string) sum(real)
  h(H) k(K) l0(L0) /* L0 in in. */
  aob(AoB)  /*ellipse axis ratio A/B */
  eps(Eps) /* phase difference between Vx and Vy*/
  airInDir(airInDir) ccw(CCW)
  dataline(line) keyword(keyword) keywords(keywords)

include "c:\\tprolog\\toolbox\\tdoms.pro"
include "c:\\tprolog\\toolbox\\tpreds.pro"
include "c:\\tprolog\\toolbox\\boxmenu.pro"

predicates
  setup  help  select_mode  operation_mode(integer)
  initialize  run_strain
  initVal(Phi0) /* Phi0 and assert L0ime,H,K,Eps,AoB */
  calc_strain(Phi0) /* and save (sum of DPhi) */
  /* Phi0 */
  checkline(line,keyword) getairindir(line,airInDir)
  getCCW(airInDir,CCW)  getEllipse(line,H,K,Eps,AoB)
  getH(line,H) getK(line,K) getEps(line,Eps)
  getAoB(line,AoB) getVal(line,Val,restline)
  get4Val(line,Time,Vx,Vy,Temp)
  atn2(Vx,Vy,Phi1) /* Vx,Vy,Phi */
  dphi(Phi0,Phi1,DPhi) /* Phi0,Phi1,Dphi */
  member(keyword,keywords)
  quit

goal /* ------------------------------ */
  setup,select_mode./* run_strain.  */

clauses /* ---------------------------- */

  Help if
    existfile("STRNHELP.BAT"),system("STRNHELP.BAT"),
    !.
```

```
    not(existfile("STRNHELP.BAT")),writedevice(screen),
    write("\nfile STRNHELP.BAT doesn't exist,"),
    readdevice(keyboard),readchar(_),nl.
 setup:-
    makewindow(11,7,0," empty window ",3,0,21,80),
    makewindow(1,7,0," show H K ",4,0,7,80),
    makewindow(2,2,0," data title ",11,15,1,55),
    makewindow(3,7,0," output data ",12,15,5,55),
    makewindow(4,7,0," edit data line ",12,0,12,80),
    makewindow(5,2,0," input/output files ",3,0,1,80),
    makewindow(23,7,0," ",23,0,1,80).

select_mode:- /* and then run it */
    Mode1=" Strain", Mode2=" Help", Mode3=" Quit",
    ModeList=[Mode1,Mode2,Mode3],
    boxmenu_leave(0,0,1,78,3,7,ModeList," Strain
      Calculation ",1,ModeNo),
    !,operation_mode(ModeNo).

    operation_mode(ModeNo):-
      ModeNo=1,/* strain */
      shiftwindow(2),clearwindow,window_attr(138),
      initialize,run_strain,shiftwindow(2),window_attr(2),
      shiftwindow(5),window_attr(138),
      readdevice(keyboard),readchar(_),window_attr(2),
      select_mode.
    operation_mode(ModeNo):- /* type STRAIN.HLP  */
      ModeNo=2,help,
      select_mode.
    operation_mode(ModeNo):-/* quit */
      ModeNo=3,quit.
    operation_mode(_):-
      select_mode.
 quit:-
    closefile(input),closefile(input1),closefile(input2),
    closefile(output),
    shiftwindow(11),system("cls"),write("Quit"),exit.

 initialize if  /* -1- */
    KeyWords=["L0","AIR","ELL"],
    asserta(keywords(KeyWords)),asserta(sum(0)),/*Sum0=0*/
    asserta(dataline("--- Dummy data line at initialize
      routine ---")),
    asserta(l0(1)),asserta(h(0)),asserta(k(0)),
    asserta(keyword("Dummy")),
    asserta(eps(45)),asserta(aob(1)),asserta(ccw(1)),
    asserta(airInDir("CCW")),/* default values, prevent
      empty error */
    shiftwindow(5),
    write("\nBy Fixed Parameters Approach :"),
    write(" source file = "),readln(XInpfile),
    upper_lower(Inpfile,XInpfile),
```

```
  asserta(inpfile(Inpfile)),
  existfile(Inpfile),openread(input,Inpfile),
  openwrite(output,"STRAIN.OUT"),
  write("input file = ",Inpfile),
  write("  output file = STRAIN.OUT"),
  readdevice(input),
  shiftwindow(1)./* display H,K, ...*/
initialize:- /* -2- input file doesn't exist */
  inpfile(Inpfile),retract(inpfile(Inpfile)),
  not(existfile(Inpfile)),
  readdevice(keyboard),writedevice(screen),
  clearwindow,
  write("\n input file ",INPFILE," does not exist"),
  readchar(_),exit.

run_strain:-
  not(eof(input)),
  initVal(Phi0),/* and L0,H,K,Eps,AoB */
  calc_strain(Phi0),
  write("\n ---------- end of run_strain routine
    ---------------").
run_strain:- /* no more valid data lines in input file */
  eof(input),inpFile(InpFile),retract(inpFile(_)),
  write("\n  no more valid data lines in file :
    ",InpFile),
  closefile(input), readdevice(keyboard),readchar(_).

initVal(Phi0):-/*also store values for L0,H,K,Eps,AoB*/
  readdevice(input),readln(Line),checkline(Line,KeyWord),
  /* store values if found */
  KeyWord<>"DATA",initVal(Phi0),
    /*retract(sum(_)),assert(sum(0)),<--if you want start
      from 0 again*/
  !./* prevent stack overflow */
initVal(Phi0):-  /* find Phi0 */
  keyword(KeyWord),
  KeyWord="DATA",dataline(Line),
  h(H),k(K),l0(L0),ccw(CCW),aob(AoB),eps(Eps),
  get4Val(Line,Time,Vx,Vy,Temp),VxH=Vx-H,
  VyK=(-1/sin(Eps*3.1416/180))*(VxH*cos(Eps*3.1416/180)
    -(AoB)*(Vy-K)),
  TempF=Temp*9/5+32,
  atn2(VxH,VyK,XPhi0),Phi0=XPhi0,Dphi0=0.0,
  sum(Sum0),Strain=CCW*Sum0/360*12.456/L0,
  writedevice(output),
  writef("\n%10.5f%10.5f%10.5f%10.3f%10.3f%10.3f%10.3f",
    Temp,Strain),
  writedevice(screen),shiftwindow(2),clearwindow,write("
    Temp.°C,  Strain(E-6) ..."),
  shiftwindow(3),
  writef("\n%10.5f%10.5f%10.5f%10.3f%10.3f%10.3f%10.3f",
    Temp,Strain),
```

```
  !. /* prevent stack overflow */

calc_strain(Phi0):-
/* when EOF -->stop calc_strain Loop  and return to
   run_strain routine */
  eof(input),retract(l0(_)),retract(h(_)),retract(k(_)),
  retract(eps(_)),retract(aob(_)),retract(airInDir(_)),
  retract(ccw(_)),retract(sum(_)),retract(dataline(_)),
  closefile(input),/* closefile(output), */
  inpFile(InpFile),retract(inpFile(_)),
  write("\n  end of data file : ",InpFile),
  readdevice(keyboard),readchar(_).
calc_strain(Phi0):-  /**** start calc_strain loop ****/
  readdevice(input),readln(Line),checkline(Line,KeyWord),
  KeyWord="DATA",h(H),k(K),l0(L0),ccw(CCW),aob(AoB),
  eps(Eps),XLine=Line,/* prevent type error ??? */
  get4Val(XLine,Time,Vx,Vy,Temp),VxH=Vx-H,
  VyK=(-1/sin(Eps*3.1416/180))*(VxH*cos(Eps*3.1416/180)
    -(AoB)*(Vy-K)),TempF=Temp*9/5+32,
  atn2(VxH,VyK,Phi1),XPhi0=Phi0,XPhi1=Phi1,
  dphi(XPhi0,XPhi1,Dphi),
  sum(Sum0),Sum1=Sum0+DPhi,Strain=CCW*Sum1/360*12.456/L0,
  /*WaveLength of He-Ne =632.8nm or 24.912uin.,CCW
    determines the air in direction */
  writedevice(output),
  writef("\n%10.5f%10.5f%10.5f%10.3f%10.3f%10.3f%10.3f",
    Temp,Strain),
  /*shiftwindow(2),*/writedevice(screen),
  writef("\n%10.5f%10.5f%10.5f%10.3f%10.3f%10.3f%10.3f",
    Temp,Strain),
  retract(sum(_)),asserta(sum(Sum1)),/* keep Sum1 for
    next data group */
  !, /* prevent stack overflow */
  XPhi1=Phi1,calc_strain(XPhi1)./* calc. strain */
calc_strain(Phi0):-/* pass any TEXT line */
  dataline(Line),keyword(KeyWord),
  KeyWord="TEXT",writedevice(screen),
  write("\n - pass TEXT line in calc_strain routine :
    ",Line),
  calc_strain(Phi0).
calc_strain(_):-/*-0- check values for L0,H,K,Eps,AoB*/
  keyword(KeyWord),keywords(KeyWords),
  member(KeyWord,KeyWords),dataline(Line),
  initVal(Phi1),XPhi1=Phi1,calc_strain(XPhi1).
calc_strain(Phi0):- /* wrong data  */
  dataline(Line),writedevice(screen),write("\n - wrong
    data line found in calc_strain routine: ","\n
    ",Line),
  readdevice(keyboard),readchar(_),/*write("\n - Quit
    from calc_strain routine "),*/
  calc_strain(Phi0).
```

```
/*returned keywords are: DATA, L0, AIR , ELL, TEXT */
  checkline(Line,KeyWord):- /* check numbers like 0.5*/
    fronttoken(Line,StrVal,_),
    str_real(StrVal,_),/* check StrVal is a number */
    retract(dataline(_)),asserta(dataline(Line)),
    KeyWord="DATA",retract(keyword(_)),
    asserta(keyword(KeyWord)),!./* ! is required */
  checkline(Line,KeyWord):- /* check numbers like .5*/
    fronttoken(Line,StrVal_1,Rest1),StrVal_1=".",
    fronttoken(Rest1,StrVal_2,Rest2),
    str_real(StrVal_2,XVal),
    retract(dataline(_)),asserta(dataline(Line)),
    KeyWord="DATA",retract(keyword(_)),
    asserta(keyword(KeyWord)),!./* ! is required */
  checkline(Line,KeyWord):- /* check numbers like -0.5*/
    fronttoken(Line,StrVal_1,Rest1),StrVal_1="-",
    fronttoken(Rest1,StrVal_2,Rest2),
    str_real(StrVal_2,XVal),
    retract(dataline(_)),asserta(dataline(Line)),
    KeyWord="DATA",retract(keyword(_)),
    asserta(keyword(KeyWord)),!./* ! is required */
  checkline(Line,KeyWord):- /* check numbers like -.5*/
    fronttoken(Line,StrVal_1,Rest1),StrVal_1="-",
    fronttoken(Rest1,StrVal_2,Rest2),StrVal_2=".",
    fronttoken(Rest2,StrVal_3,Rest3),
    str_real(StrVal_3,XVal),
    retract(dataline(_)),asserta(dataline(Line)),
    KeyWord="DATA",retract(keyword(_)),
    asserta(keyword(KeyWord)),!./* ! is required */
  checkline(Line,KeyWord):- /* check numbers like +0.5*/
    fronttoken(Line,StrVal_1,Rest1),StrVal_1="+",
    fronttoken(Rest1,StrVal_2,Rest2),
    str_real(StrVal_2,XVal),
    retract(dataline(_)),asserta(dataline(Line)),
    KeyWord="DATA",retract(keyword(_)),
    asserta(keyword(KeyWord)),!./* ! is required */
  checkline(Line,KeyWord):- /* check numbers like +.5*/
    fronttoken(Line,StrVal_1,Rest1),StrVal_1="+",
    fronttoken(Rest1,StrVal_2,Rest2),StrVal_2=".",
    fronttoken(Rest2,StrVal_3,Rest3),
    str_real(StrVal_3,XVal),
    retract(dataline(_)),asserta(dataline(Line)),
    KeyWord="DATA",retract(keyword(_)),
    asserta(keyword(KeyWord)),!./* ! is required */
  checkline(Line,KeyWord):- /* L0 */
    fronttoken(Line,XKeyWord,Rest),
    upper_lower(KeyWord,XKeyWord),
    frontstr(2,KeyWord,StrL0,_),StrL0="L0",
    getVal(Rest,XL0,Res1),
    retract(l0(_)),L0=XL0,asserta(l0(L0)),
    writedevice(screen),
    write (" sample length L0= ",XL0),nl,
```

```
    writedevice(output),
    write (" sample length L0= ",XL0),nl,
    retract(keyword(_)),asserta(keyword(KeyWord)),
    retract(dataline(_)),asserta(dataline(Line)),
    !./* prevent wrong returning */
checkline(Line,KeyWord):- /* AIR in dir */
    fronttoken(Line,XKeyWord,Rest),
    upper_lower(KeyWord,XKeyWord),
    frontstr(3,KeyWord,StrAir,_),StrAir="AIR",
    getAirInDir(Rest,AirInDir),getCCW(AirInDir,CCW),
    XAirInDir=AirInDir,retract(airInDir(_)),
    asserta(airInDir(XAirInDir)),XCCW=CCW,retract(ccw(_)),
    asserta(ccw(XCCW)),writedevice(screen),
    write(" air in dir : ",AirInDir, " --->CCW= ",CCW),nl,
    retract(keyword(_)),asserta(keyword(KeyWord)),
    retract(dataline(_)),asserta(dataline(Line)),
    !./* prevent wrong returning */
checkline(Line,KeyWord):- /* ELLipse */
    fronttoken(Line,XKeyWord,Rest),
    upper_lower(KeyWord,XKeyWord),
    frontstr(3,KeyWord,StrEll,_),StrEll="ELL",
    getEllipse(Rest,H,K,Eps,AoB),
    XH=H,XK=K,XEps=Eps,XAoB=AoB,/* prevent type error */
    retract(h(_)),retract(k(_)),retract(eps(_)),
    retract(aob(_)),asserta(h(XH)),asserta(k(XK)),
    asserta(eps(XEps)),asserta(aob(XAoB)),
    writedevice(screen),write(" Ellipse: H= ",H,", K=
      ",K,", Eps= ",Eps,", A/B= ",AoB),nl,
    retract(keyword(_)),asserta(keyword(KeyWord)),
    retract(dataline(_)),asserta(dataline(Line)),
    !./* prevent wrong returning */
checkline(Line,KeyWord):- /* TEXT lines */
    KeyWord="TEXT",writedevice(screen),write(Line),nl,
    retract(keyword(_)),asserta(keyword(KeyWord)),
    retract(dataline(_)),asserta(dataline(Line)),
    !./* prevent wrong returning */

getAirInDir(Line,AirInDir):-
    fronttoken(Line,XAirInDir,Rest),
    upper_lower(UAirInDir,XAirInDir),
    UAirInDir<>"CCW",
    getAirInDir(Rest,AirInDir).
getAirInDir(Line,AirInDir):-
    fronttoken(Line,XAirInDir,Rest),
    upper_lower(AirInDir,XAirInDir),
    AirInDir="CCW".
getAirInDir(Line,AirInDir):-
    fronttoken(Line,XAirInDir,Rest),
    upper_lower(AirInDir,XAirInDir),
    AirInDir="CW".

getEllipse(Line,H,K,Eps,AoB):-
```

```
    getH(Line,H),getK(Line,K),
    getEps(Line,Eps),getAoB(Line,AoB).
  getH(Line,H):-
    fronttoken(Line,StrH,Rest),
    upper_lower(UStrH,StrH),UStrH="H",
    getVal(Rest,XH,_),H=XH.
  getH(Line,H):-
    fronttoken(Line,StrH,Rest),
    upper_lower(UStrH,StrH),UStrH<>"H",
    getH(Rest,H).
  getK(Line,K):-
    fronttoken(Line,StrK,Rest),
    upper_lower(UStrK,StrK),UStrK="K",
    getVal(Rest,XK,_),K=XK.
  getK(Line,K):-
    fronttoken(Line,StrK,Rest),
    upper_lower(UStrK,StrK),UStrK<>"K",
    getK(Rest,K).
  getEps(Line,Eps):-
    fronttoken(Line,StrEps,Rest),
    upper_lower(UStrEps,StrEps),UStrEps="EPS",
    getVal(Rest,XEps,_),Eps=XEps.
  getEps(Line,Eps):-
    fronttoken(Line,StrEps,Rest),
    upper_lower(UStrEps,StrEps),UStrEps<>"EPS",
    getEps(Rest,Eps).
  getAoB(Line,AoB):-
    fronttoken(Line,StrAoB,Rest),
    upper_lower(UStrAoB,StrAoB),UStrAoB="AOB",
    getVal(Rest,XAoB,_),AoB=XAoB.
  getAoB(Line,AoB):-
    fronttoken(Line,StrAoB,Rest),
    upper_lower(UStrAoB,StrAoB),UStrAoB<>"AOB",
    getAoB(Rest,AoB).

  get4Val(Line,Time,Vx,Vy,Temp):-
    XLine=Line,getVal(XLine,XTime,Rest1),Time=XTime,
    XRest1=Rest1,getVal(XRest1,XVx,Rest2),Vx=XVx,
    XRest2=Rest2,getVal(XRest2,XVy,Rest3),Vy=XVy,
    XRest3=Rest3,getVal(XRest3,XTemp,_),Temp=XTemp,!.
  get4Val(Line,Time,Vx,Vy,Temp):-
    /* prompt can be inserted here */
    writedevice(screen),
    write("\n --- wrong data line : ",Line),
    write("\n --- dataline should contain 4 numbers,please
      correct it, \n press a key to continue ---"),
    readdevice(keyboard),readchar(_),/*write("\n --- Quit
      from calc_strain routine "),*/
    edit(Line,Corrected),
    get4Val(Corrected,Time,Vx,Vy,Temp).

/* getVal routines get 1st number in a given text line */
```

```
getVal(Line,Val,Rest):-/* get positive number like 0.5 */
  fronttoken(Line,StrVal,Rest),str_real(StrVal,Val).
getVal(Line,Val,Rest2):-/*get positive number like .5*/
  fronttoken(Line,StrVal_1,Rest1),StrVal_1=".",
  fronttoken(Rest1,StrVal_2,Rest2),
  fronttoken(X,"0.",StrVal_2),str_real(X,XVal),Val=XVal.
getVal(Line,Val,Rest2):-/*get negative number like -0.5*/
  fronttoken(Line,StrVal_1,Rest1),StrVal_1="-",
  fronttoken(Rest1,StrVal_2,Rest2),
  str_real(StrVal_2,XVal),Val=-XVal.
getVal(Line,Val,Rest3):-/*get negative number like -.5*/
  fronttoken(Line,StrVal_1,Rest1),StrVal_1="-",
  fronttoken(Rest1,StrVal_2,Rest2),StrVal_2=".",
  fronttoken(Rest2,StrVal_3,Rest3),
  fronttoken(X,"0.",StrVal_3),str_real(X,XVal),Val=-XVal.
getVal(Line,Val,Rest2):-/*get positive number like +0.5*/
  fronttoken(Line,StrVal_1,Rest1),StrVal_1="+",
  fronttoken(Rest1,StrVal_2,Rest2),
  str_real(StrVal_2,XVal),Val=XVal.
getVal(Line,Val,Rest3):-/*get positive number like +.5*/
  fronttoken(Line,StrVal_1,Rest1),StrVal_1="+",
  fronttoken(Rest1,StrVal_2,Rest2),StrVal_2=".",
  fronttoken(Rest2,StrVal_3,Rest3),
  fronttoken(X,"0.",StrVal_3),str_real(X,XVal),Val=XVal.
getVal(Line,Val,Rest1):- /* repeat when not numbers */
  fronttoken(Line,StrVal,Rest),getVal(Rest,Val,Rest1).

atn2(Vx,Vy,Phi):- /* -1- */
  Vx>0,Vy>=0,Phi=arctan(Vy/Vx)*180/3.14159265 .
atn2(Vx,Vy,Phi):- /* -1- */
  Vx=0,Vy>=0,Phi=90 .
atn2(Vx,Vy,Phi):- /* -2- */
  Vx<0,Vy>=0,Phi=180+arctan(Vy/Vx)*180/3.14159265 .
atn2(Vx,Vy,Phi):- /* -3- */
  Vx<0,Vy<0,Phi=180+arctan(Vy/Vx)*180/3.14159265 .
atn2(Vx,Vy,Phi):- /* -4- */
  Vx>0,Vy<0,Phi=360+arctan(Vy/Vx)*180/3.14159265 .
atn2(Vx,Vy,Phi):- /* -4- */
  Vx=0,Vy<0,Phi=270 .

dphi(Phi0,Phi1,Dphi):-
  Dphi=Phi1-Phi0,abs(Dphi)<=180 .
dphi(Phi0,Phi1,Dphi):-
  Dphi=Phi1-Phi0+360,Phi1-Phi0<-180 .
dphi(Phi0,Phi1,Dphi):-
  Dphi=Phi1-Phi0-360,Phi1-Phi0>180 .

getCCW("CCW",1).  getCCW("CW",-1).

member(X,[X|_]).  member(X,[_|T]) :- member(X,T).
```

```
************  STRAIN.HLP ******************************
Use of Fixed Parameters Approach to calculate strain from
CTE data
*************************************************************

*Ellipse parameters (0°<eps<180°) and (air in dir.) extend
 eps to (0° to 360°)
*unit used here are inches


     Data file format :

     ELLipse, h=0, k=0, aob=1, eps=45
     AIR in dir = CW
     L0 = 3

     (time)   (Vx)   (Vy)   (Temp.°C)
      0         0      1      22
      .         .      .      .
      .         .      .      .
     new ELLipse, h=0.5, k=0.5, aob=1.5, eps=55
     AIR in dir = CCW
      10      0.5     0.1      2
      .         .      .      .
      .         .      .      .

      .....

(any extra characters contained in a data line will be
skipped)



*Flies included:
   STRAIN.EXE (main prolog program, read data from a given
     source file and output to STRAIN.OUT)
   STRAIN.HLP (this file)
   STRAIN.PRO (prolog source file)
   StrnHelp.BAT (contain DOS command to print STRAIN.HLP)
   PROLOG.SYS (configuration file)
   PROLOG.ERR (prolog error message)
   source data file (filename varies)
   STRAIN.OUT (Strain output file)
   CTEREDU.PRO (pick up CTE data every one degree)
```